INFORMATION TO USERS

This manuscript has been reproduced from the microfilm master. UMI films the text directly from the original or copy submitted. Thus, some thesis and dissertation copies are in typewriter face, while others may be from any type of computer printer.

The quality of this reproduction is dependent upon the quality of the copy submitted. Broken or indistinct print, colored or poor quality illustrations and photographs, print bleedthrough, substandard margins, and improper alignment can adversely affect reproduction.

In the unlikely event that the author did not send UMI a complete manuscript and there are missing pages, these will be noted. Also, if unauthorized copyright material had to be removed, a note will indicate the deletion.

Oversize materials (e.g., maps, drawings, charts) are reproduced by sectioning the original, beginning at the upper left-hand corner and continuing from left to right in equal sections with small overlaps.

Photographs included in the original manuscript have been reproduced xerographically in this copy. Higher quality 6" x 9" black and white photographic prints are available for any photographs or illustrations appearing in this copy for an additional charge. Contact UMI directly to order.

Bell & Howell Information and Learning
300 North Zeeb Road, Ann Arbor, MI 48106-1346 USA

UMI®
800-521-0600

Viability of an Isocentric Cobalt-60 Teletherapy Unit for Stereotactic Radiosurgery

by

Brett A. Poffenbarger
Department of Medical Physics
McGill University, Montréal
March 1998

A THESIS SUBMITTED TO THE FACULTY OF GRADUATE STUDIES AND RESEARCH IN PARTIAL FULFILLMENT OF THE REQUIREMENTS FOR THE DEGREE OF MASTER OF SCIENCE IN MEDICAL RADIATION PHYSICS

Abstract

An isocentric teletherapy cobalt unit provides a viable alternative to an isocentric linac as a radiation source for radiosurgery. An isocentric cobalt unit was evaluated for its potential use in radiosurgery in three areas: (1) the physical properties of its radiosurgical beams, (2) the quality of radiosurgical dose distributions obtained with 4 to 10 non-coplanar arcs, and (3) the accuracy with which the radiosurgical dose can be delivered. In each of these areas the 10 MV beam of a linear accelerator served as a standard for comparison.

The difference between the 80%-20% penumbras of the radiosurgical fields of the cobalt-60 and 10 MV photon beams is remarkably small, with the cobalt-60 beam penumbras on the average only about 0.7 mm larger than those of the linac beam. Differences between the cobalt-60 and 10 MV plans in terms of dose homogeneity within the target volume and conformity of the prescribed isodose volume to the target volume are also minimal, and therefore of limited clinical significance. Moreover, measured obtained isodose distributions of a radiosurgical procedure performed on the isocentric cobalt unit agreed with calculated distributions to within the ±1 mm spatial and ±5% numerical dose tolerances which are generally accepted in radiosurgery. The viability of isocentric cobalt units for radiosurgery would be of particular interest for centers in developing countries where cobalt units, because of their relatively low costs, provide the only megavoltage source of radiation for radiotherapy, and could easily and inexpensively be modified for radiosurgery.

Résumé

Nous avons étudié et démontré la possibilité d'utilser une unité de télétherapie cobalt-60 pour la radiochirurgie, tout en utilisant les méthodes de localisation et de livraison de dose courammment utilisées pour la radiochirugie par accélérateur linéaire. Trois aspects de l'unité cobalt-60 AECL Theratron T-780 ont été évalués: (1) les propriétés physiques des champs de radiation cobalt-60 produits par l'unité, (2) la qualité des distributions de dose pouvant être générées utilisant ces faisceaux de radiation, et (3) l'exactitude avec laquelle la dose peut être livrée avec l'unité de cobalt. Les résultats ont été comparés avec un accélérateur linéaire 10 MV (Varian Clinac-18), ce dernier étant utilisé cliniquement pour la radiochirurgie à l'Hôpital Général de Montréal depuis plus de 10 ans.

Nous avons constaté que la différence entre les pénombres 80%-20% des champs de photons cobalt-60 et des champs de photons 10 MV est remarquablement petite (0.7 mm en moyenne), compte tenu du diamètre relativement grand de la source de cobalt-60. Concernant l'uniformité de la dose à l'intérieur du volume cible et la conformité entre la surface d'isodose de prescription et le volume du cible, nous avons constaté que la différence entre les plans utilisant des faisceaux de cobalt-60 et des faisceaux de photons 10 MV était petite, et donc insignifiante au niveau clinique. Afin d'évaluer la stabilité mécanique de l'unité cobalt, nous avons mesuré expérimentalement des distributions de dose résultant d'une procédure radiochirurgique utilisant l'unité cobalt-60 Theratron T-780, et comparé ces résultats aux distributions de dose préalablement calculées. Nos résultats indiquent que les lignes d'isodose mesurées expérimentalement sont en accord avec les lignes d'isodoses calculées, à l'intérieur des limites de tolérance spatiale (±1 mm) et numérique (±5%) généralement acceptées en radiochirurgie. Il est donc conclu que l'unité de cobalt-60 Theratron T-780, qui a l'avantage d'être relativement peu dispendieux et mécaniquement simple, représente une alternative envisageable aux accélérateurs linéaires pour la radiochirurgie stéréotactique. Cette conclusion revêt une importance particulière pour les centres de radiothérapie situés dans des pays en voie de developpement, pour lesquels les unités de cobalt-60, grâce à leur prix relativement peu élevé, sont souvent les seules sources de radiation d'énergie megavoltes disponibles pour la radiothérapie.

Acknowledgements

I would like to express my gratitude to my supervisor, Dr. Ervin B. Podgorsak, for allowing me to work independently while maintaining his open door policy of guidance whenever it is needed. In addition to his patience and wisdom, Dr. Podgorsak provided me with everything I needed to perform my work quickly and thoroughly. Financial assistance was provided through Dr. Podgorsak from the Medical Research Council of Canada.

I would also like to thank Shoukry Aboulahef who was always eager to provide assistance in the design and construction of the equipment used in our work. Many thanks also to my fellow students, especially Dr. Corey Zankowski, Francois Deblois, Arthur Curtin-Savard, and Devin Barry for showing me the ropes. I would also like to recognize the Medical Physics Unit secretaries Margery Knewstubb and Georgia Romano for their help with the many odd tasks I have encountered during my work.

Finally, I would like to thank my parents, Marjorie Gill and John Poffenbarger, for all the encouragement and support they have given me over the years.

Contents

Chapter 3

Physical Properties of Radiosurgical Beams

Chapter 4

Comparison of Radiosurgical Treatment Plans

Chapter 5

Performance of the Theratron T-780 in Radiosurgical Treatment Delivery

Chapter 6
Conclusions

Chapter 1

Introduction

1.1 INTRODUCTION

Stereotactic radiosurgery is a high precision focal brain irradiation technique used to deliver ionizing radiation to small stereotactically localized intracranial targets, while minimizing the dose to the surrounding healthy tissue. High doses of radiation (several 1000 cGy) are delivered in the form of narrow, usually circular, beams using a single fractionation. Although radiosurgery was initially developed and is still used for treatment of certain functional disorders, it has since evolved into an effective technique for treatment of vascular malformations and other benign or malignant tumors and intracranial metastatic lesions.

Risks associated with the high dose concentration place stringent demands on the accuracy of target localization and dose delivery. Pathological tissue must be stereotactically localized in three dimensions using either computed tomography *(CT)*, magnetic resonance imaging *(MRI)*, or digital subtraction angiography *(DSA)*. Furthermore, treatment planning systems must allow the superposition of volumetric dose calculations onto these diagnostic images to

assess the suitability of a treatment plan in terms of the dose deposition to radiosensitive structures of the brain (*i.e.*, brainstem and optic chiasm). Spatial and numerical accuracies of radiation delivery must be within ±1 mm and ±5%, respectively, with steep dose gradients outside the target volume.

1.2 HISTORICAL DEVELOPMENT OF RADIOSURGERY

In the early 1950s the Swedish neurosurgeon Lars Leksell used an orthovoltage (200–300 kVp) x-ray tube coupled to a stereotactic frame to irradiate deep-seated intracranial targets from multiple directions (Leksell 1951). The purpose of the technique was to produce a well defined necrotic lesion within a surgically inaccessible region of the brain and thereby relieve the tremor associated with Parkinsonism. Leksell called this technique *radiosurgery*. While it was possible to produce brain lesions with this device, the penetrating power of orthovoltage x-rays was soon deemed insufficient, and their use was discontinued. Leksell's work, however, stimulated interest in radiosurgery and the search for more suitable radiation sources began.

In the late 1950s Leksell, in collaboration with the radiobiologist Borje Larsson, used a cross-fired proton beam produced by the Uppsala University synchrocyclotron unit as a neurosurgical tool (Larsson 1958). Soon thereafter, Lawrence (1962) from Berkeley and Kjellberg (1968) from Boston reported similar work. Each group sought to exploit several advantageous depth dose characteristics of high energy (150-300 MeV/amu) proton beams, namely: the sharp increase in ionization density occurring near the end of a particle's range (*Bragg peak*); lack of lateral scattering in the dose buildup or *plateau* region; and the finite range of the ionization track determined by the particle energy. Since the late 1970s work has also been done to exploit the greater relative biological effectiveness (RBE) and the lower oxygen enhancement ratio (OER) of heavier charged particles, such as helium, carbon, and neon.

Charged particle radiosurgical techniques based on the Bragg peak and the plateau region, have been developed. In *plateau radiosurgery*, a particle beam is used of such high energy that the Bragg peak falls outside of the patient and convergent arc techniques are used to concentrated the dose (Lyman *et al.*, 1989). This technique is especially suitable for treatment of small target volumes requiring an extremely sharp dose gradient in one direction (*i.e.*, lesions in the immediate proximity of the brainstem).

More commonly employed is *Bragg peak radiosurgery*, a treatment technique which involves centering the Bragg peak within the target volume. To be of practical use the narrow Bragg peak of a monoenergetic charged particle beam must be spread using energy modulation. This spreading is achieved at the expense of the peak to plateau dose ratio; a ratio of 3 to 1 is generally considered acceptable for radiosurgery (Lyman *et al.*, 1989). The dose is concentrated within the target volume by cross-firing several static fields. As a result the treatment volume can be conformed to the target volume using simply a beam's-eye view *aperture*.

Excellent results have been reported for Bragg peak radiosurgery, especially for large targets where the importance of conformal radiosurgery increases. However, its use has been limited to only a handful of centers worldwide, because of the excessive expenses associated with the facilities, equipment, and personnel required to perform the procedure.

In the late 1960s Leksell, frustrated with the technical and time consuming aspects (transporting patients from his practice in Stockholm to Uppsala) of proton irradiation, designed the first dedicated radiosurgical device, the Leksell Gamma Unit. The prototype consisted of 179 small cobalt-60 sources radially aligned about a common point, the unit center point (*UCP*) or isocenter. It was

constructed for clinical use at the Karolinska Institute in Stockholm (Leksell 1968). A second generation unit, containing 201 cobalt-60 sources is now commercially available as the Leksell Gamma Knife (Elekta Instrument AB, Stockholm, Sweden).

Each source of the Gamma Knife is first collimated by two fixed tungsten collimators and then by one of four collimating helmets also made of tungsten. The collimating helmets produce roughly spherical dose profiles and have full widths at half maximum (FWHM) of 4, 8, 14, and 18 mm at the isocenter of the machine. During treatment, the stereotactic frame is mounted to the helmet using special brackets, and the target irradiation is initiated when the helmet and patient 'dock' with the source array. The manufacturer states field collimation and docking alignment tolerances of ±0.3 mm and ±0.1 mm, respectively (Leksell Gamma Unit technical manual).

Though the Gamma Knife is a precision instrument, it has several important disadvantages regarding its cost and versatility. The acquisition cost is high, although much lower than that of charged particle accelerators. Furthermore, the sources must be replaced every 5 to 10 years because of the 5.26 year half-life of cobalt-60; a very expensive procedure. The unit also suffers from a relatively small maximum field size of only 18 mm, resulting in a requirement that larger lesions be treated with multiple isocenters. It has been reported that on average 2.6 isocenters are used for treatments of arteriovenous malformations (AVMs), and 3.9 for tumors (Lunsford 1992). As a result, the treatment procedure is complicated and time consuming. Additionally, with the use of multiple isocenters the dose homogeneity is reduced within the target volume and a shallower dose gradient outside the target volume is observed. Moreover, the unit shows a limited potential for conformal radiosurgery as attempts at field shaping, accomplished by plugging selected beam apertures or by combining certain helmets, has been shown to have little effect on the isodose distributions at

clinically significant (≥50%) isodose levels (Flickinger *et al.* 1990). Despite these disadvantages, many thousands of patients have been treated successfully with the unit at close to one hundred facilities world-wide.

In the 1960s and 1970s radiosurgery was performed using either the Gamma unit or particle beams. During that time the high costs of the radiosurgical equipment and the limited diagnostic image quality relegated the technique to a few highly specialized centers around the world. However, excellent treatment results obtained by these centers stimulated a search for less expensive radiosurgical techniques.

In 1974 Larsson *et al.* (1974) proposed the idea of using megavoltage x-rays produced by isocentric linear accelerators (linacs) for radiosurgical procedures. Ten years later Betti and Derechinsky (1984) working in Paris and Buenos Aires, respectively, reported the first use of linac based radiosurgery, followed by Colombo *et al.* (1985) in Vicenza and Hartmann *et al.* (1985) in Heidelberg. Shortly thereafter, Lutz *et al.* (1988) in Boston and Podgorsak *et al.* (1987, 1988) in Montreal were the first institutions in North America to implement linac-based radiosurgical techniques in their radiotherapy departments. Alternatively, Barcia-Salorio *et al.*, (1979, 1982) in Valencia reported on the use of an isocentric cobalt-60 teletherapy unit for radiosurgery, however, their technique was complicated consisting of 35 fixed portals about the target, and consequently did not gain any widespread acceptance. At first there was skepticism as to whether linac-based radiosurgery could meet the demanding accuracy requirements of the procedure. It is now generally accepted that procedures performed on adequately maintained linacs result in treatment outcomes equivalent to those of the competing Gamma units.

The narrow fields used in linac-based radiosurgery are, generally, produced by special tertiary collimators, although the use of rectangular beams produced by a linac's collimating system has been reported (Colombo *et al.* 1985). The *radiosurgical* collimators are typically lead or tungsten cylinders with circular apertures (tapered, staggered, or straight) bored out of the center. Field sizes are

commonly between 0.5 and 40 mm in diameter at the linac isocenter. The effect of the tertiary collimation is threefold: it defines the field, improves the alignment of the beam central axis with the isocenter, and serves to minimize the geometric penumbra. Although most radiosurgical collimators attach directly to the head of the linac, a precision collimating system developed by Friedman and Bova (1989) rotates on its own tracks and bearings, following the gantry head to which it is coupled.

During treatment the stereotactic frame is immobilized using brackets that attach the frame to the linac couch, chair, or floor stand. In the past, floor stands were commonly used because it was believed that they provided a better immobilization and alignment of the patient. It is now believed that couch-mounting can immobilize the frame just as well as a floor stand yet it is a simpler and less expensive technique. Moreover, with couch-mounting the gantry rotation is not restricted below the patient. Consequently, most centers now use the couch-mounting method.

The orientation of the patient within the linac beam depends on the radiosurgical technique used. Most centers using *multiple* or *dynamic noncoplanar arc techniques* require the patient to be placed in the supine position on the treatment couch. For *conical arc techniques* the patient sits in a specially designed chair. Regardless of the patient support method, interlocks are commonly used to stop the gantry, couch, or chair rotations if the height of the support assembly changes by more than a given tolerance, typically ±1 mm. Floor stand mounted stereotactic frames, additionally, require the use of blocks to restrict inadvertent couch height changes because of the potential for patient injury. Other safety precautions include immobilization of the support assembly with respect to the lateral and longitudinal motions during the treatment and safety belts to strap the patient onto the support assembly to prevent injuries arising from patient movement.

Linac-based radiosurgical techniques in clinical use today fall into one of three categories: *multiple noncoplanar converging arc techniques*, *dynamic stereotactic radiosurgery*, and *conical rotation*. The first clinical implementation of

the *multiple non-coplanar converging arc technique* was by Betti and Derechinsky (1984) in Buenos Aires. Their technique involved irradiating a patient sitting on a special chair with several 120° noncoplanar arcs. In Vicenza, Colombo *et al.* (1985) used a similar technique involving five to ten 120° non-coplanar arcs with the patient in the supine position on the linac couch. A technique developed by Hartmann *et al.* (1985) in Heidelberg, used up to eleven 140° non-coplanar arcs to treat patients in the supine position. A less complicated approach consisting of only four arcs: one in the transverse plane from 50° to 310°, and the other three covering 100° for couch angles of 90° and ±45°, was shown by Lutz *et al.* (1988) in Boston to produce a reasonable dose falloff outside the target volume.

The *dynamic radiosurgery* technique developed by Podgorsak and colleagues (1987) at McGill University in Montreal involves the simultaneous motion of the gantry and couch during the irradiation of the patient. The gantry rotates 300° and the couch 150° resulting in a beam entrance trace having a baseball seam appearance. This approach has been shown to produce dose falloffs outside the target volume comparable to those of multiple noncoplanar arc techniques (Podgorsak *et al.* 1989) and those of the Gamma unit (Walton *et al.* 1987). The treatment execution is, however, more elegant and less demanding and time consuming than that of multiple noncoplanar arc techniques.

The *conical rotation technique* was developed by McGinley *et al.* (1990) at Emory University in Atlanta. During treatment the patient sits on a rotating chair, attached to the linac couch base plate, while the gantry remains stationary at a given angle off the vertical. Up to three gantry angles are used for a typical treatment resulting in a conical irradiation pattern.

The relatively low cost of linac-based radiosurgical techniques, along with the development of improved diagnostic techniques, *CT* in the 1970s and *MR* in the

1980s, have led to a tremendous increase in the number of facilities around the world (several hundred) offering radiosurgery since the late 1980s. While some fear the accessibility of linac-based techniques will lead to substandard executions of this technically demanding treatment, linac-based radiosurgery, when practiced with adequate care, represents a less expensive alternative to the Gamma knife and charged particle treatment modalities.

1.3 FUTURE TRENDS IN RADIOSURGERY

Currently, the main topics of research involving radiosurgery include: multiple fractionation, *MR* and *CT* image correlation, conformal radiosurgery, and frameless stereotaxy. An overview of these topics is presented in this section.

Radiosurgical procedures were originally intended to induce lesions within the brain using a single dose of radiation. Conventional radiation therapy experience, however, indicates that multiple fractionation will increase the differential effectiveness of the radiation tumor damage versus damage to normal tissue. This treatment technique is then known as stereotactic radiotherapy. Future protocols will be developed to compare the effectiveness of single versus multiple fractionation radiosurgery.

MRI images provide high contrast detail of soft tissues. Correlating these images with *CT* data would aid in the identification of pathological tissues from the surrounding healthy tissue. *MR* images, however, suffer from distortions caused by inhomogeneities in the main magnetic field and Eddy currents produced within the patient and stereotactic frame. Attempts are currently made to minimize and correct for these distortions. Several groups: Schad *et al.* (1987), Ehricke *et al.* (1992), Kessler and Carson (1992) use various phantoms to asses the image warping and subsequently correct for it, while Kooy *et al.* (1994) correct

distortion using an automated method for image fusion of *CT* and *MRI* volumetric image data sets. Each of these groups has reported a reduction in spatial uncertainty to approximately ±1 mm, the level required for *CT* image correlation. At the moment, however, these correlation techniques are too time consuming to be of much clinical use.

It has been estimated that the conformation of the beam profile to the target cross-section in the beam's-eye view would significantly improve the dose delivery in approximately 40-70% of the radiosurgery caseload (AAPM TG #42 Report, 1995). Several linac-based techniques have been devised to this end: a simple method described by Luxton and Jozeph (1990) uses several collimators, each with a different diameter, to irradiate a single isocenter; Leavitt *et al.* (1991) proposed the use of a four vane computer-controlled collimator to dynamically shape the field; while Bourland and McCollough (1994) used static fields, each with beam's eye view apertures; Serago *et al.* (1991) used elliptical collimators. Finally, the use of miniature (~2 mm wide at the isocenter) multileaf collimators and intensity modulation have also been proposed. Conformation techniques, although effective, are as of yet complicated and therefore not widely used.

The cumbersome and painful nature of conventional stereotactic frames has led to a search for noninvasive means of providing localization. Several methods have been devised to this end, and each of them fall under the category of frameless stereotaxy. The approaches by Jones *et al.* (1993) and Gall *et al.* (1991) rely on the use of radiographically opaque fiducial markers, surgically implanted either subcutaneously or directly into the skull. An alternative approach, developed by Adler and Cox (1995), uses a miniature linac mounted on a robotic arm and radiographic projections to continually update the cranial position. Two real-time diagnostic x-ray sources and two digital cameras acquire images during the radiosurgical procedure. The images are matched to those found within a large

digitally reconstructed radiograph (*DRR*) library, generated from *CT* slices, to determine the orientation and position of the patient's skull at a given moment so as to aim the beam toward the pre-determined target. Each of these groups report a localization precision comparable to that attainable with conventional techniques based on invasive stereotactic frames.

1.4 MOTIVATION AND STRUCTURE OF THESIS WORK

While linac-based radiosurgery represents a less expensive alternative to the Gamma knife and charged particle treatment modalities, the cost of linear accelerators nonetheless is considerable. Consequently, in developing countries the availability of linear accelerators and thus the accessibility to stereotactic radiosurgical procedures is limited. Isocentric cobalt-60 teletherapy units, on the other hand, are relatively inexpensive and can be found in most radiation oncology centers around the world, even in those in developing countries. Hence, the application of these units for radiosurgical procedures would expand further the use of stereotactic radiosurgery and also make it more readily available in developing countries.

The intent of this thesis is to investigate and demonstrate the viability of a modern isocentric cobalt-60 teletherapy unit for radiosurgery using target localization and dose delivery methods which are similar to those widely practiced with linac-based radiosurgical techniques. We modified an isocentric cobalt-60 teletherapy unit for radiosurgery and studied the physical properties of radiosurgical beams produced by the unit; the quality of radiosurgical dose distributions obtained with the unit using from 4 to 10 non-coplanar converging arcs; and the accuracy with which the radiosurgical dose can be delivered with the unit. of an isocentric cobalt-60 teletherapy unit for radiosurgery using current, widely-practiced linac-based radiosurgical methods for target localization and dose delivery. The thesis is structured as follows:

Chapter 2 contains a theoretical and practical discussion of the Theratron T-780 cobalt unit (Theratronics Int. Ltd., Ontario, Canada), the isocentric cobalt unit used for radiosurgery in our work. Also discussed is the 10 MV photon beam of a linear accelerator (Clinac-18; Varian Associates, Palo Alto, California), the beam which served as a standard by which to evaluate the radiosurgical fields of the isotope unit. Finally, a description of the radiosurgical equipment, dosimeters, and phantoms used in our work is presented.

Chapter 3 provides the physical beam parameters used for treatment plan calculation. The percentage depth dose, off-axis ratio, and relative dose factor are discussed. Measured values of these parameters for several radiosurgical fields of the cobalt-60 and 10 MV photon beams are then presented and compared.

In ***Chapter 4*** a comparison between several radiosurgical treatment plans of the cobalt-60 and 10 MV beams is presented. Cumulative dose volume histograms *(CDVH)* are used to contrast plans consisting of between 4 and 10 non-coplanar arcs in terms of the dose homogeneity within the target volume, conformity of the prescription isodose volume to the target volume, and total volume encompassed by a given isodose surface.

The radiosurgical treatment delivery performance of the Theratron T-780 is addressed in ***Chapter 5***. The techniques used to measure the practical isocenter of the isotope unit are presented, along with a discussion of the results. The accuracy with which the Theratron T-780 can deliver a radiosurgical dose distribution is then evaluated by comparing several experimentally obtained dose distributions to those calculated using the McGill Planning System.

Chapter 6 summarizes the overall results and addresses the viability of the isocentric cobalt-60 unit for radiosurgery.

1.5 REFERENCES

Adler J.R. and Cox R.S. *Preliminary clinical experience with the cyberknife: image guided stereotactic radiosurgery.* In: Kondziolka D., (ed.). Radiosurgery pp. 317-326 (1995).

American Association of Physicist in Medicine (AAPM) Report #54. *Stereotactic radiosurgery.* Report of AAPM Task Group #42, American Institute of Physics, New York (1995).

Barcia-Salorio J.L., Broseta J., Hernandez G., Ballester B., and Masbout G. *Radiosurgicaltreatment of a carotid-cavernous fistula.* Case report in Szikla, Stereotactic cerebral irradiations, Elsevier pp. 251-256 (1979).

Barcia-Salorio J.L., Hernandez G., Broseta J., Gonzalez-Darder J., and Ciudad J. *Radiosurgical treatment of carotid-cavernous fistula.* Appl. Neurophysiol. **45**: 520-522 (1982).

Betti O.O. and Derechinsky V.E. *Hyperselective encephalic irradiation with linear accelerator.* Acta Neurochir; suppl **33**: 385-390 (1984).

Bourland J.D. and McCollough K.P., *Static field conformal stereotactic radiosurgery: physical techniques.* Int. J. Radiat. Oncol. Biol. Phys. **28**: 471-479 (1994).

Colombo F., Beneditti A., Pozza F., Avanzo R.C., Marchetti C., Chierego G., and Zanardo A. *External stereotactic irradiation by linear accelerator.* Neurosurgery **16**: 154-160 (1985).

Ehricke H., Schad L.R., Gademann G., Wowra B., Engenhart R., and Lorenz W.J. *Use of MR angiography for stereotactic planning.* J. Comp. Asst. Tomography. **16**: 35-37 (1992).

Flickinger J.C., Lunsford L.D, Wu A., Maitz A.H., and Kalend A.M. *Treatment planning for Gamma Knife radiosurgery with multiple isocenters.* Int. J. Radiat. Oncol. Biol. Phys. **18**: 1495-1511 (1990).

Friedman W.A. and Bova F.J. *The University of Florida radiosurgery system.* Surg. Neurol. **32**: 334-342 (1989).

Gall K., Verhey L., and Wagner M. *Automated patient positioning for high precision radiotherapy.* AAPM Annual Meeting, 1991, St. Louis, Missouri (abstract).. Med. Phys. **18**: 604 (1991).

Hartmann G.H., Schlegel W., Sturm V., Kober B., Pastyr O., and Lorenz W.J.. *Cerebral radiation surgery using moving field irradiation at a linear accelerator facility.* Int. J. Radiat. Oncol. Bio. Phys. **11**: 1185-1192 (1985).

Jones D., Christopherson D.A., Washington J.T., Hafermann M.D., Rieke J.W.,Travaglini J.J., and Vermuelen S.S. *A frameless method for stereotactic radiotherapy.* Brit. J. Radiol. **66**: 1142-1150 (1993).

Kessler M.L. and Carson P.L. *Test object design and performance simulation for 3D imaging systems: spiral rod image distortion phantom,* Annual meeting of the Radiological Society of North America (1992). (abstract).

Kjellberg R.N., Shintani A., and Frantz A.G. *Proton beams in acromegaly.* N. Eng. J. Med. **278**: 689-695 (1968).

Kooy H.M., van Herk M., Barnes P.D., Alexander E. 3rd., Dunbar S.F., Tarbell N.J., Mulkern R.V., Holupka E.J., and Loeffler J.S. *Image fusion for stereotactic radiotherapy and radiosurgery treatment planning.* Int. J. Radiat. Oncol. Biol. Phys. **28**: 1229-1234 (1994).

Larsson B., Leksell L., and Rexed B. *The high energy proton beam as a neurosurgical tool.* Nature **182**: 1222-1223 (1958).

Larsson B., Liden K., and Sorby B. *Irradiation of small structures through intact skull.* Acta Radiol. TPB **13**: 513-534 (1974).

Lawrence J.H., Tobias C.A., Born J.L., Wang C.C., and Linfoot J.H. *Heavy particle irradiation in neoplastic and neurologic disease.* J. Neurosurg. **19**: 717-722 (1962).

Leavitt D.D., Gibbs F..A., Heilbrun M..P., Moeller J.H., and Tabach G.A. *Dynamic field shaping to optimize stereotactic radiosurgery.* Int. J. Radiat. Oncol. Biol. Phys. **21**: 1247-1255 (1991).

Leksell L. *The stereotaxis method and radiosurgery of the brain.* Acta Chir. Scand. **102**: 316-319 (1951).

Leksell L. *Cerebral radiosurgery I. Gamma thalamotomy in two cases of intractable pain.* Acta Chir. Scand. **134**: 585-595 (1968).

Lunsford L.D. *Current worldwide role of gamma knife stereotactic radiosurgery.* Stereotactic radiosurgery update proceedings of the international stereotactic radiosurgery symposium, Pittsburgh, Pennsylvania, June 1991, Elsevier (1992).

Lutz W., Winston K.R., Maleki N. *A system for stereotactic radiosurgery with a linear accelerator.* Int. J. Radiat. Oncol. Bio. Phys. **14**: 373-381 (1988).

Luxton G. and Jozsef G. *Dosimetric considerations in linac radiosurgery treatment planning of off-center and elongated targets* (abstract).. Int. J. Radiat. Oncol. Biol. Phys. (Suppl. 1). **19**: 262 (1990).

Lyman J.T., Phillips M.H., Frankel K.A, and Fabrikant J.I. *Stereotactic frame for neuroradiology and charged particle Bragg peak radiosurgery of intracranial disorders.* Int. J. Radiat. Oncol. Biol. Phys. **16**: 1615 (1989).

McGinley P.H., Butker E.K., Crocker I.R., and Landry J.C. *A patient rotator for stereotactic radiosurgery.* Phys. Med. Biol. **35**: 649-657 (1990).

Podgorsak E.B., Olivier A., Pla M., Hazel J., and deLotbiniere A. *Physical aspects of the dynamic stereotactic radiosurgery.* Appl. Neurophisiol. **50**: 263-268 (1987).

Podgorsak E.B., Olivier A., Pla M., Lefebvre P.Y., and Hazel J. *Dynamic stereotactic radiosurgery.* Int. J. Radiat. Oncol. Biol. Phys. **14**: 115-126 (1988)

Podgorsak E.B., Pike G.B., Olivier A., and Souhami L. *Radiosurgery with high energy photon beams: a comparison among techniques.* Int. J. Radiat. Oncol. Biol. Phys. **16**: 857-865 (1989).

Schad L.R., Lott S., Schmitt F., Sturm V., and Lorenz W.J. *Correction of spatial distortion in MR imaging: a prerequisite for accurate stereotaxy.* Journal of Computer Assisted Tomography **11**: 499-505 (1987).

Serago C.F., Lewin A.A., Houdek P.V., Gonzalez-Arias S., Abitbol A.A., Marcial-Vega V.A., Pisciotti V., and Schwade J.G. *Improved LINAC dose distributions for radiosurgery with elliptically shaped fields.* Int. J. Radiat. Oncol. Biol. Phys. **21**: 1321-1325 (1991).

Walton L., Bomford C.K., and Ramsden D. *The Sheffield stereotactic radiosurgery unit: physical characteristics and principles of operation.* Br. J. Radiol. **60**: 897-906 (1987).

Chapter 2

Experimental Apparatus

2.1 RADIATION SOURCES

The Theratron T-780 (Theratronics Int. Ltd., Ontario, Canada) cobalt-60 teletherapy unit was evaluated for radiosurgery in our work. This isocentric cobalt unit has been used for radiotherapy at the Montreal General Hospital since 1975, and can be considered a typical isotope unit in all accounts. In subsequent chapters the

radiosurgical performance of the Theratron T-780 is compared to that of the Varian Clinac-18 linear accelerator (Varian Associates, Palo Alto, California). The 10 MV photon beam of this linear accelerator has been used for radiosurgery at the Montreal General Hospital since 1986 and has a proven track record in terms of treatment outcome. Hence, the use of this beam as a standard of comparison is justified. A description of both the Theratron T-780 and Clinac-18 follows.

2.1.1 The Isocentric Theratron T-780 Cobalt Unit

The main components of the Theratron T-780 teletherapy unit include the sourcehead containing the cobalt-60 source, the collimating system, and the patient support assembly. The *sourcehead* is a lead-filled steel capsule that houses the source. A radiation beam is emitted from the sourcehead when the source is pneumatically positioned over the *beam portal*; a hole in the shielding. When the unit is idle, a drawer retracts the source into a depleted uranium chamber near the center of the sourcehead. At this position 99.9% of the radiation generated by the source is absorbed. The 1.5 s travel time between the storage and beam-on positions results in a 0.02 min *shutter error.*

The source consists of many cobalt-60 pellets sealed inside a 1.5 cm diameter stainless-steel cylinder, which is itself sealed within another cylinder to reduce the possibility of leakage. The cobalt-60 atoms decay to nickel-60 atoms, with a 99% probability of the emission of a β^- particle (E_{max} = 0.32 MeV), and two megavoltage photons (1.17 MeV and 1.33 MeV). Although the source and steel cylinders absorb the β^- particles, the attenuation of the megavoltage photons by these components is negligible. These photons constitute the primary radiation beam of the unit. The primary beam is, therefore, essentially monoenergetic with a mean energy of 1.25 MeV. Approximately 10% of the clinical beam intensity,

however, is attributable to scattered radiation originating from the sourcehead, collimating system, source housing, and the source itself (Kahn 1994). In October 1996, this source had an activity of 6208 Ci and yielded an exposure rate of 80.2 R/min at the mechanical isocenter (source-axis distance *SAD* = 80 cm), for a 10×10 cm^2 field.

The collimating system of the Theratron T-780 consists of a fixed shield, and two adjustable orthogonal pairs of leaves and *trimmer bars*. The depleted uranium shield surrounds the beam portal, limiting the maximum field size to 35×35 cm^2 at isocenter. The independently adjustable pairs of lead leaves are used to define rectangular fields as small as 5×5 cm^2 at *SAD*. To minimize the penumbra, these leaves are mounted in such a manner that their inner surfaces remain parallel to the edge of the beam, regardless of field size. Depleted uranium trimmer bars, located 45 cm from the source, further sharpen the field edges. Additional collimation can be performed by placing accessories into tray slots located 49.8 cm and 51.8 cm away from the source.

The sourcehead and collimating system are mounted on a rotating gantry, along with a counterweight. During arc therapy procedures, the gantry can be set to rotate at any speed between 0.2 and 1.0 rpm.

The motorized *patient support assembly* (*PSA*) consists of a patient stretcher and couch, mounted to a rotating pedestal. Nominally, the *PSA* axis of rotation is in line with the isocenter and source when the gantry is in the vertical position. Rotations of up to ±90° from the 180° position; the position at which the couch is perpendicular to the gantry plane of rotation, are possible. The couch can also travel vertically, laterally, and longitudinally.

2.1.2 The Clinac-18 Linear Accelerator

For the Clinac-18 linear accelerator the process of photon beam production begins with the emission and acceleration of electrons within the unit's electron gun. Electrons boiled off the gun's cathode are electrostatically accelerated under a 25 keV bias to a high velocity, allowing their capture by the high-powered radiofrequency pulse (5.5 MW, 2856 MHz) of the *standing waveguide* (Karzmark and Morton 1981). The *captured electrons* are further accelerated throughout the 21 disk-loaded cavities of the 1.4 m long waveguide, after which an achromatic 270° bending magnet is encountered. The magnet contains energy analyzer slits which intercept electrons varying by more than ±3% from the nominal electron energy of 10 MeV (Clinac-18 Maintenance Manual, Vol. 1). The magnet also serves to redirect the beam, focussing the electrons onto a 5 mm thick copper target. Upon striking the target, the electrons convert a portion of their kinetic energy into *bremsstrahlung* radiation. The resulting photons are radiated predominantly in the forward direction, over a continuous range of energies between 0 MeV and 10 MeV. The x-ray beam is, therefore, referred to as a 10 MV photon beam, in acknowledgement of its energy spectrum.

The electron gun, waveguide, bending magnet, and target are maintained at a vacuum pressure of 10^{-6} torr. Photons exit the evacuated chamber through a 0.25 cm thick beryllium window. The profile of the beam leaving the window is forward peaked and not suitable for therapy. The beam is, therefore, flattened using a conical-shaped tungsten-iron alloy filter. This *flattening filter* is constructed such that the profile of the beam will be rendered flat (±3%) over 80% of the longitudinal and transverse axes of a 10×10 cm^2 field at a depth of 10 cm within a tissue equivalent phantom placed at nominal *SSD* (Clinac-18 Maintenance Manual, Vol. 1).

The collimating system of the Clinac-18 consists of three parts: the primary, secondary, and variable collimators. The primary collimator is a fixed lead cone mounted just beneath the beryllium window, its purpose is to shield the room from the lateral components of the beam. The fixed secondary collimator, made of tungsten and lead, limits the maximum square field size to 35×35 cm^2 at the isocenter (*SAD* = 100 cm). Variable field definition is achieved using two pairs of independently adjustable tungsten collimators located 35.0 cm and 44.3 cm below the copper target. The movement of these collimators is constrained in such a manner that the leading edge of each block matches the beam divergence, resulting in a sharp dose fall-off outside the primary beam. Accessories placed in the tray slot, located 65.1 cm from the target, enable additional collimation to be performed.

The output of the beam is measured using independent dual transmission ion chambers, which are located just beneath the flattening filter. Charge produced by ionizing radiation passing through these detectors is collected and converted to dose monitor units (MUs). These arbitrary units are calibrated such that 1 MU corresponds to 1 cGy, measured at the depth of maximum dose (d_{max}) within a tissue equivalent phantom placed at nominal *SSD*, and irradiated by a 10×10 cm^2 field. The ionization chambers are sealed to minimize the effects of temperature and pressure variances. The dose rate of the Clinac-18 can be varied between 100-500 MU/min.

Upon leaving the linac head, the radiation beam is composed of the primary polyenergetic x-ray beam and scattered radiation originating from: the flattening filter, collimators, and ionization chambers. Additionally, some electron contamination occurs as a result of Compton interactions with these components. Monte Carlo calculations have shown that the 10×10 cm^2 field of the Clinac-18 has a mean energy of approximately 3.06 MeV (Zankowski 1994).

2.2 *RADIOSURGICAL EQUIPMENT*

2.2.1 Radiosurgical Collimators

The radiosurgical collimators in use on the Clinac-18 linac were also used for radiosurgical procedures carried out on the Theratron T-780 cobalt unit. These collimators are made of polystyrene-encased lead cylinders, each with an outer diameter of 8 cm, a height of 10 cm, and a centrally-located tapered hole which defines the radiosurgical beam. A set of radiosurgical collimators is available, producing circular radiation beams with nominal diameters (profile *FWHMs*) between 1.0 cm and 4.0 cm at the isocenter of the Clinac-18 linac with an *SAD* of 100 cm. As a result of the geometrical differences between the treatment setups on the two units, for a given collimator the nominal diameters of the Theratron T-780 radiosurgical fields are approximately 6% smaller than those of the Clinac-18 radiosurgical fields, and the collimator taper does not perfectly match the field divergence of the cobalt beam. These differences are depicted schematically in Fig. 2-1. During radiosurgery, the collimator is attached to the gantry head using a tray mount, and the variable collimator of the teletherapy unit is set to 5×5 cm^2.

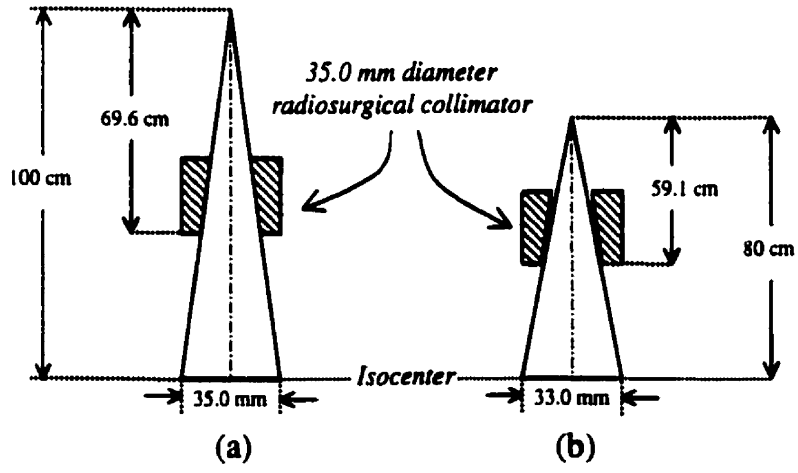

FIG. 2-1. Diagram depicting the difference in the source-axis distance and source-collimator distance between the Clinac-18 (a) and Theratron T-780 (b) for radiosurgical procedures. As a result of these differences, the nominal diameters of the Theratron T-780 radiosurgical fields are approximately 6% less than those of the Clinac-18, for a given collimator. Note that the collimator taper does not match the divergence of the Theratron T-780 beam.

2.2.2 Stereotactic Frames

Stereotactic frames are used in radiosurgery for target localization before treatment and patient immobilization during treatment. During radiosurgery the frame is usually fastened with pins to the patients skull in order to provide a fixed coordinate system (Cartesian, cylindrical, or spherical) with respect to the brain. Localization is accomplished using *CT*, *MR*, or *DSA* images of the patient's head with the frame and fiducial marker box attached. The frame coordinate system is transferred from these images to the treatment planning system, enabling 3D localization of intracranial anatomical structures.

The stereotactic frame used in this work was built in the machine shop of the Medical Physics Department at the Montreal General Hospital and is shown in Fig. 2-2. The frame has a positive-valued Cartesian coordinate system with the origin located at one corner of the box, and the center located 10.0 cm away from the origin along the X, Y, and Z coordinate axes. The frame is constructed of a rigid aluminum base with carbon fiber posts and pins, to minimize image artifacts. Transverse *CT* images of the frame's three aluminum N-shaped fiducial marker bars are used to transfer the frame coordinate system to the treatment planning system.

FIG. 2-2. Stereotactic frame and CT fiducial marker box built in the machine shop of the Medical Physics Department of the Montreal General Hospital.

2.3 *DOSIMETRIC EQUIPMENT*

High-resolution radiation detectors are required for characterization of the small radiosurgical fields. The dosimeters used in our work: the end-window parallel plate detector, semiconductor detector, and film detectors are considered suitable for such measurements. A discussion of these detectors follows.

2.3.1 Parallel-Plate Ionization Chambers

End-window parallel-plate ion chambers are designed to accurately measure dose in regions of high dose gradient. These chambers consist of an upper and lower electrode, parallel to one another, with the lower electrode surrounded by a *guard ring*. The upper electrode or *window* is constructed very thin (0.01-0.03 mm) to minimize the attenuation of incident radiation for surface dose measurements. The electrode separation is very small (0.5-1.0 mm) to provide a good depth resolution. A voltage (~150 V/mm) is applied across the electrodes to collect the ions produced in the air contained within the sensitive volume of the detector. The guard ring serves to provide a uniform electric field over the sensitive volume of the detector and to prevent leakage currents from effecting the measured signal.

Parallel-plate dosimeters exhibit polarity dependence. High energy photons may eject electrons from the chamber's electrodes through Compton interactions, producing a current. This *Compton current* adds to, or subtracts from, the 'true' ion current (current resulting from ionization events within the chamber's sensitive volume) depending on whether the upper electrode is maintained at a positive or negative potential, respectively. This polarity effect increases in significance in regions where electronic equilibrium is not achieved (Richardson 1954). Taking measurements at opposite polarities and averaging the results can cancel this

source of error. Averaging also minimizes measurement inaccuracies arising from *extracameral* currents; currents produced by ions originating outside the sensitive volume of the detector (Attix 1986).

A Nuclear Enterprises Model 2505/3 (Nuclear Enterprises Ltd., Beenham, Reading, England) end-window parallel-plate ionization chamber was used in our work. The electrode separation and sensitive diameter of the chamber are 1.0 mm and 3.0 mm, respectively, resulting in a chamber sensitive volume of 0.03 cm^3. The polyethylene window of this chamber is 0.03 mm thick. During measurements, the electrodes were maintained at polarizing potentials of –300 V and +300 V, with the average reading taken. The ionizational charge was measured using a Keithley 616 digital electrometer (Keithley Instruments Inc., Cleveland Ohio).

2.3.2 Semiconductor Detectors

Semiconductor or *diode* detectors typically consist of a small silicone crystal which has two regions containing impurities: a relatively large positively doped region (*p-r*egion) that has a high concentration of *holes*, and a very thin *n-region* that contains an excess of *conduction* electrons. Upon formation of these electrically neutral regions, there is a net electron flow out of the *n-region* toward the *p-region*, leaving positively charged donor sites behind, and a simultaneous flow of holes toward the *n-region*, leaving negatively charged acceptor sites behind. The newly formed charged regions set up an electric field that eventually halts the exchange. Between these two regions is a volume depleted of charge carriers through which current cannot flow. Ionizing radiation passing through this *depletion region* produces electron-hole pairs. The migration of the electrons to the *p-region* and the holes toward the *n-region* gives rise to a voltage that can be measured and related to dose or dose rate.

The sensitivity of an unbiased semiconductor detector is approximately 18000 times greater than that of an ionization chamber with equal sensitive volume. The difference in sensitivity results from the relatively high density of silicon compared to air ($\cong 2.3$ g/cm^3 compared to $\cong 1.3\times10^{-3}$ g/cm^3), and also from the relatively low amount of energy necessary to produce electron-hole pairs in silicon compared to air (~3 eV compared to ~33.97 eV). Because of their high sensitivity, semiconductor detectors can be made much smaller than gaseous ionization detectors, and therefore have a higher spatial resolution.

The semiconductor detector used in our work was a Scanditronix p-Si circular diode (Scanditronix AB, Uppsala, Sweden). It has a sensitive volume of approximately 0.25 mm^3, located 0.55 mm below its water-resistant epoxy surface. The effective detection area of the dosimeter is 2.5 mm in diameter.

2.3.3 Film Dosimeters and Densitometry

Film densitometry is well suited for measurements of dose distributions and stationary beam parameters of radiosurgical fields, as the spatial resolution of this detector is primarily limited by the resolution of the optical device used to analyze the film, (typically 0.1-1.0 mm). Both radiographic and radiochromic film were used for relative dosimetry in our work.

2.3.3.A Radiographic Film

Radiographic film is constructed of a 10-20 μm thick emulsion on one or both sides of an approximately 0.1 mm thick supporting polyester layer. The emulsion is composed of microscopic silver bromide grains embedded in a gelatinous layer. Radiation incident on film produces ion pairs within the emulsion, which convert silver ions into silver atoms. Grains containing the silver atoms constitute a *latent image*; an image that can be chemically processed to produce an optical record of the radiation dose and dose distribution known as a *radiograph*.

The processing begins with the administration of a *developer* solution. This solution reduces the silver ions to silver atoms, with the rate of reduction dependent on the amount of silver atoms present within a grain. Immersing the film in dilute acetic acid or *stop bath*, at some point before all the silver ions are reduced, terminates the development process. The remaining silver ions are then removed using a sodium thiosulphate solution, leaving the remaining opaque silver atoms to constitute the radiograph. The density of the silver atoms on the radiograph can be determined optically, using a densitometer, and finally related to the absorbed dose.

There are several disadvantages associated with radiographic film when used for dosimetry. This film exhibits a non-linear dose response above a relatively low dose level (~40 cGy). Relative dose measurements must, therefore, be calibrated with respect to the dose-response curve of the film, or performed within the linear portion of this curve. Film also exhibits a non-linear energy response to low energy photons (below 300 keV), as a result of the silver and bromide ions participating in photoelectric interactions (Attix 1986). Moreover, the response of film varies significantly from batch to batch, is susceptible to temperature and chemical variations in the development process, and must be handled in darkroom conditions.

Kodak X-Omat V film (Eastman Kodak Inc., Rochester, New York) was used in our work. Measurements revealed that this film had a linear dose response up to 50 cGy, with a batch-response variation of ±5.1% at the 30 cGy dose level, as shown in Fig. 2-3. When comparisons were to be made between films, each was taken from the same batch and developed at the same time to minimize inaccuracies. All measurements were performed in the linear portion of the dose-response curve.

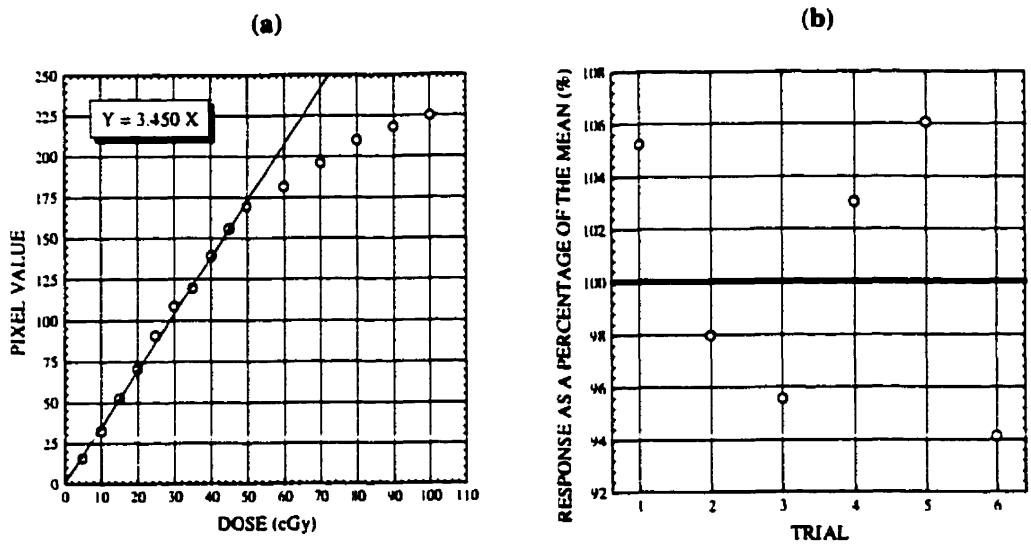

FIG. 2-3. (a) The Kodak X-Omat V dose-response calibration curve for the 10 MV photon beam, and (b) response variability of the radiographic film at the 30 cGy dose level. Pixel values were determined using an He-Ne laser microdensitometer.

2.3.3.B Radiochromic Film

Radiochromic film, film that changes color immediately following exposure to radiation, was first proposed for use in dosimetry by McLaughlin and Chalkey (1965). This film has several advantages over conventional radiographic films for relative dosimetry as it requires no processing to bring out the color change, is relatively photo-insensitive, and can be handled in ambient light conditions. Furthermore, radiochromic film exhibits relatively little energy dependence (±5% between 0.127-1.71 MeV), is essentially tissue equivalent over the range of therapeutic beam energies, and exhibits a relatively small (~2%) batch-response variation (Sayeg 1990, Muench 1991).

GafChromic MD-55 (ISP Technologies Inc., Wayne, New Jersey) radiochromic film was used in our work. Each film was cut from lot number 970106. The film exhibited a linear dose response up to 60 Gy, with a response variation of ±2.1% at the 50 Gy dose level, for densitometry performed with an He-Ne laser

microdensitometer, as shown in Fig. 2-4. These values are in agreement with those reported by Ramani (1994) and McLaughlin *et al.*, (1994). All measurements were carried out within the linear region of the film's dose-response curve.

2.3.3.C Film Densitometry

Film densitometry was performed using either the scanning infrared densitometer of the RFA (Scanditronix AB, Uppsala, Sweden) or the He-Ne laser microdensitometer of the LINX Clinical Review System (E.J. Dupont De Nemours and Co. Inc., Wilmington, Delaware).

The infrared densitometer of the RFA has a density resolution of 0.01 optical units (O.D.) over a range of 0.0-4.0 O.D., with a scanning area of 49.5x49.5 mm^2 (RFA Operation Manual). The manufacturer states a spatial resolution of 0.5 mm and 0.8 mm between the 90%-50% and 50%-10% optical density levels, respectively, when scanning over an edge.

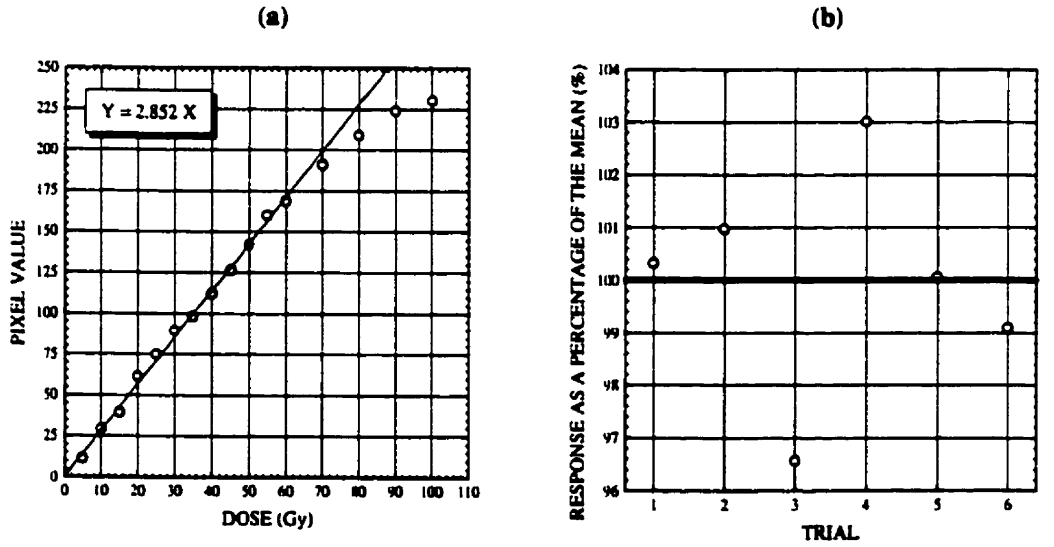

FIG. 2-4. (a) The GafChromic MD-55 dose-response calibration curve for the cobalt-60 photon beam, and (b) the response variability of the radiochromic film at the 50 Gy dose level. Pixel values were determined using an He-Ne laser microdensitometer.

The LINX laser microdensitometry system has a scanning area equal to 35.4×43.0 cm^2, with a maximum spatial resolution of 0.21 mm (LINX Clinical Review System operation manual). The helium-neon (He-Ne) laser has a focal spot size of 100 μm and a wavelength of 632.8 μm.

2.4 PHANTOMS

It is seldom possible to perform measurements *in-vivo*. Dose calculations are, therefore, derived from data measured within *tissue equivalent* materials called *phantoms*. Water is the most commonly used phantom material, because it closely approximates the radiation absorption and scattering properties of muscle and soft tissues, and is also readily available. It is not possible, however, to immerse into water some detectors such as parallel-plate ionization chambers; the water pressure would distort or collapse the chamber's thin window and the humidity would increase the chamber leakage currents to unmanageable levels. Solid phantoms have been designed to interact with radiation in a manner equivalent to water to overcome this problem.

Ideally, for a material to be considered water equivalent, it must have an effective atomic number Z_{eff}, number of electrons per gram ρ_e, and mass density ρ_m equal to that of water. For megavoltage photon beams, however, the Compton effect is the primary mode of interaction. Since the Compton cross-section is dependent only on the electron density of a material, a phantom that merely possesses an electron density similar to that of water can be considered water equivalent. The solid phantoms used in our work are constructed of such materials include: polystyrene, Solid Water™ (RMI, Middleton, Wisconsin), and Lucite™. Relevant physical properties of these materials are listed in Table 2-1. From this table it is evident that Solid Water™ most closely approximates water equivalence, therefore, this material was preferentially used in our work.

MATERIAL	ρ_m *(g/cm^3)*	ρ_e *(Electrons/g)*	Z_{eff}
Water	1.00	3.34×10^{23}	7.42
Polystyrene	1.03–1.05	3.24×10^{23}	5.69
Solid Water™	1.00	3.34×10^{23}	7.35
Lucite™	1.16–1.20	3.24×10^{23}	6.48

TABLE 2-1. The mass density ρ_m, electron density ρ_m, and effective atomic number Z_{eff} of various phantom materials. (Khan 1994)

2.4.1 The Scanditronix Radiation Field Analyzer 300

The Scanditronix Radiation Field Analyzer 300 (Scanditronix AB, Uppsala, Sweden), or simply RFA, is essentially a cubical water phantom designed to automate the acquisition of 3D dose distributions. It consists of an Lucite™ water tank, dual channel electrometer, radiation dosimeter, and computer. The RFA has a scanning volume of 50×50×50 cm^3 with a positional accuracy and reproducibility of 0.5 mm and 0.1 mm, respectively. The manufacturer states a dose resolution of 0.1% at any depth. The p-Si semiconductor, mentioned in the Section 2.3.2, was used with the RFA for photon beam dosimetry. Measurements of the Clinac-18 photon beam required the additional use of an identical *reference* detector, to cancel out beam intensity fluctuations.

2.4.2 Stereotactic Head Phantom

A phantom suitable for radiosurgical treatment planning and verification procedures was designed and built in-house. This phantom, shown in Fig. 2-5, consists of a hollow head-shaped Lucite™ shell, approximately 2.0-3.0 mm thick. A stereotactic frame can be affixed to the phantom by driving the frame's four pins into indentations present on the shell. During measurements, the shell is filled with water to render it approximately tissue equivalent.

FIG. 2-5. Phantom and stereotactic frame built in the machine shop of the Medical Physics Department at the Montreal General Hospital for verification of radiosurgery treatment plans and techniques.

A space exists within the head phantom into which a cylindrical insert may be placed. Two inserts are available: one for target localization procedures, the other for treatment planning verification procedures. The hollow *localization insert* has 4.0 mm thick Lucite™ walls. During localization procedures, one of several tumor phantoms is mounted within this cylinder and the insert is filled with water. Diagnostic images of the phantom, with the fiducial marker box attached, provide contours suitable for treatment planning procedures.

The *verification insert* is constructed of polystyrene. It contains a cavity into which a cylindrical *film mount*, also made of polystyrene, can be placed. Two of these film mounts exist: one for transverse dose distribution measurements, the other for sagittal and coronal measurements. A 4.8 cm diameter circular film can

be loaded into the transverse mount, whereas a 4.8×8.0 cm^2 rectangular film can be loaded into the sagittal-coronal mount. Pegs are used to align a given mount with the sectional plane of interest. Because the head phantom and inserts are not light-tight, radiochromic film was used for the measurements.

2.5 SUMMARY

Meeting the stringent accuracy demands of radiosurgery begins with a thorough understanding of the apparatus and materials required to develop and execute this procedure. In this chapter a detailed description of the teletherapy units and ancillary equipment used for radiosurgical procedures was presented, along with a theoretical and practical discussion of the dosimetric equipment used to characterize the radiosurgical beams.

2.6 REFERENCES

Attix F.H., *Introduction to radiological physics and radiation dosimetry*. John Wiley and Sons Inc. (1986).

Karzmark C.J. and Morton R.J. *A primer on theory and operation of linear accelerators in radiation therapy*. U. S. Department of Health and Human Services, Food and Drug Administration, Bureau of Radiological Health, Rockville, Maryland, (1981).

Khan F.M. *The Physics of Radiation Therapy*. 2nd edition, Williams and Wilkins, (1994).

McLaughlin W.L. and Chalkey L., *Low atomic numbered dye systems for ionizing radiation measurements*, Photo. Sci. Eng. **9**: 159-165 (1965).

McLaughlin W.L., Soares C.G., Sayeg J.A., McCullough E.C., Kline R.W., Wu A., and Maitz A.H. *The use of a radiochromic detector for the determination of stereotactic radiosurgery dose characteristics*. Med. Phys. **21**: 379-388 (1994).

Muench P.J., Meigooni A.S., Nath R., and McLaughlin W.L. *Photon energy dependence of the sensitivity of radiochromic film and comparison with silver halide film and LiF TLDs used for brachytherapy dosimetry.* Med. Phys. **18**: 769-775 (1991).

Ramani R., Lightstone A.W., Mason D.L.D., and O'Brien P.F., *The use of radiochromic film in treatment verification of dynamic stereotactic radiosurgery.* Med. Phys. **21**: 389-392 (1994).

Richardson, C. *Effect of chamber voltage on electron build-up measurements.* Radiology **62**: 584 (1954).

Sayeg J.A., Coffey C.W., and McLaughlin W.L. *The energy response of GafChromic radiation detectors*, Med. Phys. **17**: 521 (1990). (Proc. of 1990 AAPM Meeting).

Zankowski C. *Monte Carlo analysis of the 10 MV x-ray beam from a CLINAC-18 linear accelerator.* M.Sc. Thesis, McGill University, Montreal (1996).

Chapter 3

Physical Properties of Radiosurgical Beams

3.1 INTRODUCTION

To evaluate the suitability of the Theratron T-780 cobalt-60 gamma-ray beam for radiosurgery it is necessary to formulate treatment plans based on its radiosurgical field properties. The McGill Planning System was used in our study for this purpose. This program, developed in-house (Pla 1994), calculates 3-D dose distributions from the *percentage depth doses (PDDs)* and *off-axis ratios (OARs)*, using the relationship proposed by Pike *et al.*, (1987):

$$D_Q(d,A_Q) = P\left(d, A_i \frac{f_i - d_i + d}{f_i + d}, f_i\right)\left(\frac{f_i + d}{f_i + d_{max}}\right)^2\left(\frac{f_i}{f_i - d_i + d}\right)^2 OAR(d,r_Q), \qquad (3.1)$$

where d is the depth of the point of interest Q within the head; f_i is the source-axis distance; d_{max} and d_i are the depth of maximum dose and the isocenter depth, respectively; A_Q and A_i are the field diameters at point Q and at isocenter, respectively; and r_Q is the distance from the central axis to point Q at depth d. The dose rate is calculated from the relative dose factor *(RDF)* of the radiosurgical fields. The algorithm has been verified by Pike *et al.*, (1987) for various megavoltage photon beams and the planning system has been developed, verified, and described by Pla (1994).

A discussion of the percentage depth dose, off-axis ratio, and relative dose factor appears in this chapter. Measured values for several radiosurgical fields of the cobalt-60 and 10 MV photon beams are presented and compared. An evaluation of these physical quantities with respect to the guidelines recommended by the AAPM TG #42 Report (1995), a report on the quality assurance of radiosurgery, is also presented.

3.2 PERCENTAGE DEPTH DOSE

3.2.1 Definition

The percentage depth dose is used to characterize the central axis dose D as a function of depth within a phantom placed at nominal *SSD*. Values are given relative to the maximum dose [$D(d_{max})$], which appears at the depth of dose maximum d_{max} beneath the phantom surface and is assigned a value of 100. Mathematically, the percentage depth dose can be expressed as:

$$P(d,A,f,E) = 100\ \frac{D(d)}{D(d_{max})}. \qquad (3.2)$$

The percentage depth dose is dependent on the depth d, the field area at the phantom surface A, the source-surface distance f, and the beam energy E. A graphical definition of these field parameters is shown in Fig. 3-1.

The percentage depth dose *(PDD)* increases with depth from the surface dose up to the maximum value attained at d_{max}; beyond this depth the dose decreases. Fig. 3-2 illustrates this behavior for the 10×10 cm^2 field of the cobalt-60 and 10 MV clinical photon beams. The surface dose of megavoltage photon beams occurs as a result of electron contamination, and photons scattered from the sourcehead, collimators, air, and phantom. For higher energy beams, the surface dose decreases, because the more energetic secondary electrons deposit their energy at a greater depth, and also because the amount of scattered radiation seen at the surface decreases.

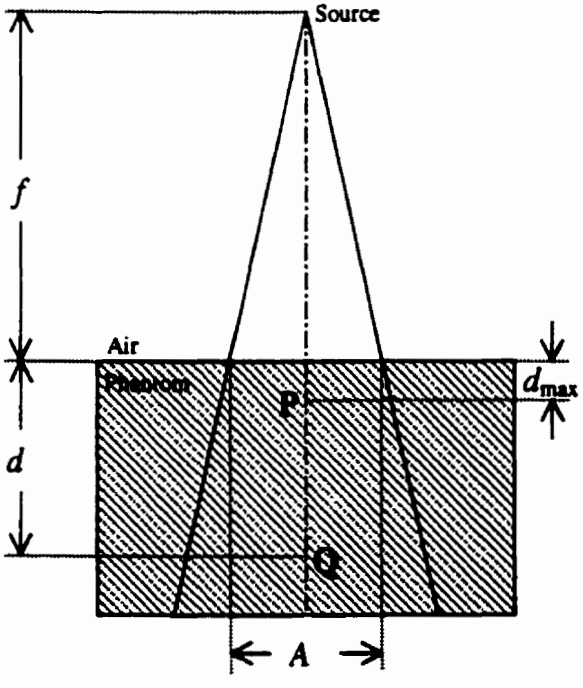

FIG. 3-1. Schematic representation of the parameters involved in the definition of the percentage depth dose.

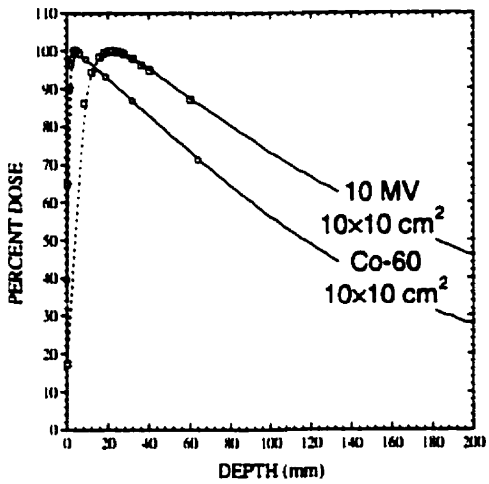

FIG. 3-2. Percentage depth doses as a function of depth for the 10x10 cm² field of the cobalt-60 beam (source-surface distance = 80 cm) and the 10 MV beam (source-surface distance = 100 cm). Measurements were performed using the diode (solid lines) and the parallel plate ion chamber (data points) in water-equivalent phantoms. A second degree polynomial was fit to the measurements in the build-up region (dashed lines).

The region between the surface dose and the maximum dose is known as the *dose build-up region.* Within this region a steep dose gradient is seen as the dose increases from the surface value to the maximum value. Dose build-up occurs as a result of the high energy secondary electrons depositing their energy a significant distance away from their site of origin. The secondary electron fluence, and thus the absorbed dose, increases with depth until a condition of transient electronic equilibrium occurs at approximately d_{max}. The thickness of material required to achieve the transient electronic equilibrium increases with beam energy. This is illustrated by the relative d_{max} values of the cobalt-60 and 10 MV photon beams shown in Fig. 3-2.

The depth at which the maximum dose is attained is also dependent on the field size. For a given photon beam energy a maximum value of d_{max} is found for fields of approximately 5×5 cm². Smaller fields show a migration of d_{max} toward the surface, with a similar yet more gradual decrease in d_{max} seen for fields larger

than 5×5 cm^2. It is generally believed that the cause of the shift for larger fields is due to electron contamination (Padikal and Deye (1978), Biggs and Ling (1979), Galbraith and Rawlinson (1985), and Leung *et al.*, (1976)). For small fields, however, it has been put forth that the shift is caused by scattered photons, originating within the phantom, progressively adding to the central axis dose as the field is increased, until the contribution saturates for fields of approximately 5×5 cm^2 (Sixel and Podgorsak 1994, and Zankowski 1996).

The percentage depth dose also exhibits field size dependence; for a constant depth, source-surface distance, and beam energy the *PDD* increases as the field area is increased. For very small fields, the dose delivered to a medium occurs almost entirely from primary radiation. As the field is enlarged, the contribution of scattered radiation to the dose increases, because more scattering material is present within the beam. The field size has less effect on the *PDD* for higher beam energies, because the scattering probability decreases and the radiation that is scattered is predominantly forward directed.

For a constant depth, field area, and energy, the percentage depth dose increases with an increase in the source-surface distance. This property can be illustrated by examining an alternative expression of the *PDD* which accounts for the primary beam component alone:

$$P(d, A, f, E) \propto \left(\frac{f + d_{max}}{f + d} \right)^2 e^{-\mu (d - d_{max})}, \qquad (3.3)$$

where the first term is simply the ratio of the reduction in beam intensity due to the inverse square law at depths d and d_{max}, and the exponential term is the ratio of the beam attenuation occurring at the same depths within a phantom possessing a linear attenuation coefficient μ, respective of the mean photon energy. Taking the limit of this equation as $f \rightarrow \infty$, the expression becomes:

$$\lim_{f \rightarrow \infty} P(d, A, f, E) \propto e^{-\mu (d - d_{max})}. \qquad (3.4)$$

Thus, the difference in the geometrical reduction of the beam intensity at depths d and d_{max} becomes diminished at greater isocenter distances, resulting in a relatively greater percentage depth dose. Although it is desirable to have as large a percentage depth dose as possible, the increase in the *PDD* with the source-surface distance comes at a cost of dose rate. Therapy units are, therefore, designed with an isocenter distance which provides a compromise between the dose rate and the *PDD*. For linacs this distance is commonly 100 cm, whereas for isotope units the cost and size of the source required to produce a reasonable dose rate generally limits the source-axis distance to 80 cm.

3.2.2 Results and discussion

Measurements of the percentage depth dose were performed by combining results obtained using two detectors: a diode and an end-window parallel-plate ionization chamber. The diode was used with the radiation field analyzer to quickly acquire relative depth dose measurements. It is difficult, however, to perform absolute depth measurements using this dosimetric system, because the surface tension surrounding the diode inhibits accurate alignment of the detector reference point with the water surface. There is also uncertainty as to how the silicone detector performs in regions of electronic imbalance, *i.e.*, the build-up region. Measurements made with the semiconductor detector are, therefore, considered valid only at depths greater than d_{max}.

The end-window parallel-plate ionization chamber was used to determine the depth doses in the build-up region. For measurements of the 10 MV beam, Solid Water™ sheets 2 mm and 3 mm thick were used. These sheets, however, were too thick to provide the depth resolution necessary to measure the shallower d_{max} of the cobalt-60 photon beam. For these measurements polystyrene sheets with thicknesses 0.56, 1.32, and 3.2 mm were used. At a given depth, the measurement was repeated three times at both chamber polarities with the average taken. The results were then plotted as a function of depth, with the average of six

estimations of d_{max} used for percentage depth dose calculations. These depth doses were also used to determine the absolute depths of the RFA measurements.

Depth doses for several radiosurgical fields of the cobalt-60 and 10 MV photon beams are plotted in Fig. 3-3. The differences between the beams are clearly visible. For a given field, the surface dose of the cobalt-60 radiosurgical beam

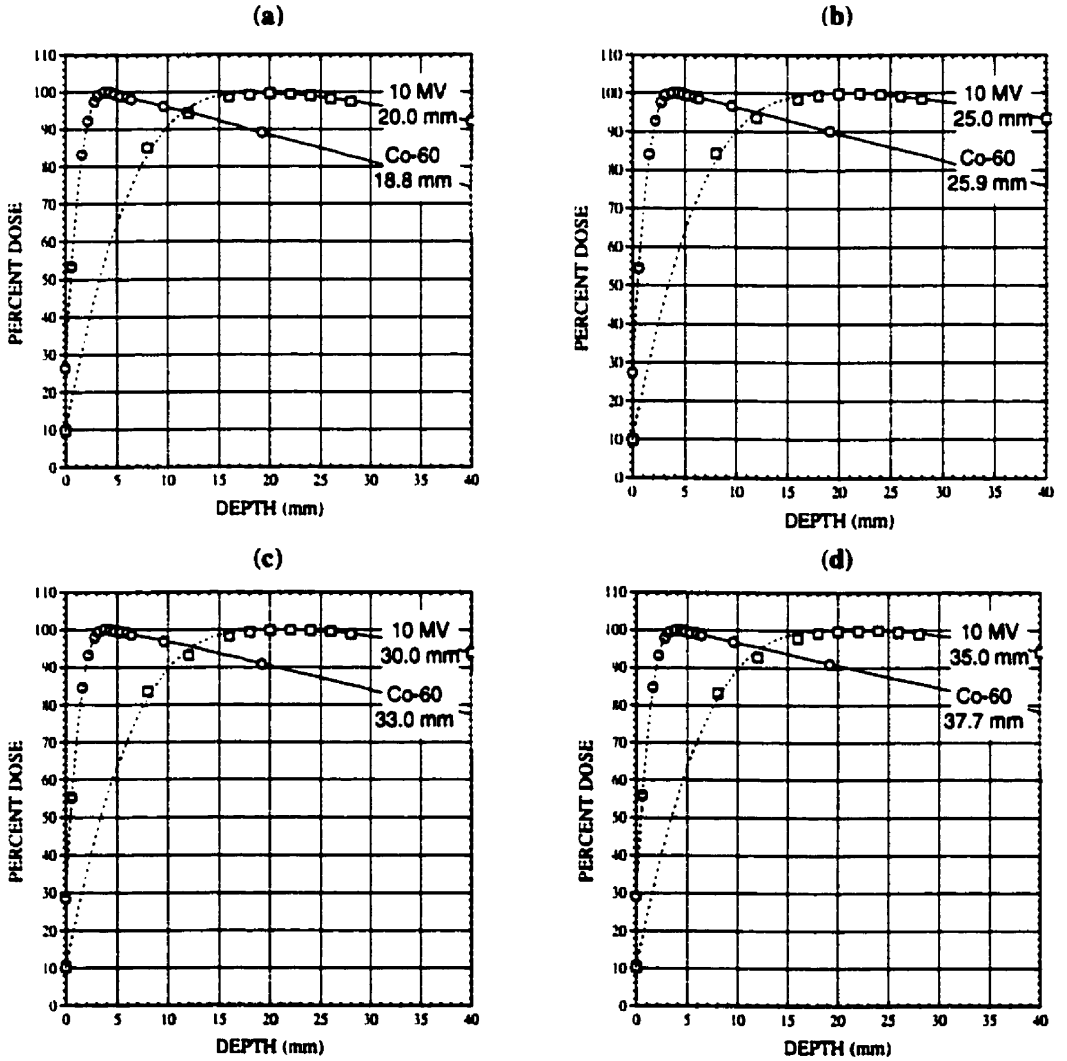

FIG. 3-3. Percentage depth doses in the region near the surface for (a) the 18.8 and 20.0 mm, (b) 25.9 and 25.0 mm, (c) 33.0 and 30.0 mm, and (d) 37.7 and 35.0 mm diameter radiosurgical fields of the cobalt-60 and 10 MV photon beams, respectively. Measurements were performed using the diode (solid lines), and the parallel plate ionization chamber (data points) in water-equivalent phantoms. A second degree polynomial was fit to the measurements in the build-up region (dashed lines).

is nearly three times greater than that of the 10 MV radiosurgical beam (~29% compared to ~10%, respectively). The transition from the build-up region to the exponential region is also sharper for the cobalt-60 beam, with a slightly shallower dose fall-off within the exponential region. Additionally, the depth of maximum dose is clearly greater for the 10 MV photon beams.

Fig. 3-4 shows the depths of dose maximum for several standard radiotherapeutic square fields and radiosurgical circular fields for the Theratron T-780 cobalt unit and the Clinac-18 linear accelerator. For the 10 MV radiotherapeutic square fields a maximum value of d_{max} equal to 22.6 mm was found for an approximately 5×5 cm^2 field. Square fields larger than 5×5 cm^2 exhibited a gradual decrease in d_{max}, down to 19.3 mm for the 20×20 cm^2 field. Similarly, the depth of maximum dose decreased for fields smaller than 5×5 cm^2 to a value of 21.9 mm for the 3×3 cm^2 field. These results are in agreement with the

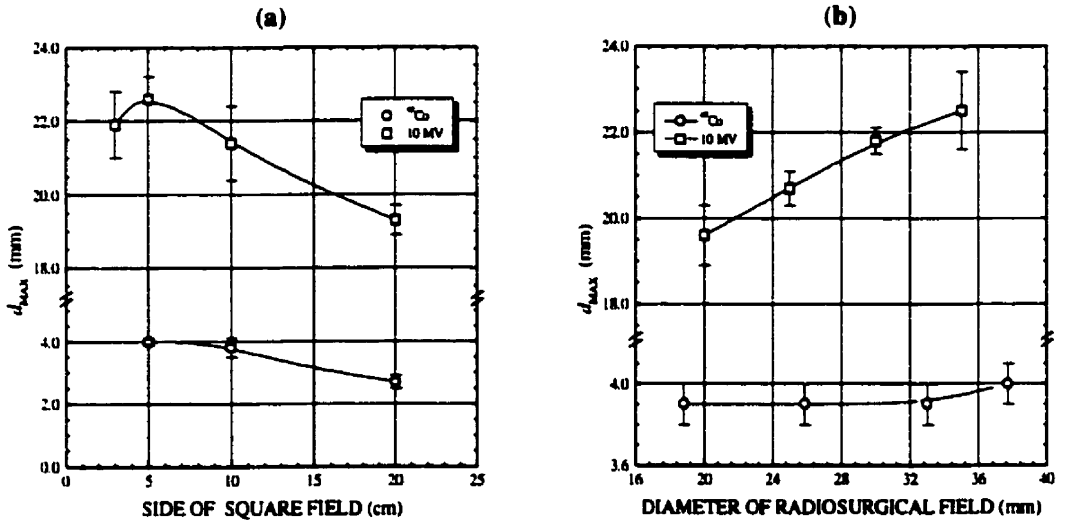

FIG. 3-4. Depth of dose maximum values (d_{max}) as a function of field size for (a) various standard radiotherapeutic square fields, and (b) various radiosurgical circular fields of the cobalt-60 and 10 MV photon beams.

values obtained by Sixel and Podgorsak (1994) and Zankowski (1996), as shown in Table 3-1. With regard to the radiosurgical fields (Fig. 3-4B) the depth of maximum dose increased from 19.6 mm to 22.5 mm, as the field was increased from 20.0 mm to 35.0 mm in diameter, respectively. These results are also in agreement with those obtained by Sixel and Podgorsak (1994).

The square fields of the cobalt-60 photon beam also exhibited depth of maximum dose shifts, as shown in Fig. 3-4A. It was determined that a maximum d_{max} value of 4.0 mm occurred for an approximately 5×5 cm^2 field. A significant shift was seen for larger fields, down to 2.7 mm for the 20×20 cm^2 field. These d_{max} values are similar to those reported by Leung *et al.*, (1976) for the Theratron T-780; 4.5 mm and 3.0 mm for the 5×5 cm^2 and 15×15 cm^2 fields, respectively. Regarding the radiosurgical fields, the 37.7 mm diameter field had a d_{max} value equal to that of the 5×5 cm^2 field. The smaller 33.0 mm, 25.9 mm, and 18.8 mm diameter fields exhibited a 0.1 mm shift in d_{max} toward the surface, as shown in Fig. 3-4B. Between these fields, however, a shift in d_{max} was not detected. Any change in the depth of maximum dose between these fields was, therefore, considered to be less than the 0.1 mm experimental uncertainty in the depth measurement.

	d_{max} (mm)		
Field Size	Measured	Sixel (1994,[1] 1990)	Zankowski (1996)
20×20 cm^2	19.3(0.4)	20.7	18.4
10×10 cm^2	21.4(1.0)	22.0	21.0
5×5 cm^2	22.6(0.6)	23.3	22.0
3×3 cm^2	21.9(0.9)	21.4	22.6
35.0 mm*	22.5(0.9)	24.0[1]	-
30.0 mm*	21.8(0.3)	23.4[1]	-
25.0 mm*	20.7(0.4)	22.7[1]	-
20.0 mm*	19.6(0.7)	20.9[1]	-

* *diameter of circular radiosurgical field*

TABLE 3-1. Depth of maximum dose (d_{max}) values for various radiotherapeutic and radiosurgical fields of the Clinac-18 10 MV. Standard deviations are shown in parentheses.

The percentage depth doses for several fields of the cobalt-60 and 10 MV photon beams used for radiosurgical treatment planning appear in Fig. 3-5. Depth doses were obtained to a depth of only 20 cm, since this distance is already larger than the maximum surface separation of the head and radiosurgery is only used for treatment of intracranial lesions.

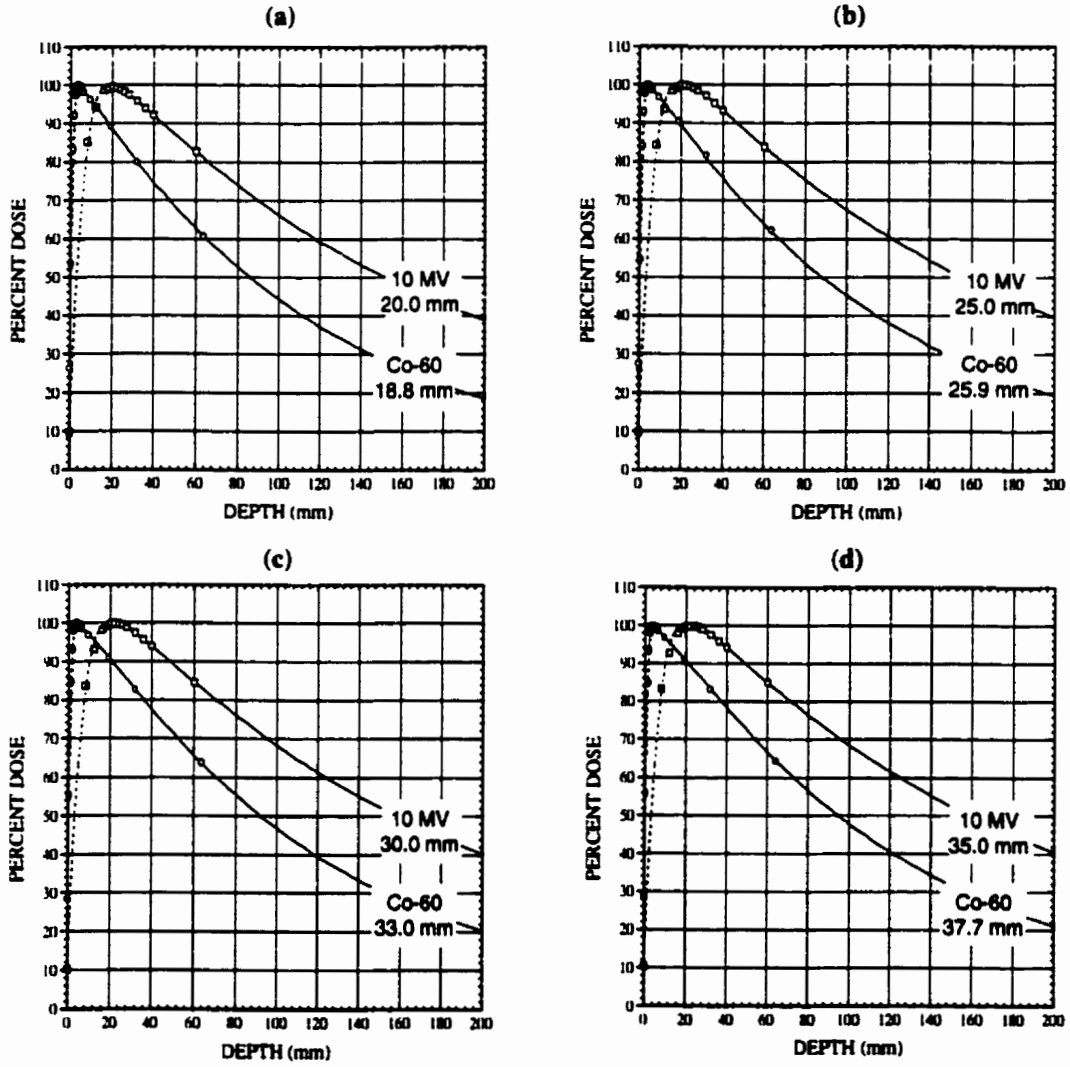

FIG. 3-5. Percentage depth doses of the (a) 18.8 and 20.0 mm, (b) 25.9 and 25.0 mm, (c) 33.0 and 30.0 mm, and (d) 37.7 and 35.0 mm diameter radiosurgical fields for the cobalt-60 and 10 MV photon beams, respectively. Measurements were performed using the diode (solid lines), and the parallel plate ion chamber (data points) in water-equivalent phantoms. A second degree polynomial was fit to the measurements in the build-up region (dashed lines).

With the determination of the percentage depth doses, the radiosurgical fields have been characterized along the central axis of the beam. The fields, however, must also be characterized in a plane perpendicular to the beam before volumetric dose distributions can be calculated. The off-axis ratio, discussed below, is used for this purpose.

3.3 OFF-AXIS RATIO

3.3.1 Definition

The *off-axis ratio* is used to characterize the dose delivered to points off-axis with respect to the central axis dose value. Profiles can be measured using either a constant source-surface distance *(SSD)* or constant source-axis distance *(SAD)*. For a constant *SSD*, the profiles acquired at a given depth *d* are a distance of *SSD* plus depth *d* from the source. Profiles acquired at different depths will, therefore, have different widths as a result of the beam divergence. For *SAD* profiles the source to profile distance remains constant regardless of profile depth and for radiosurgical beams all profiles appear nearly identical, with only slight differences occurring as a result of the increased amount of phantom scattering seen at greater depths. Most radiosurgical treatment planning systems, including the McGill Planning System, calculate 3-D dose distributions from profiles taken at a single depth (usually d_{max}) and correct for beam divergence at the depth of interest.

Ideally, one would like the beam intensity to remain constant over the field area and drop immediately to zero outside of it. In practice, however, the intensity varies over the field and some radiation is delivered to points lying outside the geometrical field limits, as shown in Fig. 3-6. The dose fall-off near the beam edges is quantified by the beam *penumbra*, defined as the separation between two dose levels (e.g., 80%-20% or 90%-10%).

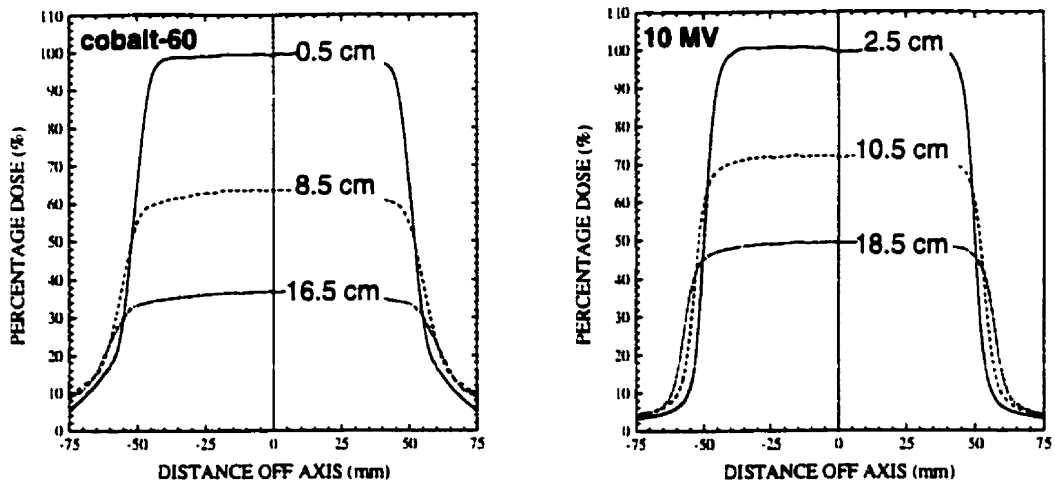

FIG. 3-6. SSD beam profiles for the 10×10 cm² field of the cobalt-60 and 10 MV photon beams at several depths in water. Measurements were performed using a diode detector within water.

Several physical properties associated with the radiation beam contribute to the overall beam penumbra. As a result of the exponential nature of photon attenuation, some radiation is always transmitted through the collimating system, producing what is known as the *transmission penumbra*. A lack of lateral electronic equilibrium near the field edges also contributes to the penumbra. Additionally, scattered radiation originating from the collimating system, unit head, and phantom further degrades the dose fall-off. While the penumbra arising from electronic imbalance cannot be significantly reduced, in radiosurgery the collimators of a therapy unit are commonly designed to match the beam divergence in an attempt to minimize the transmission penumbra, and the contribution of scattered radiation to the penumbra is reduced using tertiary beam collimation.

A *geometric penumbra* is also associated with a radiation beam. This term refers to the penumbra caused by the finite source dimensions. A diagram useful for mathematically defining the penumbra, caused by a source of diameter *s*, appears in Fig. 3-7. Points beyond the edge of the geometrically defined field are

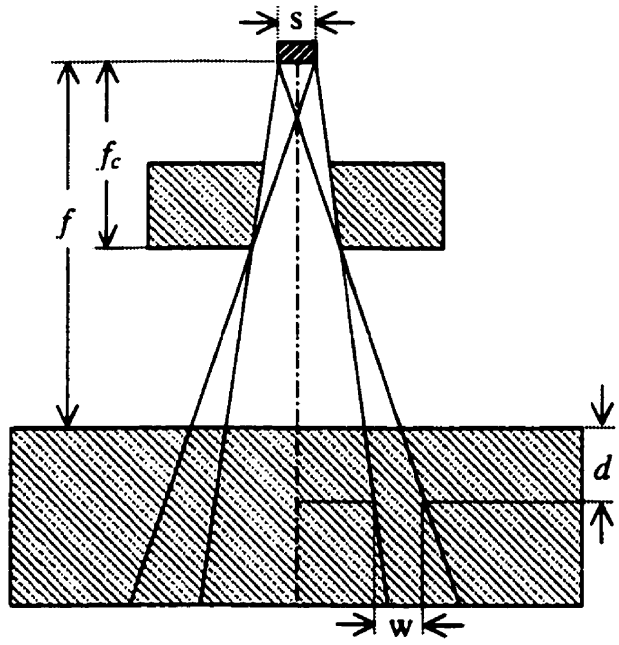

FIG. 3-7. Schematic representation of the parameters involved in the definition of the geometric beam penumbra.

exposed to only a fraction of the source. As a result, the dose fall-off is degraded. The width w of this penumbra at any given depth d can be determined using similar triangles:

$$\frac{w}{s} = \frac{f - f_c + d}{f_c} \quad \Rightarrow \quad w = \frac{s \cdot (f - f_c + d)}{f_c}, \tag{3.5}$$

where f is equal to source-surface distance, and f_c is the source-collimator distance. It is evident from this equation that the geometrical penumbra can be reduced by increasing the source to collimator distance. This is accomplished in radiosurgery by using tertiary beam collimation. It is also notable that the penumbra is directly proportional to the source size.

Measurements of radiosurgical field penumbras and profile characteristics can be significantly influenced by detector dimensions (Dawson *et al.*, 1986; Rice *et al.*, 1987). A geometrical penumbra occurs when the detector's sensitive volume is partially hidden from the source, by the collimators, near the edges of the field. Also, since profile measurements are made over a volume rather than a point, the beam's intensity profile is effectively convolved with the detector's response profile. To minimize these detector effects, the AAPM TG #42 Report (1995) recommends that the detector diameter be 2 mm or less for radiosurgical field profile measurements. The effective diameters of the semiconductor and film-densitometry detectors used for profile measurements in our work are 2.5 mm and 1.3 mm, respectively. Although the diameter of our semiconductor detector is slightly larger than recommended, it is shown in the following section that the profiles measured using this detector are essentially identical to those measured by film densitometry.

3.3.2 Results and discussion

The off-axis ratios for several radiosurgical fields of the cobalt-60 and 10 MV photon beams are shown in Fig. 3-8 and Fig. 3-9, respectively. These profiles were acquired using an *SAD* setup. Other than an increase in the magnitude of the profile 'tails' when the depth was increased, the profiles of a given field appeared identical irrespective of the depth of measurement. Compared to the cobalt-60 fields, the increase in the magnitude of the tails with depth was less pronounced for the 10 MV photon beam, because this higher energy beam exhibits less lateral scattering.

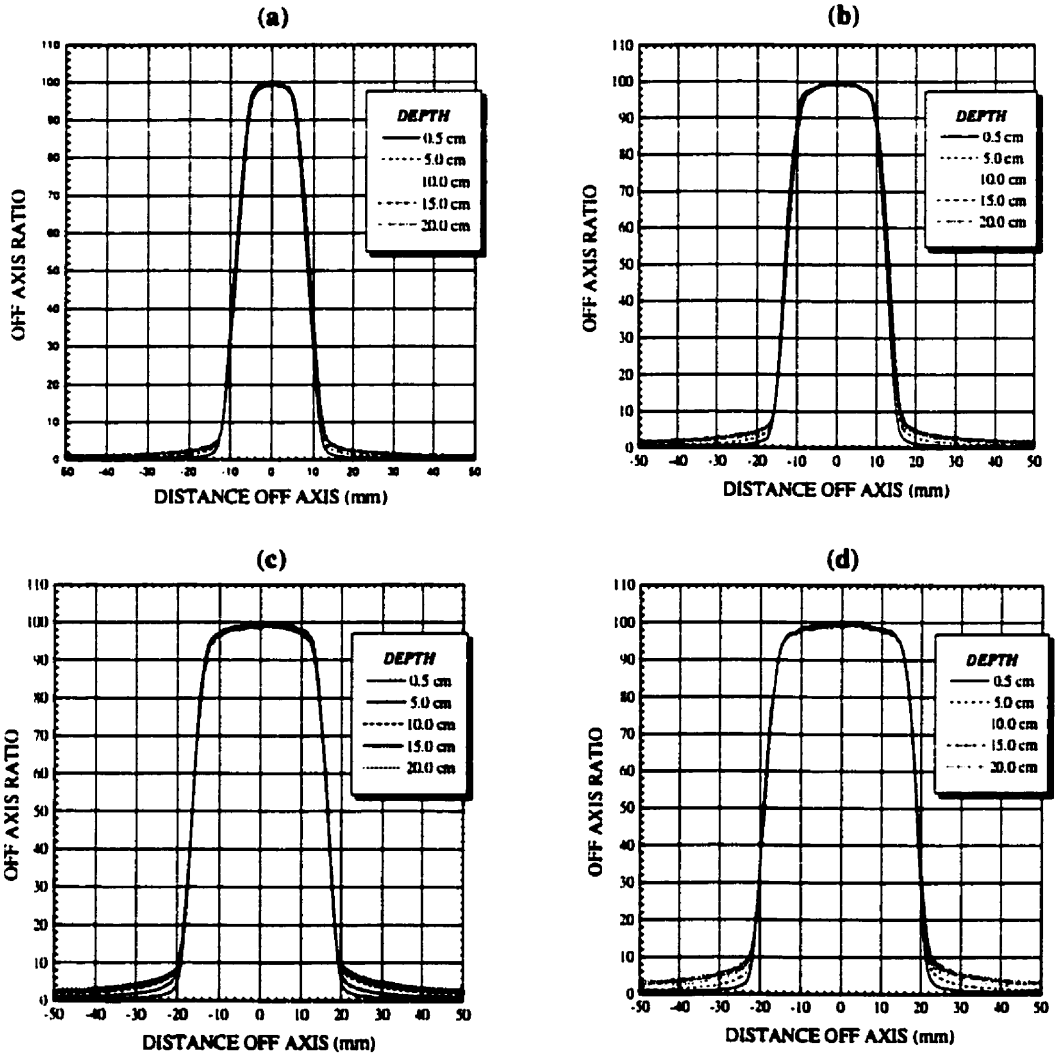

FIG. 3-8. SAD Beam profiles of (a) the 18.8 mm, (b) 25.9 mm, (c) 33.0 mm, and (d) 37.7 mm diameter radiosurgical fields of the cobalt-60 photon beam at various depths. Measurements were performed using a semiconductor detector within water.

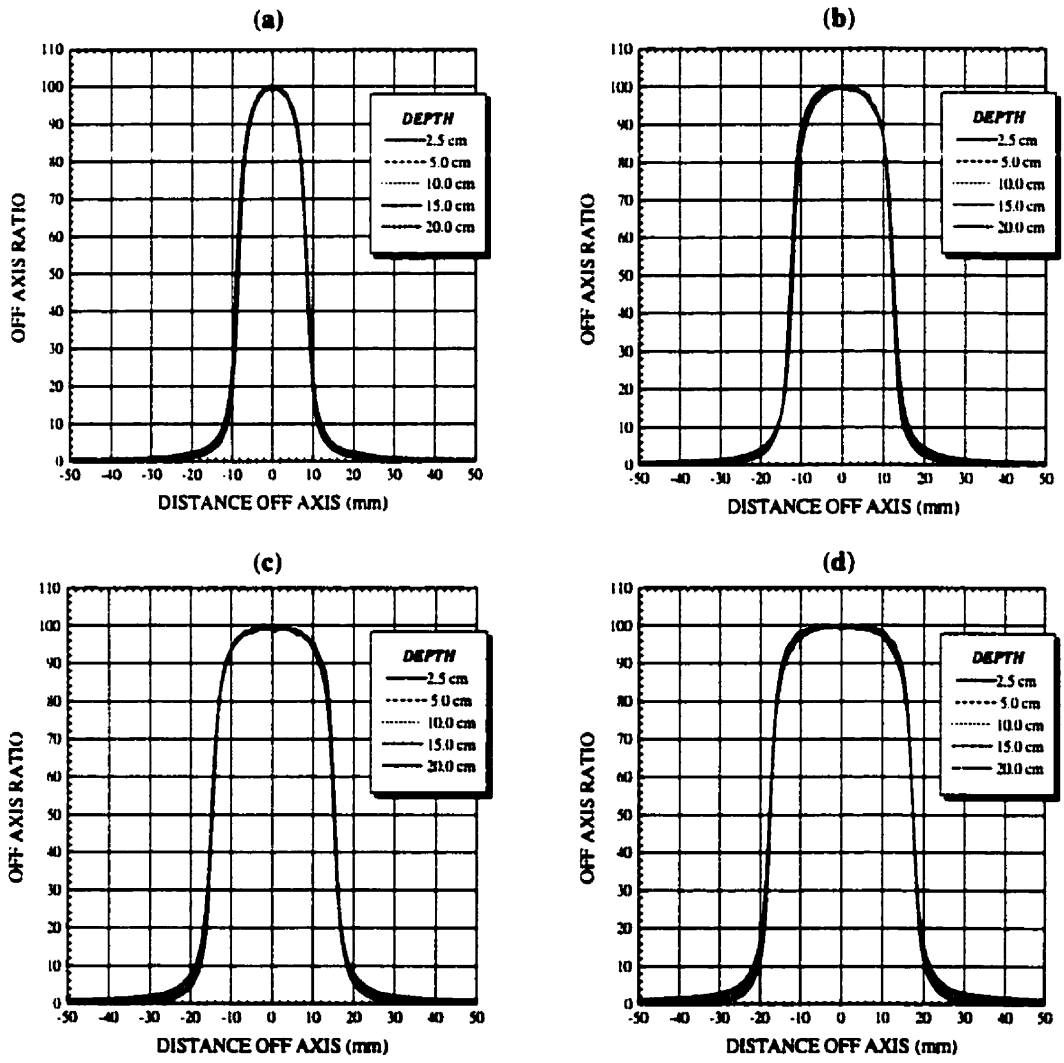

FIG. 3-9. SAD Beam profiles of (a) the 17.5 mm, (b) 25.0 mm, (c) 30.0 mm, and (d) 35.0 mm diameter radiosurgical fields of the 10 MV photon beam at various depths. Measurements were performed using a semiconductor detector within water.

To illustrate the differences between *SAD* and *SSD* beam profiles, the cobalt-60 radiosurgical beam profiles, shown in Fig. 3-10, were also acquired using a constant source-surface distance. The beam divergence is clearly reflected by the increase in the profile width at larger phantom depths. It is also evident that the geometrical penumbra width increases with depth for the *SSD* setup.

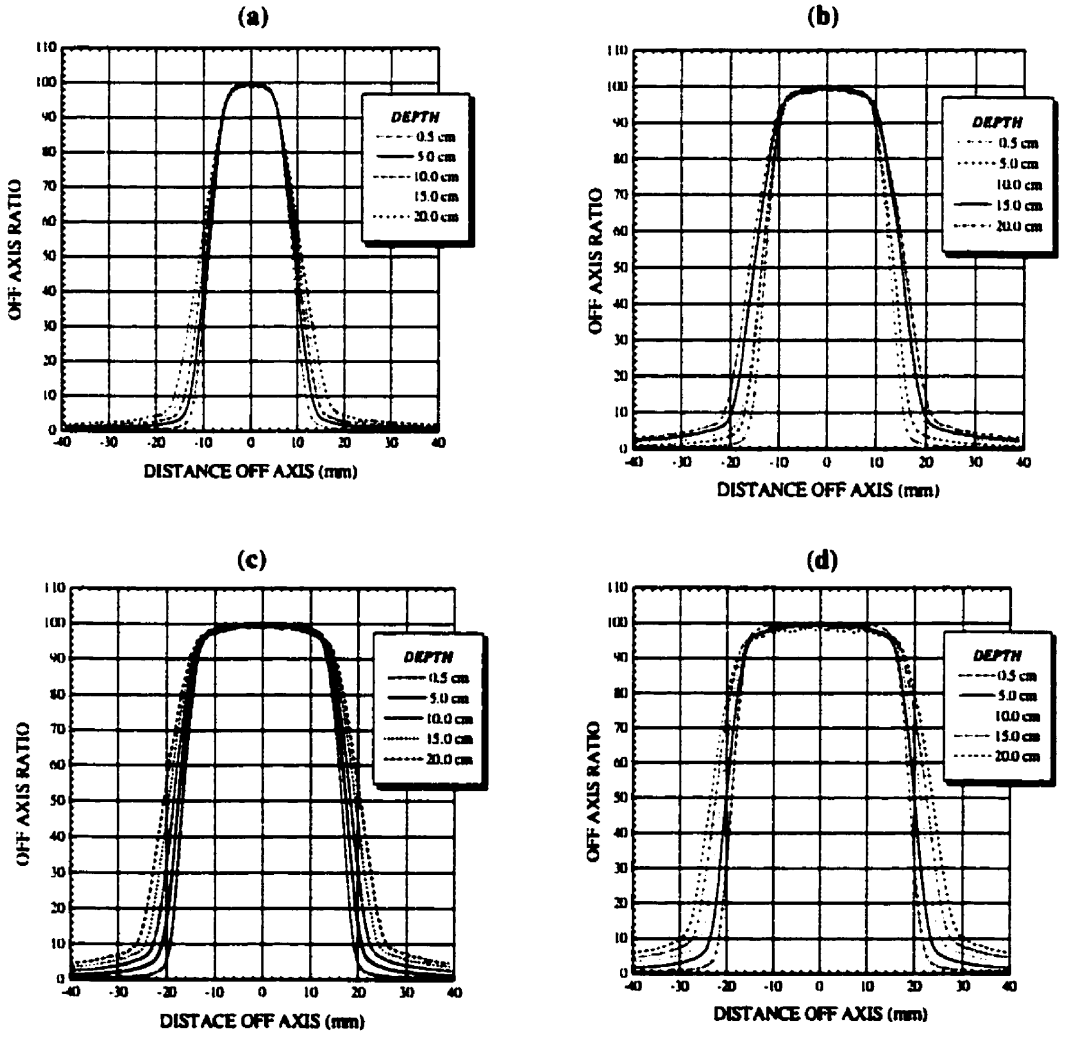

FIG. 3-10. SSD Beam profiles of (a) the 18.8 mm, (b) 25.9 mm, (c) 33.0 mm, and (d) 37.7 mm diameter radiosurgical fields of the cobalt-60 photon beam at various depths. Measurements were performed using a semiconductor detector within water.

Profile measurements, taken with film at a depth of 5 cm in Solid Water™, were used to verify the radiosurgical field profiles measured with the diode in water. On average, the profile widths, determined using film and diode, agreed to within 1 mm, as shown in Fig. 3-11. Larger discrepancies were apparent below the 15% dose level, likely resulting from low-energy scattered photons engaging in photoelectric interactions with the silver of the film. Profile disagreements at these low dose levels, however, are not clinically significant. The film and diode profile measurements can, therefore, be assumed to agree.

A graphical comparison of the dose fall-offs, measured using the semiconductor detector, for several radiosurgical fields of the cobalt-60 and 10 MV photon beams are shown in Fig. 3-12. It is evident that the slope of the cobalt-60 profiles appears almost constant between the 90% and 10% dose levels, regardless of field diameter. The 10 MV photon beam profiles have a more gaussian appearance, with a steeper dose fall-off seen between the 90%-20% dose levels than the cobalt-60 profiles of similar field size. Below the 10% dose level, however, the slopes of the 10 MV and cobalt-60 profiles are nearly identical.

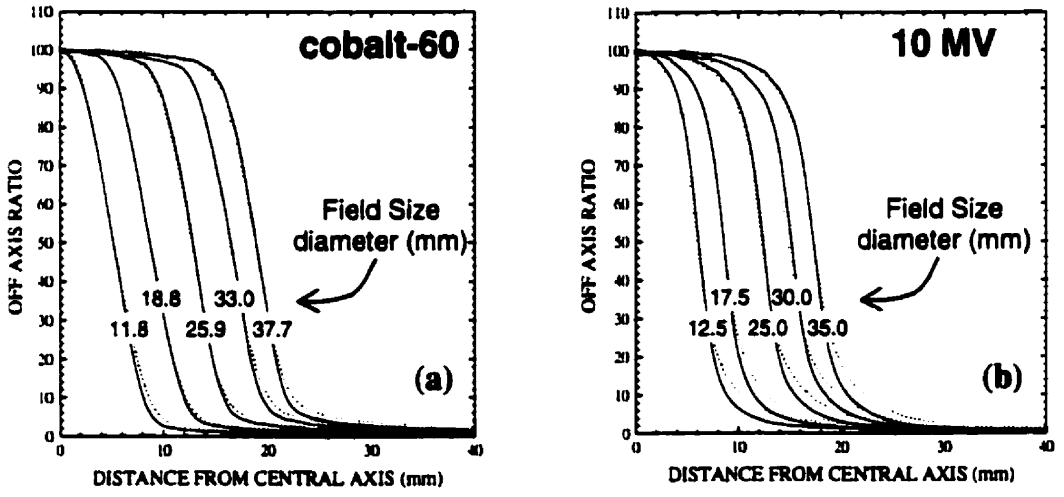

FIG. 3-11. SAD Beam profiles of the cobalt-60 (a) and the 10 MV (b) photon beams for various radiosurgical fields. Profiles were taken at a depth of 5 cm in water-equivalent material. Measurements carried out with a semiconductor detector are depicted by solid lines and with film by dashed lines.

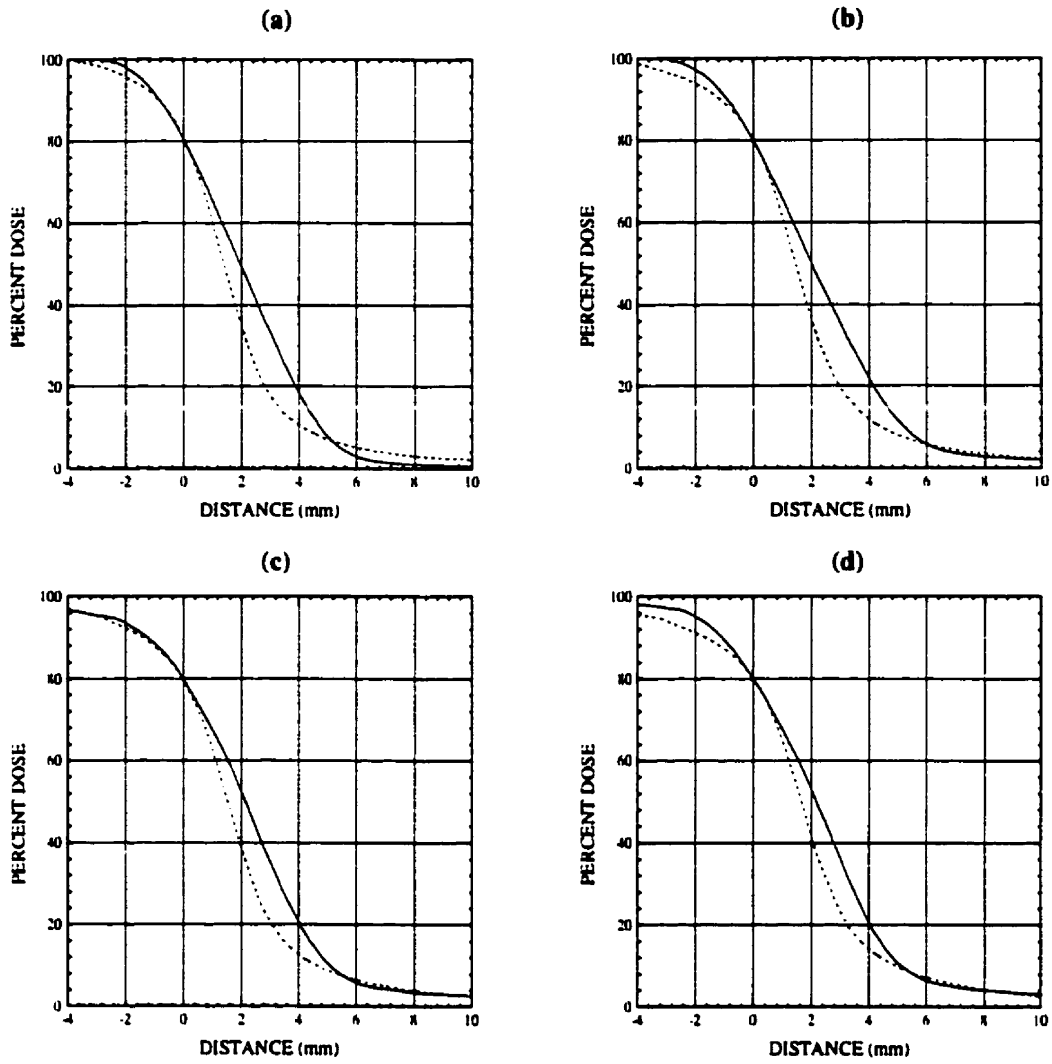

FIG. 3-12. A comparison of the (a) 11.8 mm and 12.5 mm, (b) 18.8 mm and 12.5 mm, (c) 25.9 mm and 25.0 mm and (d) 33.0 mm and 35.0 mm diameter, cobalt-60 (solid) and 10 MV (dashed) SAD radiosurgical field profiles, respectively. Measurements were carried out with a semiconductor detector at a depth of 5 cm within water. Distances are shown relative to the 80% dose level to facilitate comparison of the 80%-20% beam penumbras. The data are normalized to 100 on the central axis.

A quantitative analysis of the 80%-20% radiosurgical field penumbra values was performed, and the results are given in Table 3-2. The values were calculated from *SAD* profiles, measured using both the semiconductor and radiographic film detectors, at a depth of 5 cm within a tissue equivalent phantom.

The mean penumbra of the cobalt-60 profiles was 4.2 ± 0.1 mm, 0.7 mm larger than the 3.5 ± 0.2 mm mean penumbra value of the 10 MV profiles.

The difference in the mean penumbra values between the 10 MV and cobalt-60 photon beams is not as large as one might expect, considering that the 15 mm diameter source of the Theratron T-780 is significantly larger than the approximately 1-3 mm diameter focal spot of the Clinac-18 photon beam, and also considering that while the taper of the collimators matches the 10 MV beam divergence, the taper does not match the divergence of the cobalt-60 beams. This can be partially explained if one compares the radiosurgery treatment setups. The ratio of the collimator-isocenter distance to the source-collimator distance for the Clinac-18 is approximately 27% greater than that of the Theratron T-780. By examining Eq. (4-5) it is evident that the geometric penumbra is proportional to this ratio for *SAD* setups. Consequently, the geometric penumbra of the Theratron T-780 is relatively reduced. Regarding the divergence of the radiosurgical collimators, it has been reported that the taper has little effect on the penumbra for radiosurgical fields between the energies of 4 and 24 MV (Serago 1992).

cobalt-60				10 MV			
Field diameter	Diode (mm)	Film (mm)	Mean (mm)	Field diameter	Diode (mm)	Film (mm)	Mean (mm)
37.7 mm	4.0	4.3	4.2	35.0 mm	3.3	4.2	3.8
33.0 mm	4.1	4.3	4.2	30.0 mm	3.3	3.9	3.6
25.9 mm	4.0	4.1	4.1	25.0 mm	3.2	3.7	3.5
18.8 mm	4.2	4.2	4.2	17.5 mm	3.0	3.6	3.3
11.8 mm	4.1	4.2	4.2	12.5 mm	2.8	3.5	3.2
Mean	4.1	4.2	4.2	Mean	3.1	3.8	3.5

TABLE 3-2. The 80% to 20% penumbras for several circular cobalt-60 and 10 MV radiosurgical fields. Data were obtained from SAD profiles, measured at a depth of 5 cm in tissue equivalent material, using both a semiconductor detector(diode) and radiographic film.

The clinical significance of the difference between the radiosurgical field penumbra values of the Theratron T-780 and Clinac-18 is difficult to determine. It is notable, however, that the penumbra values for most fields of both radiation beams are greater than 3 mm, the value recommended by the AAPM TG #42 Report (1995). This recommendation, however, is based on what is generally achievable and has a limited clinical basis. Of more importance than the stationary beam penumbra, is the dose fall-off of the volumetric dose distribution produced by a radiosurgical technique. This topic is addressed in the following chapter.

3.4 RELATIVE DOSE FACTOR

3.4.1 Definition

For dose calculations it is often useful to consider a radiation beam in terms of its primary and scattered dose components. Primary dose refers to the dose deposited by photons originating from the focal spot or source of a unit. The dose delivered by the primary beam component to any given point is, therefore, independent of the field area as opposed to the dose that results from radiation scattered by the collimator and phantom. The contribution of scattered radiation to the dose or dose rate is quantified by the *relative dose factor (RDF)*, sometimes called the *total scatter factor*.

The relative dose factor is defined as the ratio of the dose delivered to a point located at depth d_{max} within a phantom placed at nominal *SSD* by a given field *A* over the dose delivered to the same point in phantom by a reference field A_{ref} usually chosen as a 10×10 cm^2 field. Mathematically, the *RDF* can be expressed as:

$$RDF(A) = \frac{D(A)}{D(A_{ref})}. \qquad (3.6)$$

The measured relative dose factors of the cobalt-60 and 10 MV photon beams for various radiotherapeutic fields are shown in Fig. 3-13. The *RDF* increases with field size, with the increase becoming less pronounced at higher energies. Insight can be gained into this behavior by examining the *RDFs* two components, the *scatter factor (SF)* and the *collimator factor (CF)*:

$$RDF(A) = SF(A)CF(A). \tag{3.7}$$

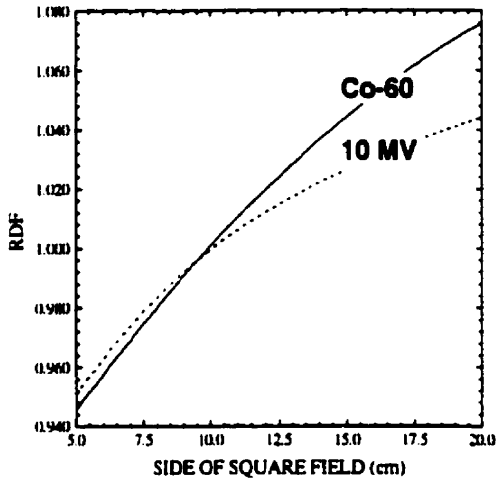

FIG. 3-13. Relative dose factors for the cobalt-60 (solid line) and 10 MV (dashed line) radiotherapy beams with nominal field sizes between 5×5 cm² and 20×20 cm².

The *collimator factor*, also called the *head scatter factor* or *relative exposure factor (REF)*, describes the contribution of scattered radiation, originating from the collimators and unit head, to the total central axis dose of a given field, relative to that of the 10×10 cm² field. The collimator factor can be defined as:

$$CF(A) = \frac{D'(A)}{D'(10)}, \tag{3.8}$$

where D' denotes the dose delivered to a small mass of phantom material, located in air, at a distance of *SSD* plus d_{max} from the source. The collimator factor increases with field size, as a greater scattering surface area is present within the beam. While the collimator factor varies significantly over the field sizes used in standard radiotherapy, it remains nearly constant for radiosurgical fields (Sixel 1990; Rice *et al.*, 1987). Any variation in the *RDF* with field size is, therefore, associated with the behavior of the scatter factor.

Before discussing the scatter factor it is useful to define another quantity, the *peak scatter factor (PSF)*. The *PSF* represents the ratio of the dose delivered to a point located at d_{max} within a phantom placed at nominal *SSD*, to that delivered to a small mass placed at the same position in air, mathematically:

$$PSF(A) = \frac{D(A)}{D'(A)}. \qquad (3.9)$$

The peak scatter factor is commonly used to express the *scatter factor*; a quantity which accounts for the contribution of radiation scattered within the phantom to the total central axis dose at d_{max}:

$$SF(A) = \frac{PSF(A)}{PSF(10)}. \qquad (3.10)$$

The scatter factor increases with field size, with the increase being less significant at higher energies for the reasons mentioned in Section 4.2.1. Consequently, the relative dose factor exhibits a similar field and energy dependence.

3.4.2 Results and discussion

Relative dose factors were measured using an end-window parallel-plate ionization chamber and radiographic film. With regard to the ionization chamber measurements, the *RDFs* were calculated from the depth dose measurements by simply renormalizing the d_{max} charge reading of each field to that obtained for the 10×10 cm^2 field. These values were then verified using film densitometry. Both dosimeters have effective diameters smaller than 3 mm and, therefore, meet the AAPM TG #42 Report (1995) recommendations concerning the measurement of the *RDF* for radiosurgical fields.

The relative dose factors for several radiosurgical fields of the cobalt-60 and 10 MV photon beams are given in Table 3-3. On average, the ion chamber and film measurements agreed to within ±1.6% for the cobalt-60 radiosurgical fields, and to within ±1.0% for the 10 MV fields. A plot of the relative dose factors as a function of field size, given in Fig. 3-14, reveals that this beam parameter roughly exhibits a second degree polynomial dependence on field diameter for both the cobalt-60 and the 10 MV photon beams.

cobalt-60				10 MV			
Field diameter	Ion C. (mm)	Film (mm)	Mean (mm)	Field diameter	Ion C. (mm)	Film (mm)	Mean (mm)
20×20 cm^2	1.067	1.091	1.079	*20×20 cm^2*	1.057	1.043	1.050
10×10 cm^2	1.000	1.000	1.000	*10×10 cm^2*	1.000	1.000	1.000
5×5 cm^2	0.950	0.948	0.949	*5×5 cm^2*	0.947	0.945	0.946
*37.7 mm**	0.938	0.927	0.932	*35.0 mm**	0.934	0.919	0.927
*33.0 mm**	0.934	0.915	0.925	*30.0 mm**	0.924	0.916	0.920
*25.9 mm**	0.927	0.910	0.919	*25.0 mm**	0.909	0.882	0.895
*18.8 mm**	0.905	0.897	0.901	*20.0 mm**	0.873	0.857	0.865

* *diameter of circular radiosurgical field*

TABLE 3-3. Relative dose factors for several radiotherapy and radiosurgical cobalt-60 and 10 MV beams. Measurements were performed using both an end-window parallel-plate ionization chamber and radiographic film within water-equivalent phantoms.

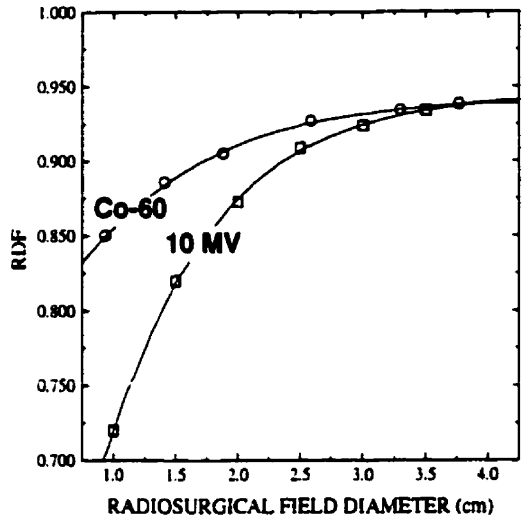

FIG. 3-14. Relative dose factors for the cobalt-60 and 10 MV radiosurgical beams with nominal diameters between 1 cm and 4 cm. The data points represent the average value of the RDFs measured with a semiconductor detector and an end-window parallel plate ionization chamber. The data are normalized to 1.0 for standard 10×10 cm² fields.

3.5 SUMMARY

In this chapter the physical beam parameters relevant to radiosurgical treatment plan calculations were discussed. The percentage depth doses, off-axis ratios, and relative dose factors for several radiosurgical fields of the Theratron T-780 cobalt-60 photon beam and the Clinac-18 10 MV photon beam were presented and compared. The measurement techniques and results were shown to agree reasonably with the guidelines suggested by the AAPM TG #42 Report (1995) on radiosurgery. Similar to the differences between the *PDDs* of the standard cobalt-60 and 10 MV beams, the cobalt-60 radiosurgical beams exhibit a greater surface dose, have a shallower depth of dose maximum (d_{max}), and are less penetrating in comparison with the 10 MV radiosurgical beams of similar field diameter. While these beam characteristics were to be expected, the relatively small difference between the 80%-20% penumbras of the two beams, with cobalt radiosurgical beam penumbras on average only 0.7 mm larger than those of the linac beam, was not expected considering the relatively large source size of the Theratron T-780. The clinical significance of these stationary field differences is examined in the following chapter.

3.6 REFERENCES

American Association of Physicist in Medicine (AAPM) Report #54. *Stereotactic radiosurgery*. Report of AAPM Task Group #42, American Institute of Physics, New York (1995).

Biggs P.J. and Ling C.C. *Electrons as the observed d_{max} shift with field size in high energy photon beams*. Med. Phys. **6**: 291-299 (1979).

Dawson D.J., Schroeder N.J., and Hoya J.D. *Penumbral measurements in water for high energy x-rays*, Med. Phys. **13**: 101 (1986).

Galbraith D.M. and Rawlinson J.A. *Direct measurement of electron contamination in cobalt beams using a charge detector*. Med. Phys. **12**: 273-280 (1985).

Leung P.M.K., Sontag M.R., Harrideo M., Chenery S. *Dose measurements in the build-up region for cobalt-60 therapy units*. Med. Phys. **3**: 169-172 (1976).

Padikal T.N. and Deye J.A. *Electron contamination of a high energy x-ray beam*. Phys. Med. Biol. **23**: 1086-1091 (1978).

Pike B., Podgorsak E.B., Peters T.M., and Pla C. *Dose distributions in dynamic stereotactic radiosurgery*. Med. Phys. **14**: 780-791 (1987).

Pla. C. *A Macintosh based treatment planning system for brachytherapy and stereotactic radiosurgery*. In: Hounsell A.R., Wilkinson J.M., and Williams P.C., eds. Proc. 11th Int. Conf. on the use of computers in radiation therapy. Manchester, United Kingdom: 138-139 (1994).

Rice R.K., Hansen J.L., and Svensson G.K. *Measurements of dose distributions in small beams of 6 MV x-rays*, Phys. Med. Biol. **32**: 1087 (1987).

Serago C.F., Houdek P.V., Hartmann G.H., Saini D.S., Serago M.E., and Kaydee A. *Tissue maximum ratios (and other parameters) of small circular 4, 6, 10, 15, and 24 MV x-ray beams for radiosurgery*. Phys. Med. Biol. **37**: 1943-1956 (1992).

Sixel K.E. *Physical parameters of narrow photon beams in radiosurgery.* M.Sc. Thesis, McGill University, Montreal (1990).

Sixel K.E. and Podgorsak E.B. *Build-up region and depth of dose maximum of megavoltage x-ray beams.* Med. Phys. **21**: 411-416 (1994).

Zankowski C. *Monte Carlo analysis of the 10 MV x-ray beam from a CLINAC-18 linear accelerator.* M.Sc. Thesis, McGill University, Montreal (1996).

Chapter 4

Comparison of Radiosurgical Treatment Plans

4.1 INTRODUCTION

The goal of radiosurgery is to deliver a highly localized dose of radiation uniformly throughout the target volume, while minimizing the dose to the surrounding tissues. To achieve these ends, current treatment planning systems can quickly calculate cumulative dose volume histograms *(CDVH)*; the total volume encompassed by a given isodose surface as a function of dose. By comparing the *CDVHs* of the target volume, the surrounding tissue, and those of the sensitive structures of the brain, an optimized treatment plan can be developed to suit a particular case. Although *CDVHs* are now the tool of choice for optimizing radiosurgery treatment plans, at this time there is no definite biological model linking the *CDVHs* to the tissue response, normal or otherwise.

The RTOG Protocol #93-05 (1994) has been designed and implemented to determine this relationship. In this chapter the treatment planning quality assurance guidelines and figures of merit presented in the RTOG Protocol #93-05

(1994) are used to compare several treatment plans formulated using the cobalt-60 beam of the Theratron T-780 to similar plans developed using the 10 MV photon beam of the Clinac-18 linear accelerator; the beam used clinically for radiosurgery at the Montreal General Hospital.

4.2 TREATMENT PLAN COMPARISONS

4.2.1 Basis of Comparison: The RTOG Protocol #93-05

Although the use of dose volume histograms to characterize radiosurgical dose distributions produced by various linac-based arc techniques has been well established (Phillips *et al.*, (1989), Schell *et al.*, (1991), and Serago *et al.*, (1992)), at this time the tissue response as a function of dose and volume remains uncertain. The RTOG Protocol #93-05 (1994) has been designed and implemented to address this issue. Eighteen facilities, including McGill University, are participating in this study which began in February 1994 and is slated to close in October 2001. Specifically, the object of the study is to determine the radiotoxicity of single fractionation radiosurgery as a function of dose and irradiation volume. Although our work is not directly concerned with the biological effects of radiosurgery, the treatment planning quality assurance conventions outlined in the protocol provide a useful means for comparing radiosurgery treatment plans, and were therefore used in our work.

For accurate target volume and isocenter determination the RTOG Protocol #93-05 (1994) states that the target volume must be determined from either serial *CT* or *MR* images, with the slice thicknesses not exceeding 4 mm. The protocol also states that the maximum isodose surface that fully encompassed the target volume is to be taken as the prescription isodose level, and the isodose distributions are to be renormalized to read 100 at this dose level. For the

prescription isodose level to be considered per protocol, the target volume must be completely covered by an isodose level equal to or larger than 90% of the prescription isodose. A minor deviation from protocol occurs, if this condition is not met but an isodose level between to 80% and 90% of the prescription isodose level encompasses the target volume. If a lesser isodose level is required to fully encompass the target volume, the prescription is considered a major, but acceptable, deviation from protocol. This prescription classification system is summarized in Table 4-1.

Maximum Isodose Level Covering Target	Classification
≥90 % of Prescription Isodose Level	Per Protocol
≥80 %-90 % of Prescription Isodose Level	Minor Deviation
≤80 % of Prescription Isodose Level	Major Acceptable Deviation

TABLE 4-1. Prescription isodose (PI) classification system outlined in the RTOG Protocol #93-05 (1994)

To describe the dose homogeneity within the target volume, the protocol proposes the use of the maximum target dose to prescription dose ratio *(MDPD)* as a figure of merit. An *MDPD* less than or equal to 2.0 is considered to be per protocol, whereas an *MDPD* between 2.0 and 2.5 is considered a minor acceptable deviation from protocol, and an *MDPD* greater than 2.5 is considered a major acceptable deviation. These conventions are listed in Table 4-2.

Range	Classification
MDPD ≤ 2.0	Per Protocol
2.0 < MDPD ≤ 2.5	Minor Acceptable Deviation
MDPD > 2.5	Major Acceptable Deviation

TABLE 4-2. Maximum target dose to prescription dose ratio (MDPD) classification system outlined in the RTOG Protocol #93-05 (1994).

The prescription isodose volume to target volume ratio *(PITV)* is used to describe the conformity of the prescription isodose volume to the target volume. A *PITV* ratio between 1.0 and 2.0 is classified as per protocol. A *PITV* ratio greater

that or equal to 0.9 and less than 1.0 is considered a minor acceptable deviation from protocol, as is a *PITV* less than or equal to 2.5 but greater than 2.0. A *PITV* ratio greater than 2.5 is considered a major acceptable deviation from protocol. The *PITV* conventions are given in Table 4-3.

Range	Classification
1.0 ≤ PITV ≤ 2.0	Per Protocol
0.9 ≤ PITV < 1 or 2.0 < PITV ≤ 2.5	Minor Acceptable Deviation
PITV > 2.5	Major Acceptable Deviation

TABLE 4-3. Prescription isodose volume to target volume ratio (PITV) classification system outlined in the RTOG Protocol #93-05 (1994).

4.2.2 Treatment Plan Formulation

To provide the cranial and tumor contours required for treatment planning a Picker PQ-2000 CT–simulator (Picker International, Cleveland, Ohio) was used to generate serial *CT* images of the stereotactic radiosurgery phantom, which was described in Section 2.4.2., the procedure was as follows: After affixing the spherical tumor phantom, which has a diameter of 26 mm, to the *localization insert* of the head phantom the insert was slipped into the cavity located within the head phantom. Next, the stereotactic frame was secured to the head phantom and the fiducial marker box was attached to the frame. The frame-phantom assembly was then mounted to a special patient tray; designed to immobilize the stereotactic frame during the *CT* scanning procedure, and transverse images were acquired over the volume enclosed by the fiducial marker box. Each image had a field of view equal to 280×280 mm^2, matrix dimensions of 256×256, and a slice thickness of 2.0 mm. The voxel volume was, therefore, equal to 0.9×0.9×2.0 mm^3 or 1.6 mm^3. Each transverse slice was indexed 2 mm from the previous one resulting in a total of 56 slices.

After importing the *CT* images into the McGill Planning System (Pla 1994), the coordinate system of the fiducial marker box was transferred to the *CT* images by digitizing the nine fiducial marker points that appeared on each slice. The skull and tumor phantom contours were then digitized.

The arc lengths and arc planar angles used for treatment plan development were based on the work of Schell *et al.*, (1991) and Serago *et al.*, (1992). They compared the cumulative dose volume histograms for different non-coplanar and dynamic radiosurgical arc techniques and reported that the normal tissue dose is minimized if: (a) the total arc traversal is greater than 400° per isocenter, (b) the arc planes are distributed evenly, and (c) individual arc lengths are less than 180°. Before discussing the arc geometries used in our work, it is useful to adopt a set of gantry and couch angle conventions.

A different set of gantry and couch angle conventions exist for the Clinac-18, the Theratron T-780, and the McGill Planning System *(MPS)*. To avoid confusion, the *MPS* angle conventions alone will be used for discussions of the radiosurgical arc techniques. For the McGill Planning System the gantry reference angle (i.e., 0°) corresponds to the position at which the beam is directed upwards. Subsequent gantry angles increase in the clockwise direction. The couch reference angle denotes the position at which the couch is perpendicular to the gantry's plane of rotation. Subsequent angles increase positively in the clockwise direction and negatively in the counterclockwise direction. These angle conventions are shown in Fig. 4-1.

Treatment plans were devised using 4, 6, 8, and 10 non-coplanar arcs, with each arc traversing 120°. The minimum total arc traversal was, therefore, 480°. The arc planes were distributed evenly over the coronal plane between the maximum couch angles of ±75°. The radiosurgical techniques used in our work thus meet the treatment planning optimization criteria described by Schell *et al.*, (1991) and Serago *et al.*, (1992).

For radiosurgical techniques planned with the cobalt beam it was determined that the 37.5 mm cone, which produces a 35.3 mm diameter stationary beam profile at the Theratron T-780 isocenter, yielded the optimum *CDVH*. The 35.0 mm cone, which produces a 35.0 mm diameter stationary beam profile at the

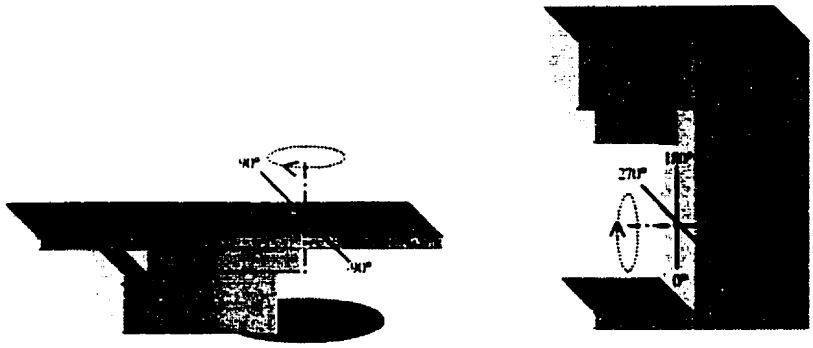

FIG. 4-1. Diagram illustrating the patient support assembly (PSA) and gantry angle conventions adopted for our work. When oriented as depicted, the PSA and gantry angles are equal to 0° and 180°, respectively.

Clinac-18 isocenter, was selected for the 10 MV radiosurgical treatment plans. In accordance with the RTOG Protocol #93-05 (1994) the maximum isodose line that fully encompassed the target volume was chosen as the prescription isodose surface *i.e.*, 100%, and the isodose distributions were renormalized to this dose level.

4.1.1 Results and Discussion

The coronal, sagittal, and transverse isodose distributions for the cobalt-60 and 10 MV beam radiosurgical treatment plans for various multiple non-coplanar converging arc techniques appear on the following three pages. Qualitatively speaking, it is evident from these figures that for a given number of arcs the differences between equal isodose surfaces of the cobalt-60 and 10 MV plans are primarily noticeable below the 50% and above the 100% dose levels; dose levels which are generally given little consideration during treatment planning. Between the prescription dose and 50% dose levels the isodose distributions for the two beams are very similar, with the isodose surfaces of the 10 MV plans appearing slightly more spherical than those of the cobalt-60 plans. The prescription isodose surface of the 10 MV plans can, therefore, be expected to show a greater degree of conformity to the spherical target volume. As expected, these differences become less pronounced as the number of arcs used is increased from 4 to 10.

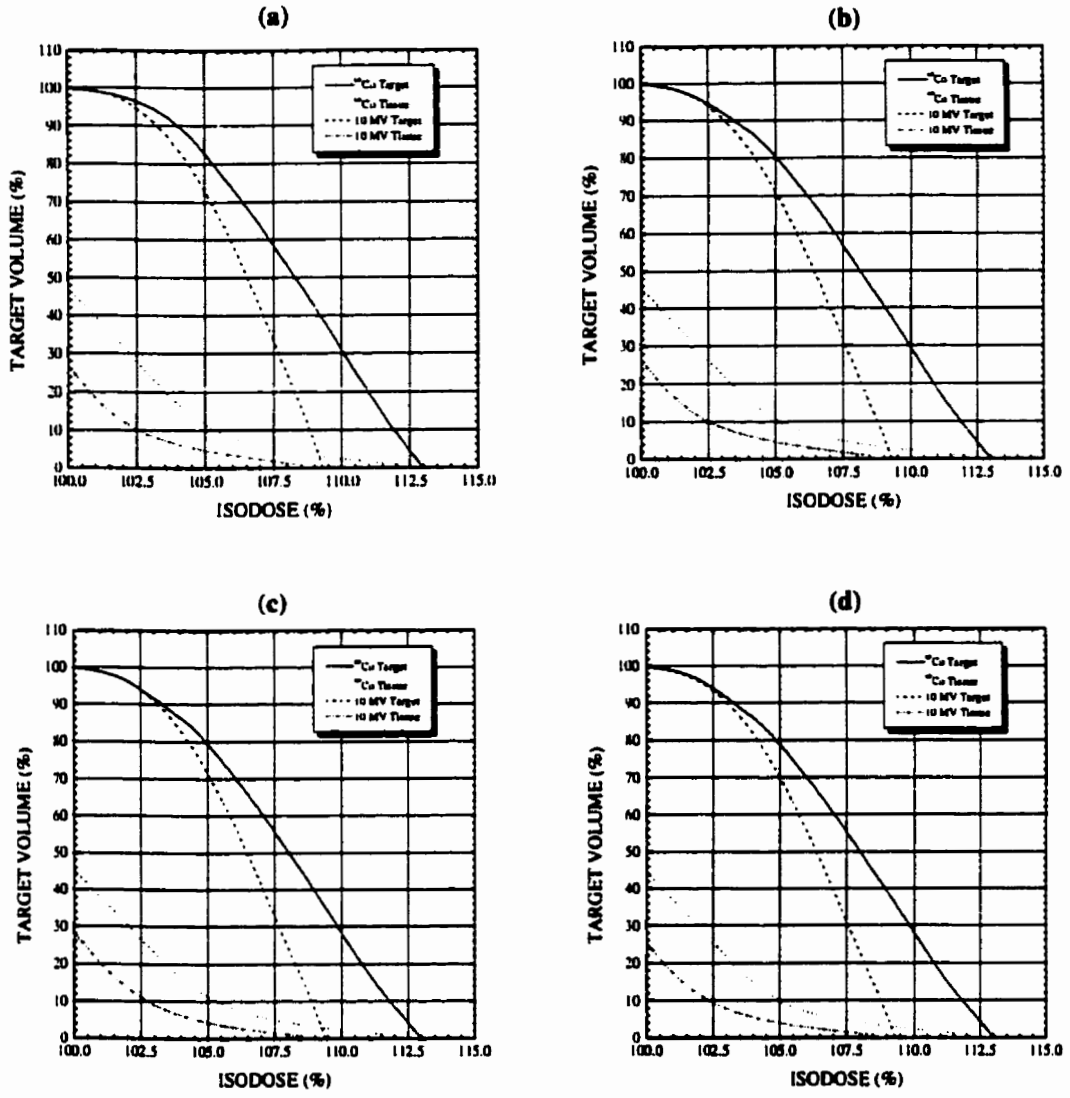

FIG. 4-5. Target and tissue volumes raised to a dose equal to or greater than the prescription isodose for (a) 4, (b) 6, (c) 8, and (d) 10 non-coplanar arc radiosurgical treatment plans calculated for our head phantom and the 35.3 mm nominal diameter cobalt-60 beam and the 35.0 mm nominal diameter 10 MV photon beam. Volumes are normalized to the target volume equal to 10.11 cm^3 and the dose matrix voxel size was equal to 2.8 mm^3.

A quantitative examination of the treatment plans was performed by evaluating each plan's target and tissue cumulative dose volume histograms (CDVH), shown in Fig. 4-5 and Fig. 4-6, with respect to the figures of merit outlined in the RTOG Protocol #93-05 (1994). Regarding the dose homogeneity over the target volume, the maximum target dose to prescription dose

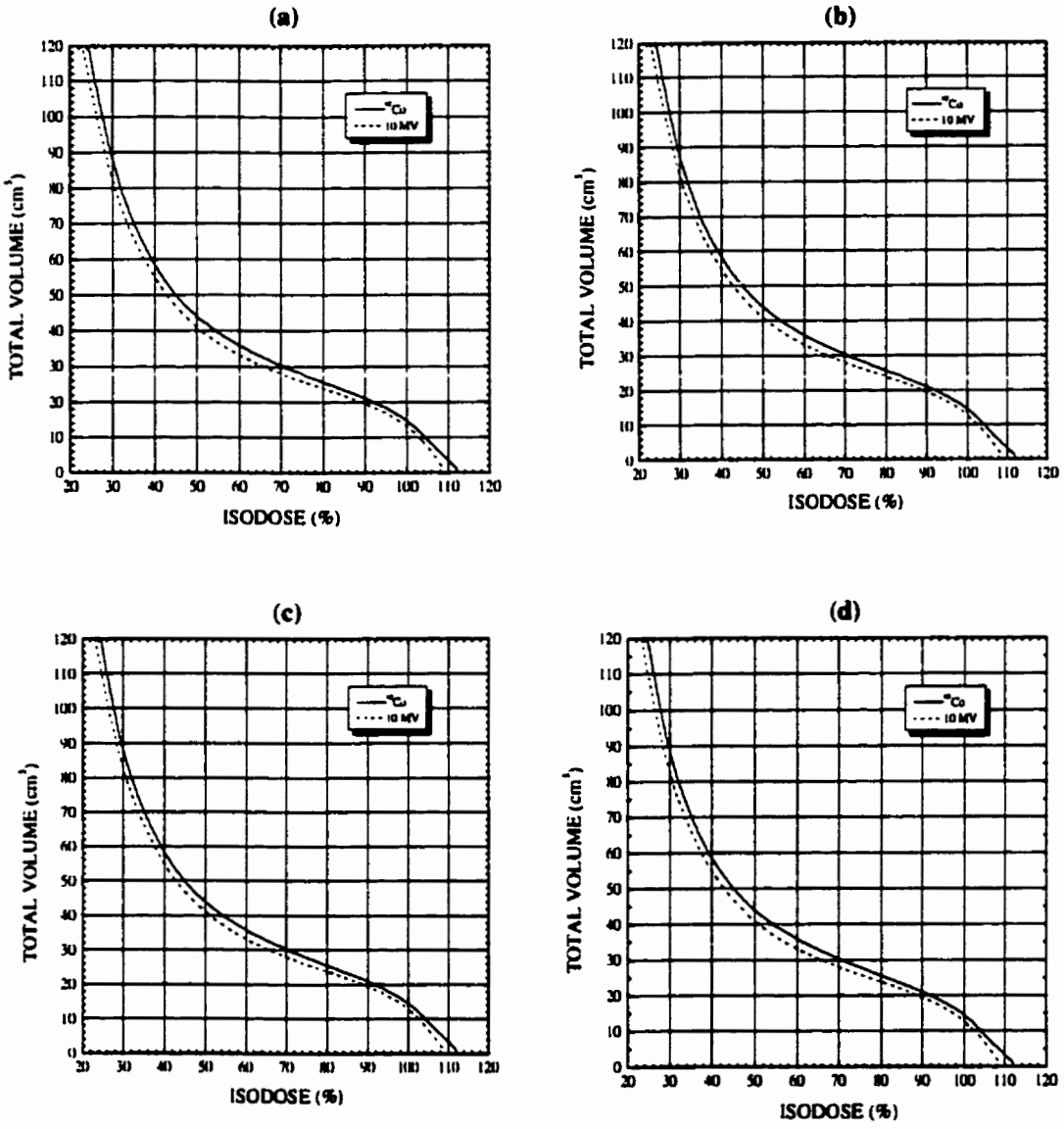

FIG. 4-6. Total volumes encompassed by the 20%-110% isodose surfaces for the (a) 4, (b) 6, (c) 8, and (d) 10 non-coplanar arc radiosurgical techniques, and calculated for our head phantom and the 35.3 mm nominal diameter cobalt-60 beam and the 35.0 mm nominal diameter 10 MV photon beam. Volumes are normalized to the target volume equal to 10.11 cm³ and the dose matrix voxel size was equal to 2.8 mm³.

ratio *(MDPD)* of the cobalt-60 beam treatment plans was equal to 1.130, 3.4% greater than the 1.093 *MDPD* of the 10 MV photon beam, regardless of the number of arcs used. Dependence of the *MDPD* on the number of arcs was, therefore, considered to be less than ±0.5%; the uncertainty of the McGill

Planning System target *CDVHs*. For both beams the *MDPD* values were less than 2.0 and, therefore, considered per the RTOG Protocol #93-05 (1994) quality assurance guidelines. Although the 10 MV photon beam produces a slightly more homogeneous dose distribution within the target volume, the clinical significance of the 3.4% difference in the *MDPD*s of the cobalt-60 and 10 MV treatment plans is likely to be negligible.

The prescription isodose volume to target volume ratios *PITV*s of the cobalt-60 and 10 MV photon beam treatment plans are given in Table 4-4. For both beams the *PITV* values are between 1.0 and 2.0, regardless of the number of arcs used, and are therefore considered per protocol. The *PITV* of the 4 arc cobalt-60 plan was 11.2% greater than that of the similar 10 MV plan. As the number of arcs used was increased from 4 to 6 the difference in the *PITV*s between the beams increased to 15.0%. The use of additional arcs did not appreciably change the *PITV* difference that occurred between the two beams. Considering that a *PITV* value of up to 2.0 is considered clinically acceptable (RTOG Protocol #93-05, 1994), the difference in the *PITV* values of the two beams, 0.180 or 14.1% on average, is of limited significance.

	cobalt-60		10 MV		
Arcs	PI (cm^3)	PITV	PI (cm^3)	PITV	PITV Difference
4	14.94	1.477	13.43	1.328	0.149(11.2%)
6	14.71	1.455	12.79	1.265	0.190(15.0%)
8	14.69	1.453	12.75	1.261	0.192(15.2%)
10	14.59	1.443	12.70	1.256	0.187(14.9%)

TABLE 4-4. PITV ratios of Prescription isodose volume (PI) to target volume (TV) for various non-coplanar converging arc radiosurgical treatment plans formulated using the cobalt-60 and 10 MV photon beams with nominal diameters of 35.3 mm and 35.0 mm, respectively. The target volume was equal to 10.11 cm^3 and the dose matrix voxel size was equal to 2.8 mm^3.

The differences that exist between the cobalt-60 and 10 MV treatment plans, in terms of the total volumes encompassed by several isodose surfaces, are given in Table 4-5. On average, the volume encompassed by the 100%, 80%, 50%, and 30% isodose surfaces of the cobalt-60 plan are 2.07 cm^3, 1.84 cm^3, 3.21 cm^3, and 5.90 cm^3, respectively, greater than those of the 10 MV plan. The 6 arc cobalt-60 treatment plan, therefore, raises 14.1% more tissue to the prescription dose level and 7.2%, 7.3%, and 6.8% more tissue to the 80%, 50%, and 30% dose levels, respectively. For perspective, these volumes are only equal to 0.2%, 0.2%, 0.2%, and 0.4% of the total brain volume (~1300 cm^3), respectively. The differences in the cobalt-60 and 10 MV photon beam treatment plans in terms of the total volume raised to a given dose level are, therefore, unlikely to be of clinical significance, neglecting the presence of sensitive structures of the brain in or near the target volume.

	Volume encompassed by isodose surface (cm^3)							
	100%		*80%*		*50%*		*30%*	
	^{60}Co	**10 MV**	**^{60}Co**	**10 MV**	**^{60}Co**	**10 MV**	**^{60}Co**	**10 MV**
4 arcs	14.94	13.43	25.57	23.84	43.92	40.98	88.36	82.75
6 arcs	14.71	12.79	25.52	23.82	43.88	40.91	88.32	82.71
8 arcs	14.69	12.75	25.48	23.81	43.91	40.89	88.29	82.66
10 arcs	14.59	12.70	25.50	23.77	43.89	40.88	88.30	82.68
Mean Difference	+14.1%		+7.2%		+7.3%		+6.8%	

TABLE 4-5. Volumes encompassed by several isodose surfaces of the 4, 6, 8, and 10 non-coplanar converging arc radiosurgical treatment plans formulated using the cobalt-60 and 10 MV photon beams with nominal diameters of 35.3 mm and 35.0 mm, respectively. Differences are expressed as percentages of the volume emcompassed by a given isodose surface of the 10 MV plan. The target volume was equal to 10.11 cm^3 and the dose matrix voxel size was equal to 2.8 mm^3.

4.3 SUMMARY

In this chapter several radiosurgical treatment plans developed using the cobalt-60 beam of the Theratron T-780 and the 10 MV photon beam of the Clinac-18 linac were compared and evaluated. Based on the quality assurance guidelines described in the RTOG Protocol #93-05 (1994) it was demonstrated that the cobalt-60 beam treatment plans exhibited less dose homogeneity within the target volume and also less dose conformity to the target volume than the 10 MV beam treatment plans. Given the relatively small magnitude of the differences, however, their clinical significance is likely to be minor. The radiosurgical beams of the Theratron T-780 isocentric cobalt unit, therefore, present a viable alternative to linac-produced radiosurgical beams for multiple non-coplanar convergent arc radiosurgical techniques. It should be noted, however, that the uncertainties associated with the actual execution of a radiosurgical technique on the Theratron T-780 can not be assessed using treatment plans alone. The practical application of the isocentric cobalt unit for use in radiosurgery forms the topic of the following chapter.

4.4 REFERENCES

Chierego G., Marchetti C., Avanzo R.C., Pozza F., and Colombo F. *Dosimetric considerations on multiple arc stereotaxic radiotherapy.* Radiotherapy and Oncology **19**: 141-152 (1988).

Phillips M.H., Frankel K.A., Lyman J.T., Fabrikant J.I., and Levy R.P. *Comparison of different radiation types and irradiation geometries in stereotactic radiosurgery.* Int. J. Radiat. Oncol. Biol. Phys. **18**: 211-220 (1989).

Pla. C. *A Macintosh based treatment planning system for brachytherapy and stereotactic radiosurgery.* In: Hounsell A.R., Wilkinson J.M., and Williams P.C., eds. Proc. 11th Int. Conf. on the use of computers in radiation therapy. Manchester, United Kingdom: 138-139 (1994).

RTOG Protocol #93-05 *Radiosurgery Quality Assurance Guidelines*, Radiation Therapy and Oncology Group, Dosimetry Department, Philadelphia, Pennsylvania (1994).

Schell M.C., Smith V., Larson D.A., Wu A., and Flickinger J.C. *Evaluation of radiosurgery techniques with cumulative dose volume histograms in linac-based stereotactic external beam irradiation.* Int. J. Radiat. Oncol. Biol. Phys. **20**: 1325-1331 (1991).

Serago C.F., Houdek P.V., Hartmann G.H., Saini D.S., Serago M.E., and Kaydee A. *Tissue maximum ratios (and other parameters) of small circular 4, 6, 10, 15, and 24 MV x-ray beams for radiosurgery.* Phys. Med. Biol. **37**: 1943-1956 (1992).

Serago C.F., Houdek P.V., Bauer-Kirpes B., Lewin A., Abitbol A., Gonzalez-Arias S., Marcial-Vega V., and Schwade J. *Stereotactic radiosurgery: Dose-volume analysis of linear accelerator techniques.* Med. Phys. **19**: 181-185 (1992).

Chapter 5

Performance of the Theratron T-780 in Radiosurgical Treatment Delivery

5.1 INTRODUCTION

The stringent spatial demands associated with convergent arc radiosurgery require a tight alignment between the radiation-field axis and the rotational axes of the gantry and the patient support assembly *(PSA)*. Ideally, there is a common intersection between these three axes, and the focus of each arc occupies the same point in space; the isocenter. In practice, however, for arbitrary angles of the gantry and *PSA*, the axes do not intersect at a point, and the isocenter is alternatively defined as a sphere that has a radius equal to the maximum distance between the axes, found over all possible combinations of

gantry and *PSA* angles encountered in radiosurgery. It is generally agreed that this 'best compromise' sphere should have a radius of less than 1 mm for radiotherapy machines used in radiosurgery (AAPM TG #42 Report, 1995). In this chapter the techniques used to measure the practical isocenter of the Theratron T-780 unit are presented along with a discussion of the results. The dosimetric effects of the isocenter size, determined experimentally by evaluating the dose distribution produced by a radiosurgical procedure, are also discussed.

5.1 ISOCENTER OF THE THERATRON T-780

Before describing the isocenter measurements, we describe the coordinate system of the treatment room in relation the couch and gantry. The positioning lasers of the Theratron T-780 were used for this purpose. The room which houses the Theratron T-780 has three lasers: two wall-mounted on opposite sides of the unit, and one mounted on the ceiling. These lasers define the coordinate system shown in Fig. 5-1, with the origin located at the point of laser intersection. The position of this intersection is routinely adjusted to coincide with the practical isocenter of the Theratron T-780. Translations of the gantry, *PSA*, and radiation-field axes with gantry or *PSA* rotation were measured relative to this point. A description of these measurements follows.

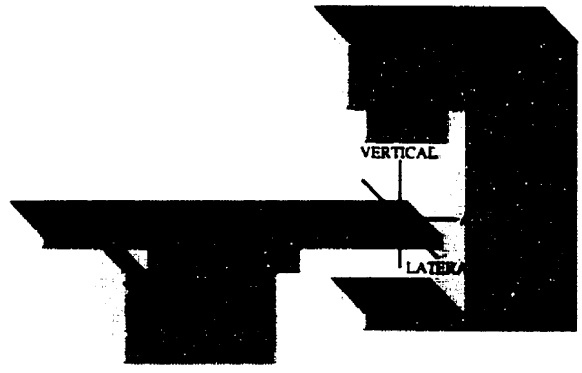

FIG. 5-1. Coordinate system useful for describing the practical isocenter of an isocentrically mounted teletherapy unit. The gantry rotates about the axial axis, while the patient support assembly rotates about the vertical axis.

5.1.1 Rotational Tolerance of the Gantry

The considerable weight of the source shielding, collimation system, frame, and counterweight all forming the gantry cause the rotational axis of the gantry to shift during rotation, spreading the focal point of an arc. Pointing rods were used to determine the axis position at various angles. With the gantry at 180°, the *isocenter distance gauge* of the Theratron T-780; an L-shaped rod that locates the gantry's nominal axis-of-rotation, was attached to the gantry head with its pointing tip aligned with the laser intersection. A second pointing rod was affixed to the patient support assembly *(PSA)* table top, and also aligned with the laser intersection. The lateral, axial, and vertical translations that occurred between the tips of the pointing rods, as the gantry was rotated, were measured every 45° over one full rotation. The results are shown in Fig. 5-2.

Over one rotation and five trials the gantry axis translated by as much as 0.8 mm in the lateral direction, and by as much as 0.2 mm and 0.9 mm in the axial and vertical directions, respectively. Relative to the average axis position, however, the maximum and minimum radial translations varied in magnitude between approximately 0.4 mm at 245° and 0.6 mm at 305°.

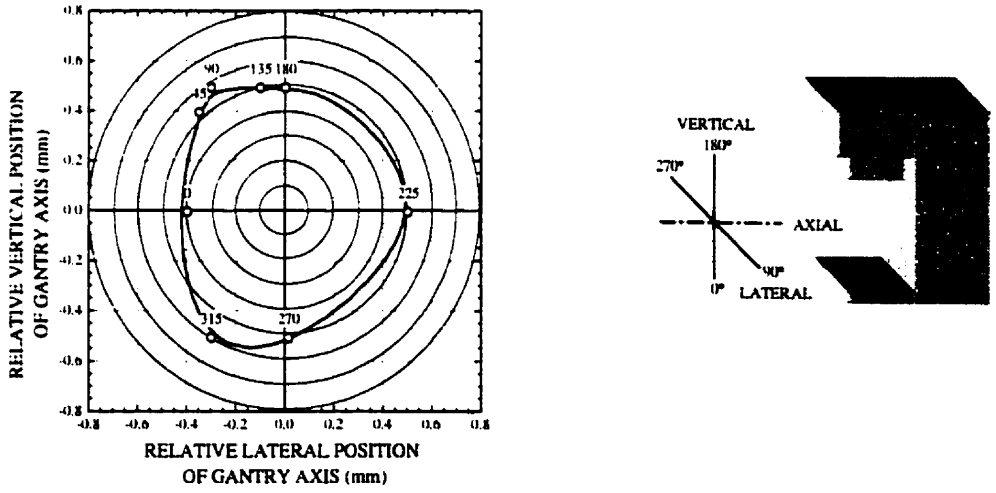

FIG. 5-2. Position of the gantry axis-of-rotation versus angle (data labels), relative to the average axis position. Also depicted are the adopted spatial coordinate system and the gantry angle conventions.

5.1.2 Rotational Tolerance of the Patient Support Assembly

In radiosurgery the patient support assembly *(PSA)* angle determines the arc plane. The convergence of multiple non-coplanar arc planes is limited by the rotational tolerance of the *PSA*. The position of the *PSA* axis-of-rotation was recorded at five angles between ±85°. At *PSA* angles of –85°, -45°, 0°, 50°, and 85° the ceiling laser cross-hairs were traced onto the same sheet of paper, which was taped to the *PSA* table top. The tracings were then digitized and magnified, enabling the position of the laser intersection to be determined at each of the *PSA* angles. The entire procedure was repeated five times.

The position of the *PSA* axis-of-rotation as a function of angle, relative to the position of the axis when the *PSA* is at 0°, is shown in Fig. 5-3. This point of reference was chosen because it is the position at which the target alignment procedure takes place during radiosurgery. As the *PSA* was rotated away from the reference angle, the axis position shifted up to approximately 0.45 mm at -85° and 0.50 mm at 85°. These axis translations were directed primarily in

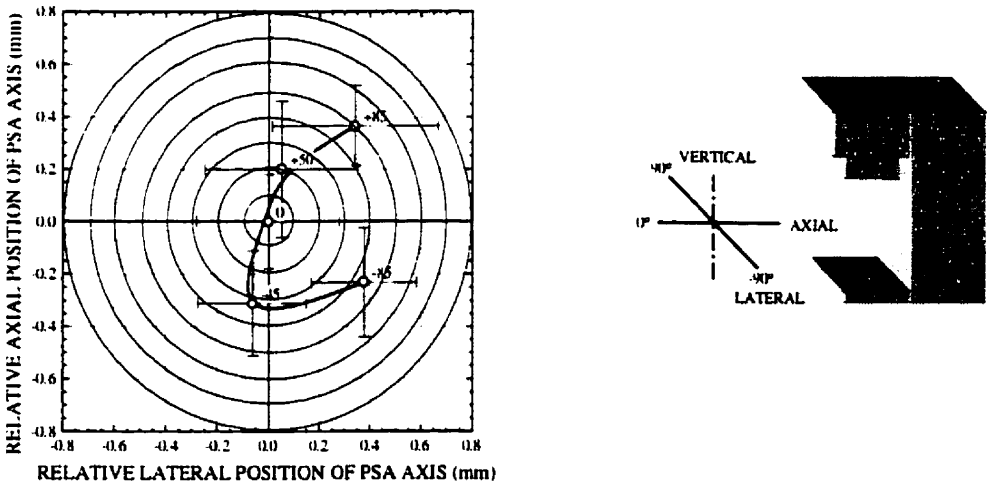

FIG. 5-3. Position of patient support assembly (PSA) axis-of-rotation versus angle (data labels), relative to the 0° PSA position; the position at which the target alignment procedure takes place during radiosurgery. Also depicted are the adopted spatial coordinate system and PSA angle conventions.

the right lateral direction; away from the gantry for negative *PSA* angles, and towards the gantry for positive angles. Additionally, it was determined that the patient stretcher itself had a significant amount (approximately ±0.5 mm) of rotational play, regardless of the *PSA* angle.

The shift in the patient stretcher height as a function of *PSA* angle was also measured and the procedure was as follows: With the gantry at 180°, a pendulum was attached to the unit head, and its tip aligned with the laser intersection. A level surface was then placed on the patient stretcher and raised to within 1 mm of the pendulum tip. For several *PSA* angles between ±90° a relative measurement of the stretcher height was then performed by counting the number of 0.1 mm thick acetate films that could be inserted between the table top and the tip of the pendulum without disturbing the pendulum. It was determined that the maximum change in couch height was less than 0.1 mm from the nominal position, and therefore is insignificant.

5.1.3 Radiation-Field Alignment

At a given gantry angle, the position of the radiosurgical field axis is dependent upon the alignment of the radiosurgical collimator with the axes of the rectangular fields defined by the adjustable and fixed collimators of the Theratron T-780. Radiographic film densitometry was used to determine the position of the field axis relative to the laser intersection. A film *ready-pack* was placed perpendicular to the beam, at a source-surface distance *(SSD)* of 160 cm. By placing the film at twice the unit's nominal source-axis distance, the distance between the field axis and the laser intersection, at the isocenter, is magnified by a factor of two. Hence, the resolution of the detection system is effectively doubled. To denote the lateral and axial directions on the film, the cross-hairs of the ceiling

lasers were marked using pinpricks. A pinprick was also used to mark the point of laser intersection and a reference point, the latter point was used to denote the orientation of the film during exposure. A dose of 35 cGy was then delivered to the film. These procedures were repeated five times for the 5×5 cm^2 radiotherapy field of the Theratron T-780, and the 33.0 mm diameter radiosurgical field.

The method used to determine the relative position of the field axis from the exposed film is best described by referring to Fig. 5-4. After digitizing the film, optical density profiles were taken in the axial direction (denoted by pinpricks *A* and *B*) and in the lateral direction (denoted by pinpricks *C* and *D*). At

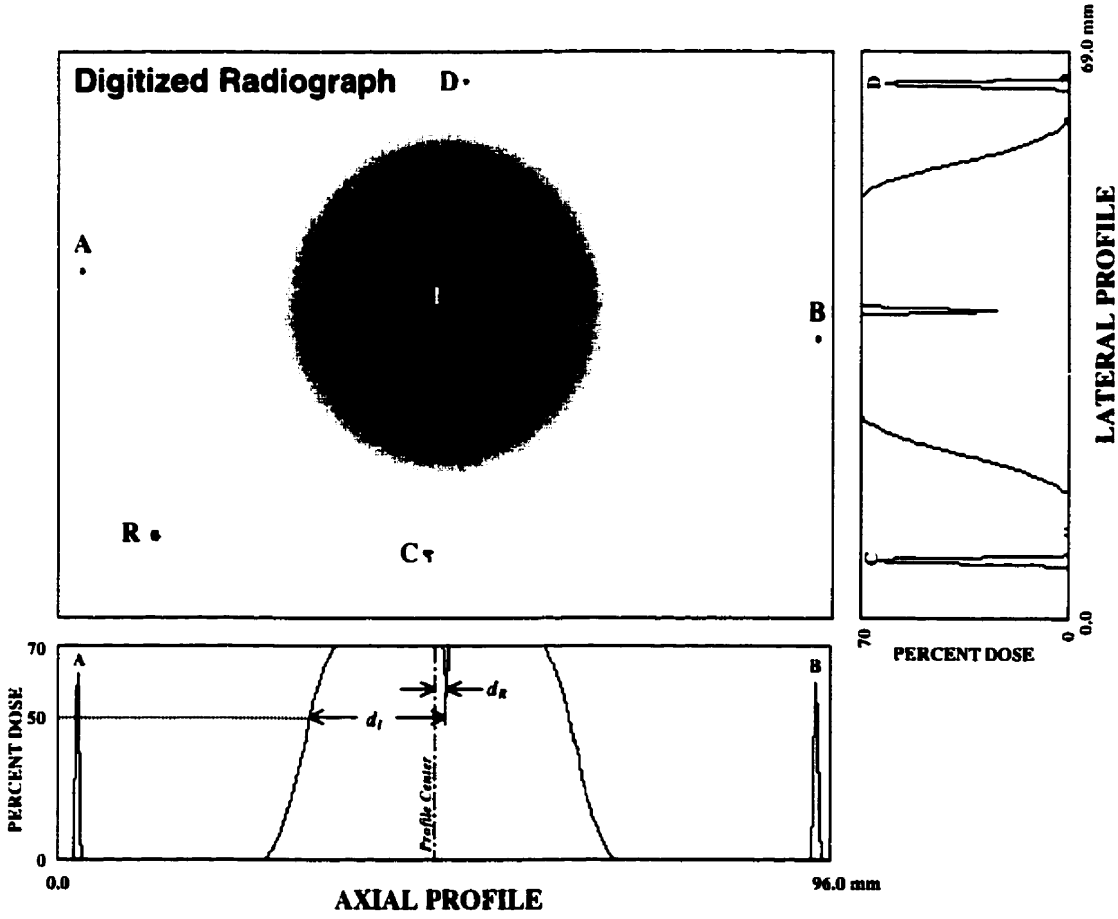

FIG. 5-4. Schematic diagram illustrating the method used to measure the displacement (d_R) of the radiosurgical beam axis from the point of laser intersection (I). The bottom profile was taken along line AB and is perpendicular to the gantry plane of rotation. The right hand profile was taken along the line CD and is parallel to the gantry plane of rotation. The reference point R denotes the directions towards and to the left of the gantry.

a given dose level, the distance d_R between the field axis and the laser intersection is equal to the difference between the profile edge to laser intersection distance d_l, and one half the profile width. At the 50% dose level, this relation can be expressed mathematically as:

$$d_R = \frac{FWHM}{2} - d_l \ . \qquad (5.1)$$

For the 5×5 cm^2 field of the Theratron T-780 it was determined that the radiation-field axis was displaced from the point of laser intersection by a distance of (1.6 ± 0.2) mm in the left-lateral direction, and by (0.8 ± 0.1) mm toward the gantry in the axial direction. Similarly, the radiosurgical field measurements revealed a field axis displacement of (1.1 ± 0.3) mm in the left-lateral direction, and (0.6 ± 0.2) mm toward the gantry.

The resolution of this detection method was investigated by measuring the field axis displacement caused by misaligning the radiosurgical cone by a known distance. Measurements were performed for left-lateral light-field translations of 0.5 mm and 1.0 mm at the isocenter, and then for similar translations in the axial direction toward the gantry. Measurements were repeated three times for each translation. The results are shown in Fig. 5-5.

The translation of the radiosurgical cone in a given direction resulted in radiation-field displacements of similar magnitude and direction, with only slight field displacements seen in the perpendicular direction, as expected. On average, the difference between the measured displacement and the known displacement was 0.3 mm. The spatial resolution of this detection method was, therefore, considered to be of similar magnitude.

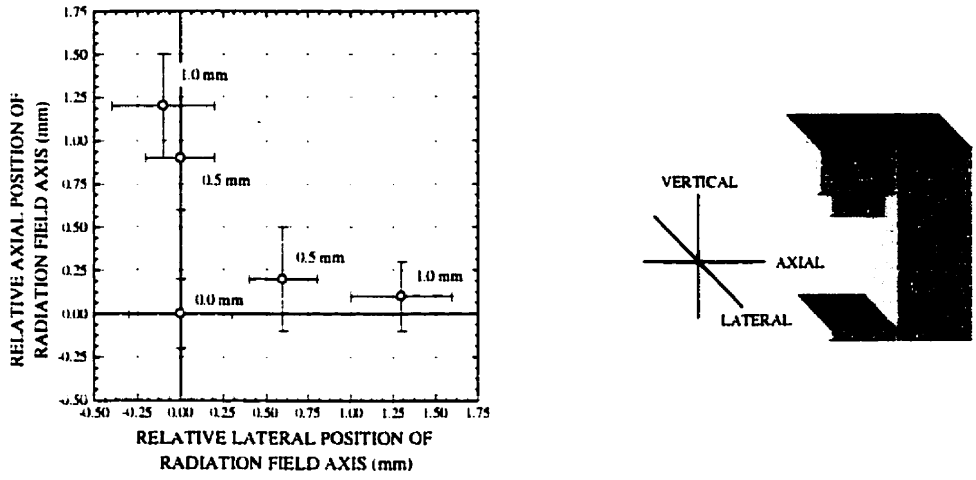

FIG. 5-5. Effect of cone misalignment on the position of the radiation-field axis with respect to the mean position of the aligned radiation field, for the 33.0 mm diameter field of the Theratron T-780. The data labels refer to the magnitude of the light-field displacement at isocenter. Measurements were performed using radiographic film densitometry. Also shown is the adopted spatial coordinate system.

5.1.4 Practical Isocenter of the Theratron T-780 Unit

For an isocentrically mounted therapy unit the practical isocenter is defined by a sphere which has a radius equal to the maximum distance between the patient support assembly axis, the gantry axis, and the radiation-field axis, over all the possible combinations of gantry and *PSA* angles used for radiosurgery. Mathematically, the distance Δ between the axes at a given *PSA* and gantry angles, ϕ and θ, respectively, can be expressed as:

$$\Delta = \Big(\big(d_{PSA}(\phi) - d_G(\theta) - d_R(\theta)\big)^2_{LAT} + \big(d_{PSA}(\phi) - d_G(\theta) - d_R(\theta)\big)^2_{AXIAL} + \big(d_{PSA}(\phi) - d_G(\theta) - d_R(\theta)\big)_{VERT} \Big)^{1/2}, \qquad (5.2)$$

where $d_{PSA}(\phi)$, $d_G(\theta)$, and $d_R(\theta)$ are equal to the distance between an arbitrary point (taken as the position of laser intersection in our work), and the position of the *PSA*, gantry, and radiation-field axes, respectively, at a given angle. The practical isocenter is equal to the maximum value of this expression found over all the combination of *PSA* and gantry angles used in radiosurgery.

Two sets of *PSA* angle-gantry angle combinations are encountered in non-coplanar arc radiosurgery; arcs delivered to left cranial hemisphere consist of *PSA* angles between 0° and 90° combined with gantry angles ranging from 0° and 180°, those delivered to the right cranial hemisphere are composed of *PSA* angles between 0° and -90° combined with gantry angles ranging from 180° and 360°. The practical isocenter was, therefore, determined from combinations of gantry and *PSA* angles taken from these sets.

After evaluating Eq. 5.2 for 61 combinations of gantry and *PSA* angles, it was determined that the maximum value of Δ, equal to 1.9 mm, occurred when the *PSA* is placed at approximately 70° and the gantry at approximately 270°. This tolerance decreases to 0.9 mm if the spatial uncertainty introduced by the radiation-field axis is neglected. Hence, for the Theratron T-780 at the Montreal General Hospital the radiation-field axis displacement is the main source of mechanical instability.

The ±1.9 mm isocenter tolerance of the Theratron T-780 is nearly twice the ±1.0 mm tolerance achievable by modern linacs. Although there is no quantitative relationship between the isocenter tolerance and treatment outcome, some perspective can be gained by taking into account the other sources of spatial uncertainty inherent to the radiosurgical procedure. These sources are listed in Table 5-1. Considering the 1.0 mm uncertainty introduced by both the tissue motion and the stereotactic frame, the 1.9 mm uncertainty introduced by the *CT* image resolution, and the uncertainty associated with the target definition which has been estimated to be as small as 1.0 mm for well defined AVMs (AAPM TG #42 Report, 1995), and as large as 10.0 mm for an invasive malignancy (Halperin *et al.*, 1989), it can be shown that the isocenter tolerance of the Theratron T-780 increases the net spatial uncertainty by only 0.4 mm at most; an amount that is unlikely to affect the treatment outcome.

Source of Spatial Uncertainty	Achievable Uncertainty	
	Linac (mm)	*Theratron T-780 (mm)*
Practical Isocenter	1.0[a]	1.9
Stereotactic Localization[a]	1.0	1.0
CT Image Resolution	2.4	2.4
Tissue Motion[a]	1.0	1.0
Target Definition	1.0[a] - 10.0[c]	1.0[a] – 10.0[c]
Net Uncertainty	**3.1 – 10.4**	**3.5 – 10.5**

[a] *Uncertainty associated with the target definition of a well circumscribed AVM, taken from the AAPM TG #42 Report (1995).*
[b] *CT image resolution based on a voxel volume of 0.9×0.9×2.0 mm³.*
[c] *Uncertainty associated with the target definition of a glioblastoma multiforme, reported by Halperin et al., (1989).*

TABLE 5-1. Sources of spatial uncertainty in stereotactic radiosurgery and their practical magnitude.

5.3 RADIOSURGICAL TREATMENT DELIVERY EVALUATION

To evaluate the dosimetric effects of the practical isocenter it was necessary to quantitatively evaluate the results of an actual radiosurgical procedure. The radiosurgery head phantom was used for this purpose. A discussion of the evaluation procedure and results follows.

5.3.1 Treatment Planning and Setup

A 6 arc radiosurgical technique with the 33.0 mm nominal diameter cobalt beam was chosen for the performance evaluation procedure. Because the bottom of this collimator was only 20.6 cm from the isocenter, couch and angle combinations were limited by possible collisions between the radiosurgical collimator and stereotactic frame, and also by collisions between the *PSA* and one of the treatment room walls. To accommodate these constraints and achieve arc lengths of 120°, the maximum and minimum *PSA* angles were limited to ±60° and ±15°, respectively. *PSA* angles of ±15°, ±38°, and ±60° were therefore used. The coronal, sagittal, and transverse isodose distributions of the 6 arc radiosurgical technique, calculated using the McGill Planning System, appear in Fig. 5-6.

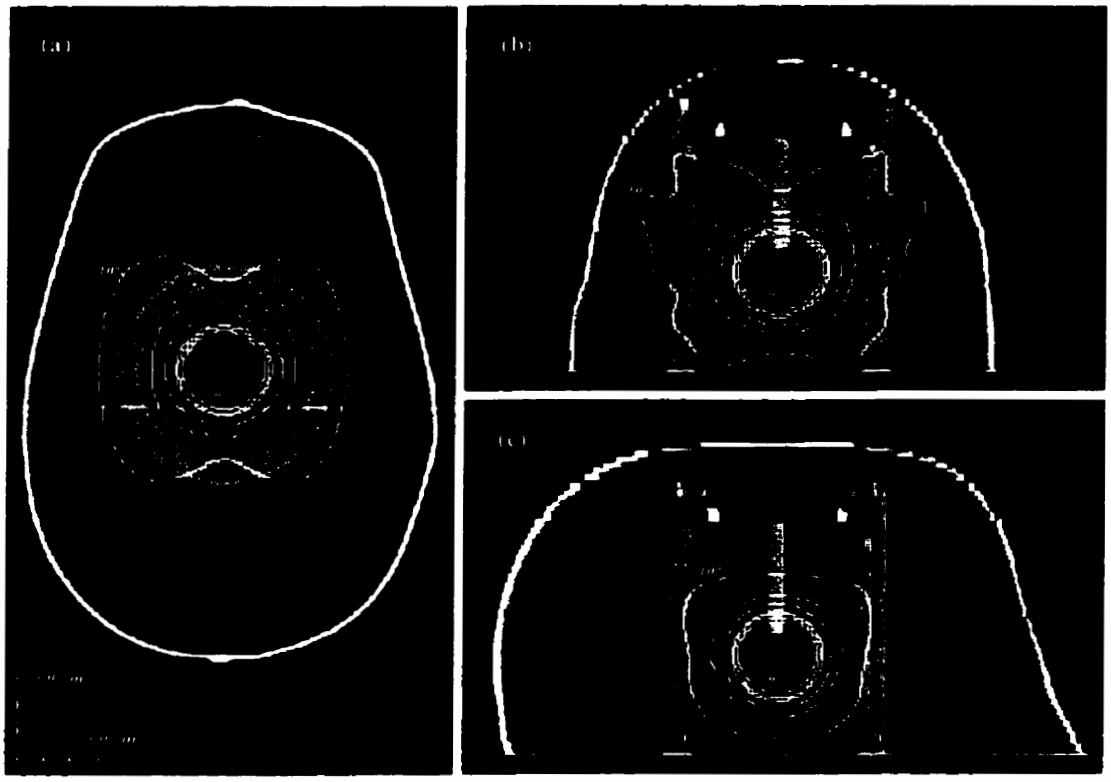

FIG. 5-6. (a) Coronal, (b) sagittal, and (c) transverse isodose distributions of a 6 arc radiosurgical technique, calculated for our head phantom with the 33.0 mm nominal diameter cobalt-60 beam, and used for treatment delivery evaluation of the Theratron T-780 cobalt-60 teletherapy unit. The isodose lines shown are equal to 110%, 100% (prescription isodose surface), 90%, 80%, 50%, 30%, and 10%.

The patient tray designed to immobilize the stereotactic frame during *CT* scans was used to hold the frame and head phantom during the radiosurgical procedure. Alignment of the treatment isocenter with the mechanical isocenter of the Theratron T-780 was facilitated using templates generated by the McGill Planning System. These templates were affixed to the anterior plane, and the left and right lateral planes of the frame's fiducial marker box. The treatment isocenter position, denoted by cross-hairs printed on the templates, was then aligned with the mechanical isocenter, denoted by the wall and ceiling laser cross-hairs, after which the frame was locked in place, and the couch and gantry were rotated to the starting position of the first arc.

Just prior to irradiation, the film mount of the radiosurgical head phantom was loaded with radiochromic film, described in Section 2.3.3.B, and then inserted into the phantom. Because this radiochromic film exhibits a linear dose response

up to 60 Gy, see Fig. 2-4A, a dose of 50 Gy was prescribed to the target. The dose rate of the 33.0 mm diameter radiosurgical beam was equal to 1.43 Gy/min at the depth of maximum dose in tissue for an *SAD* setup. Each arc, therefore, required a beam-on time of 10.30 min to deliver a total dose of 50 Gy to the prescription isodose surface which typically corresponded to an average *TMR* of 0.6. During the irradiation, the gantry was set to rotate continuously between the arc limits at a rate of 1.0 rpm. After all six arcs were completed, the film was removed and stored in a light-tight box. The radiosurgical procedure was then repeated for the other two sectional planes, after which the entire procedure was repeated to gauge the reproducibility of the experiment.

After storing the films for approximately 36 hours, high resolution optical density scans of the films were performed using the laser densitometer, described in Section 2.3.3.C. The radiochromic dose-response calibration curve, shown in Fig. 2-4, was used to convert the measured optical density values to absorbed dose. The dose values of the digitized images were then *binned* to produce isodose bands, and superimposed onto the *MPS* treatment plan isodose lines to facilitate comparison between the measured and calculated dose distributions.

5.3.2 Results and Discussion

The coronal, sagittal, and transverse isodose lines calculated with the McGill Planning System and overlaid onto measured isodose bands are shown on the following three pages. Between the 50% and the prescription dose level, *i.e.*, the 100% dose level, the experimentally determined isodose lines matched those of the treatment plan to within ±1 mm; *i.e.*, within the tolerance specified by the AAPM TG #42 Report (1995). Greater deviations occurred, however, at the 110% dose level and to a lesser degree at the 30% dose level. These discrepancies are most likely a result of the shallow dose gradients found at these dose levels. In any event, the isodose distributions at these dose levels are, generally, given little consideration during treatment planning. The measured isodose distributions can, therefore, be said to agree reasonably with those of the treatment plan.

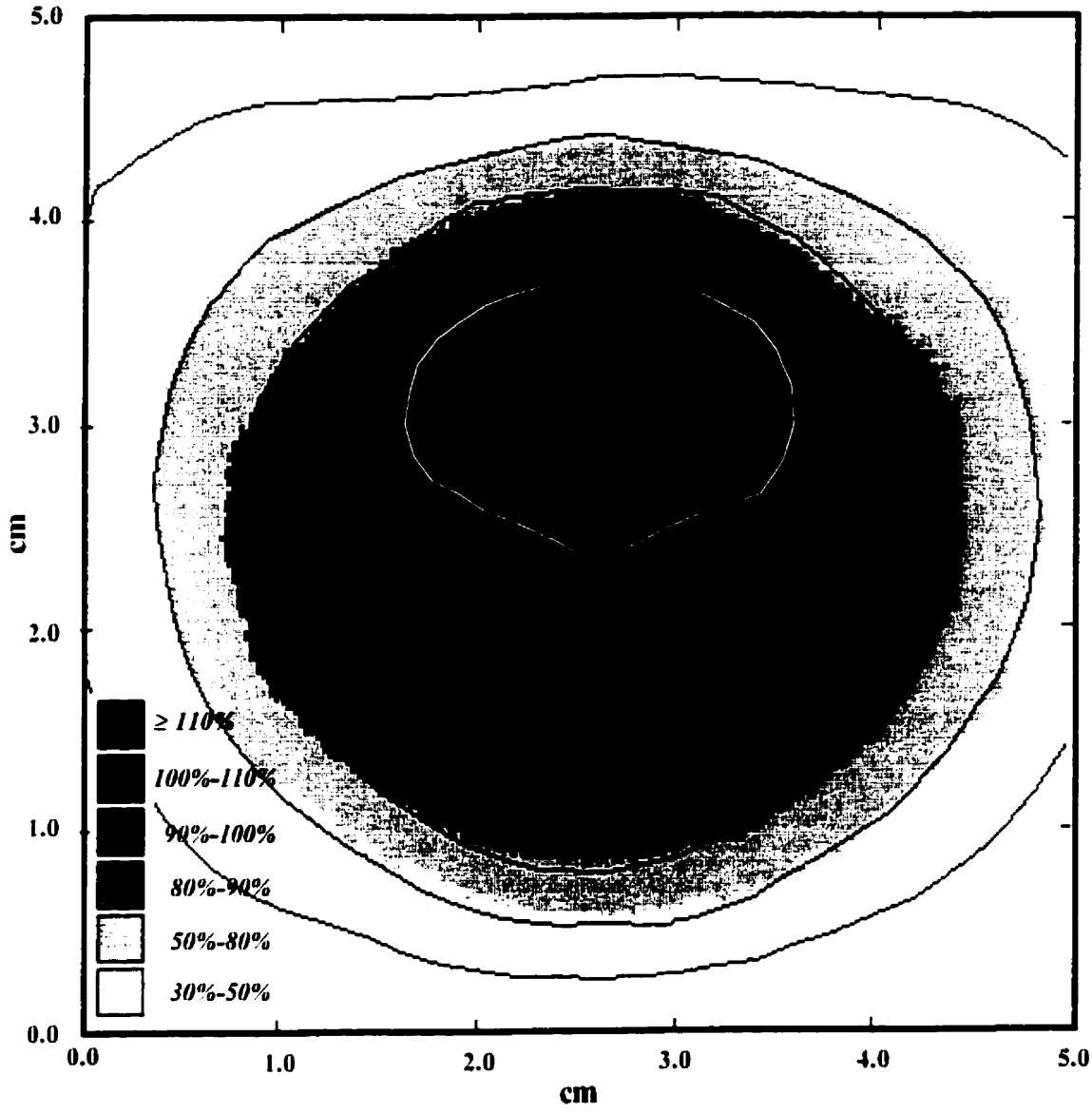

FIG. 5-7. Coronal isodose distributions for a radiosurgical technique consisting of 6 non-coplanar converging arcs with the 33.0 mm nominal diameter cobalt beam, calculated for our head phantom with the McGill Planning System (lines) and superimposed onto isodose distributions obtained experimentally using radiochromic film densitometry (shaded bands). The isodose surfaces are normalized to the prescription dose level (i.e., 100%). The calculated 110% isodose surface is shown as a white line for contrast.

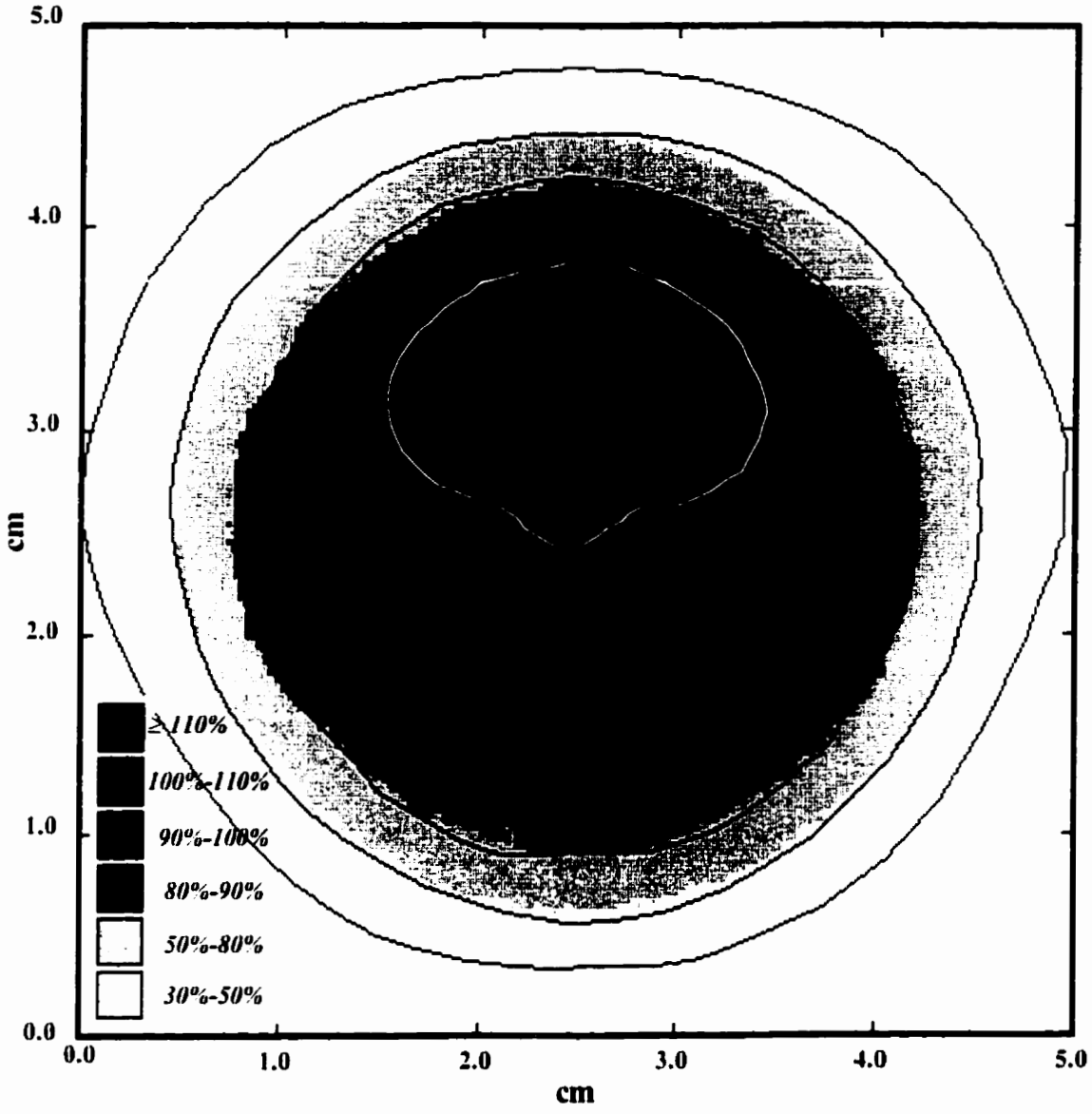

FIG. 5-8. Sagittal isodose distributions for a radiosurgical technique consisting of 6 non-coplanar converging arcs with the 33.0 mm nominal diameter cobalt beam, calculated for our head phantom with the McGill Planning System (lines) and superimposed onto isodose distributions obtained experimentally using radiochromic film densitometry (shaded bands). The isodose surfaces are normalized to the prescription dose level (i.e., 100%). The calculated 110% isodose surface is shown as a white line for contrast

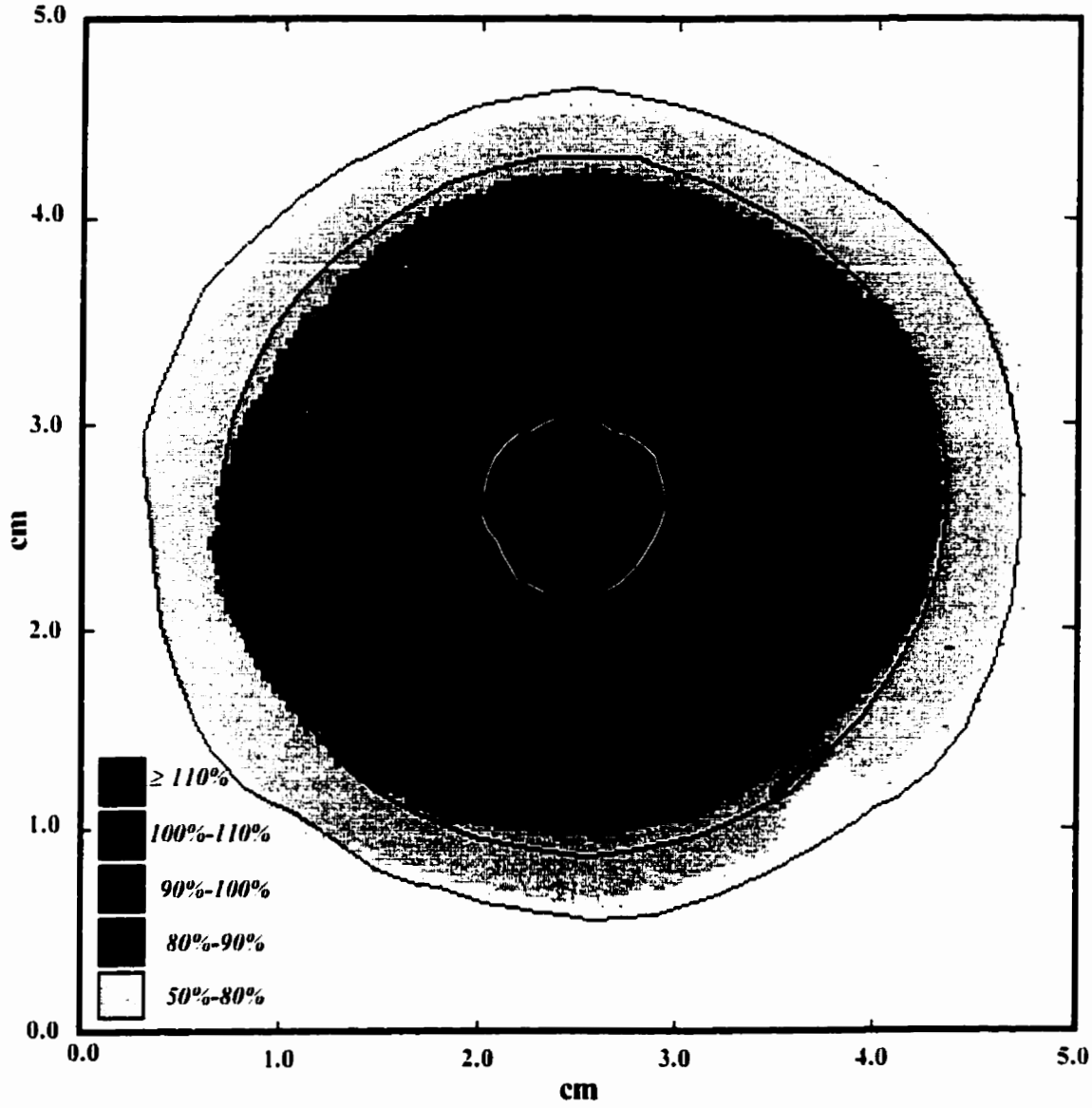

FIG. 5-9. Transverse isodose distributions for a radiosurgical technique consisting of 6 non-coplanar converging arcs with the 33.0 mm nominal diameter cobalt beam, calculated for our head phantom with the McGill Planning System (lines) and superimposed onto isodose distributions obtained experimentally using radiochromic film densitometry (shaded bands). The isodose surfaces are normalized to the prescription dose level (i.e., 100%). The calculated 110% isodose surface is shown as a white line for contrast. The notch in the 50%-80% isodose band at the bottom right is an artifact caused by an alignment peg.

To determine the numerical dose uncertainty of the 6 arc radiosurgical procedure, comparisons were made between the calculated and measured doses delivered to the point of dose maximum in the coronal, sagittal, and transverse planes. These comparisons are given in Table 5-2. In each of the planes, the mean difference between the measured and calculated maximum doses was less than ±5%; the value recommended by the AAPM TG #21 Report (1983) to achieve tumor control and avoid complications. Hence, the radiosurgical performance of the isocentric Theratron T-780 cobalt unit found at the Montreal General Hospital is acceptable for radiosurgery.

	Point of Dose Maximum in Plane		
Plane	**Calculated**	**Measured**	**Difference**
Coronal	5882 cGy	5645 cGy	4.0%
Sagittal	5882 cGy	5627 cGy	4.3%
Transverse	5860 cGy	5635 cGy	3.8%

TABLE 5-2. Comparison of the calculated and measured absorbed doses found at the point of dose maximum in the coronal, sagittal, and transverse planes of a radiosurgical isodose distribution produced using a radiosurgical technique consisting of 6 non-coplanar converging arcs with the 33.0 mm nominal diameter cobalt beam of the Theratron T-780. The measurements were carried out using our radiosurgical head phantom and radiochromic film densitometry.

5.4 SUMMARY

In this chapter the treatment delivery performance of the Theratron T-780 cobalt-60 unit was assessed for use in radiosurgery. It was determined that the maximum displacement between the gantry, patient support assembly *(PSA)*, and radiation-field axes (*i.e.*, the practical isocenter) was equal to ±1.9 mm. The displacement of the radiation-field axis from the gantry and *PSA* rotational axes

was found to be the greatest source of mechanical uncertainty. Although the practical isocenter of the Theratron T-780 is nearly twice the ±1.0 mm tolerance commonly recommended for radiosurgery, it was demonstrated that a radiosurgical dose distribution produced by the unit could meet the spatial and numerical dose uncertainty recommendations of the AAPM TG #42 Report (1995) and TG #21 Report (1983), respectively. The performance of the Theratron-T-780 cobalt-60 unit found at the Montreal General Hospital is therefore acceptable for radiosurgery.

5.5 REFERENCES

American Association of Physicist in Medicine (AAPM) Report #21. *A protocol for absorbed dose from high-energy beams.* Report of the AAPM Task Group #21, Med. Phys. **10**: 741 (1983).

American Association of Physicist in Medicine (AAPM) Report #54. *Stereotactic radiosurgery.* Report of AAPM Task Group #42, American Institute of Physics, New York (1995).

Halperin E.C., Bentel G., and Heinz E.R. *Radiation therapy treatment planning in supratentorial glioblastoma multiforme: an analysis based in postmortem. Topographic anatomy with CT correlations.* Int. J. Radiat. Oncol. Biol. Phys. **17**: 1347 (1989).

RTOG Protocol #93-05. *Radiosurgery Quality Assurance Guidelines*, Radiation Therapy and Oncology Group, Dosimetry Department, Philadelphia, Pennsylvania (1994).

Chapter 6

Conclusions

6.1 VIABILITY OF THE THERATRON T-780 FOR RADIOSURGERY

We have investigated and demonstrated the viability of an isocentric cobalt-60 teletherapy unit for radiosurgery using target localization and dose delivery methods similar to those widely-practiced with linac-based radiosurgical techniques. An isocentric AECL Theratron T-780 cobalt-60 teletherapy unit was evaluated in three areas: (1) the physical properties of radiosurgical fields produced by the unit, (2) the quality of radiosurgical dose distributions generated using the cobalt-60 beam parameters, and (3) the accuracy with which the radiosurgical dose could be delivered using the cobalt unit. For each of these evaluative areas, the 10 MV radiosurgical beam of a Varian Clinac-18 linear accelerator, which has been used for radiosurgery at the Montreal General Hospital for over a decade, served as a standard for comparison.

The percentage depth doses, off-axis ratios, and relative dose factors were used to calculate radiosurgical treatment plans with the McGill Radiosurgical Planning System. These beam parameters were therefore measured and compared for several radiosurgical fields of the cobalt-60 and 10 MV photon beams. The differences between the *PDDs* of the two types of beams followed analogous

trends to the differences observed between the *PDDs* in the standard radiotherapy fields produced by the two machines; the cobalt-60 radiosurgical beams exhibit a larger surface dose, have a shallower depth of maximum dose (d_{max}), an are less penetrating in comparison with the 10 MV radiosurgical beams of the same field diameter.

Contrary to the relatively large 80%-20% penumbra differences that exist between the radiotherapy fields of the two types of beams, the differences between the radiosurgical field penumbras were remarkably small, with the cobalt-60 beam penumbras on the average only about 0.7 mm larger than those of the linac beam. Although we expected that the difference would be larger considering the relatively large diameter of the cobalt-60 source, it was determined that the geometric penumbra of the Theratron T-780 radiosurgical fields had been significantly reduced by performing the tertiary beam collimation relatively close to the isocenter.

A quantitative evaluation of several radiosurgical treatment plans calculated using the cobalt-60 and 10 MV photon beams with nominal diameters of 35.3 mm and 35.0 mm, respectively, and formulated to treat a 26 mm spherical target with between 4 and 10 non-coplanar converging arcs, was carried out using cumulative dose volume histograms. Comparisons were based in part on the RTOG Protocol #93-05 (RTOG 1994) recommendation that the *maximum dose* to *prescription dose* ratio *(MDPD)* and the *prescription isodose volume* to *tumor volume* ratio *(PITV)* be used as quality indices of dose homogeneity within the target volume and conformity of the prescription isodose volume to the target volume, respectively. *MDPDs* of the cobalt beam radiosurgical plans were only negligibly larger (3.4%) than the *MDPDs* of the 10 MV beam plans, regardless of the number of arcs used. The average *PITV* of the cobalt-60 plans was equal to 1.46 compared

to the 1.28 average *PITV* value of similar 10 MV plans, a difference of limited significance, considering that *PITV* values of up to 2.0 are considered clinically acceptable. Additionally, the total volume encompassed by a given isodose surface of the cobalt-60 treatment plans was on average only 8.8% greater than the volume encompassed by the same isodose line of the 10 MV plans, an acceptable difference considering that this extra volume of irradiated tissue constitutes on average a very small fraction of the total brain volume. Given the relatively insignificant differences between the cobalt-60 and 10 MV treatment plans, the radiosurgical beams generated by the Theratron T-780 cobalt unit can be considered suitable for use in radiosurgery.

The evaluation of treatment plans only shows the potential of a cobalt unit for use in radiosurgery. To evaluate the practical application of the Theratron T-780 for radiosurgery it was also necessary to determine whether or not the unit could produce radiosurgical dose distributions that agreed with the treatment plan to within an acceptable tolerance. Although measurements of the cobalt unit's practical isocenter revealed that the isocenter sphere has a radius of approximately 2.0 mm, nearly twice the 1.0 mm tolerance generally recommended for radiosurgery, it was shown by accounting for the major uncertainties inherent in radiosurgery that the inferior isocenter of the Theratron T-780 unit increases the net spatial uncertainty of the procedure by at most a mere 0.4 mm, an amount that is unlikely to play a significant role in the treatment outcome.

The coronal, sagittal, and transverse isodose distributions of a 6 arc radiosurgical procedure performed on the Theratron T-780 agreed with calculated treatment plan isodose distributions to within the ±1 mm spatial and ±5% numerical dose tolerances recommended by the AAPM TG #42 Report (AAPM 1995) and TG #21 Report (AAPM 1983), respectively. Hence, the performance of the isocentric Theratron-T-780 cobalt unit found at the Montreal General Hospital

is acceptable for radiosurgery. Moreover, the mechanical tolerances of the gantry and treatment couch could be improved on newly-manufactured isocentric cobalt units, if their use in radiosurgery is seriously contemplated.

In conclusion, the radiosurgical dose distributions produced with isocentric Theratron T-780 cobalt units meet the quality assurance guidelines recommended by the AAPM TG #42 Report (1995) and TG #21 Report (1983), as well as those of the RTOG Protocol #93-05 (1994). The drawbacks of using this unit for radiosurgery in comparison with linac-based radiosurgery include longer treatment times because of the inherently lower machine output and the need to restrict the couch-gantry angle combinations to avoid possible collisions between the radiosurgical collimator and the stereotactic frame. The latter problem is of course specific to the 80 cm *SAD* unit and will not be present for the newer, *SAD* 100 cm cobalt units.

Radiosurgery with the relatively inexpensive and technologically simple isocentric cobalt-60 teletherapy unit is a viable alternative to linear accelerator-based radiosurgery. The use of isocentric cobalt units for radiosurgery would be of particular interest for centers in developing countries where cobalt units, because of their relatively low costs, provide the only megavoltage source of radiation for radiotherapy and could relatively easily and inexpensively be modified for radiosurgery.

6.2 FUTURE WORK

Future work might include an investigation of the Theratron T-780 radiosurgical cobalt-60 beam parameters using Monte Carlo simulations. In addition to verifying the measurements presented in this work, Monte Carlo simulations would provide insight into the components and behavior of the radiosurgical cobalt beam penumbra.

6.3 REFERENCES

American Association of Physicist in Medicine (AAPM) Report #21. *A protocol for absorbed dose from high-energy beams.* Report of the AAPM Task Group #21, Med. Phys. **10**: 741 (1983).

American Association of Physicist in Medicine (AAPM) Report #54. *Stereotactic radiosurgery*. Report of AAPM Task Group #42, American Institute of Physics, New York (1995).

RTOG Protocol #93-05 *Radiosurgery Quality Assurance Guidelines*, Radiation Therapy and Oncology Group, Dosimetry Department, Philadelphia, Pennsylvania (1994).

List of Figures

List of Tables

Bibliography

Adler J.R. and Cox R.S. *Preliminary clinical experience with the cyberknife: image guided stereotactic radiosurgery.* In: Kondziolka D., (ed.). Radiosurgery. **pp.** 317-326 (1995). 9

American Association of Physicist in Medicine (AAPM) Report #21. *A protocol for absorbed dose from high-energy beams.* Report of the AAPM Task Group #21, Med. Phys. **10**: 741 (1983). 91, 92, 95, 96

American Association of Physicist in Medicine (AAPM) Report #54. *Stereotactic radiosurgery.* Report of AAPM Task Group #42, American Institute of Physics, New York (1995). 9, 35, 47, 54, 57, 58, 77, 84, 85, 87, 92, 95, 96

Attix F.H., *Introduction to radiological physics and radiation dosimetry.* John Wiley and Sons Inc. (1986). 24, 26

Barcia-Salorio J.L., Broseta J., Hernandez G., Ballester B., and Masbout G. *Radiosurgicaltreatment of a carotid-cavernous fistula.* Case report in Szikla, Stereotactic cerebral irradiations, Elsevier pp. 251-256 (1979). 5

Barcia-Salorio J.L., Hernandez G., Broseta J., Gonzalez-Darder J., and Ciudad J. *Radiosurgical treatment of carotid-cavernous fistula.* Appl. Neurophysiol. **45**: 520-522 (1982). 5

Betti O.O. and Derechinsky V.E. *Hyperselective encephalic irradiation with linear accelerator.* Acta Neurochir; suppl **33**: 385-390 (1984). 5, 7

Biggs P.J. and Ling C.C. *Electrons as the observed d_{max} shift with field size in high energy photon beams.* Med. Phys. **6**: 291-299 (1979). 38

Bourland J.D. and McCollough K.P., *Static field conformal stereotactic radiosurgery: physical techniques.* Int. J. Radiat. Oncol. Biol. Phys. **28**: 471-479 (1994). 9

Colombo F., Beneditti A., Pozza F., Avanzo R.C., Marchetti C., Chierego G., and Zanardo A. *External stereotactic irradiation by linear accelerator.* Neurosurgery **16**: 154-160 (1985). 5, 7

Dawson D.J., Schroeder N.J., and Hoya J.D. *Penumbral measurements in water for high energy x-rays*, Med. Phys. **13**: 101 (1986). 47

Ehricke H., Schad L.R., Gademann G., Wowra B., Engenhart R., and Lorenz W.J. *Use of MR angiography for stereotactic planning.* J. Comp. Asst. Tomography. **16**: 35-37 (1992). 8

Flickinger J.C., Lunsford L.D, Wu A., Maitz A.H., and Kalend A.M. *Treatment planning for Gamma Knife radiosurgery with multiple isocenters.* Int. J. Radiat. Oncol. Biol. Phys. **18**: 1495-1511 (1990). 5

Friedman W.A. and Bova F.J. *The University of Florida radiosurgery system.* Surg. Neurol. **32**: 334-342 (1989). 6

Galbraith D.M. and Rawlinson J.A. *Direct measurement of electron contamination in cobalt beams using a charge detector.* Med. Phys. **12**: 273-280 (1985). 38

Gall K., Verhey L., and Wagner M. *Automated patient positioning for high precision radiotherapy*. AAPM Annual Meeting, 1991, St. Louis, Missouri (abstract).. Med. Phys. **18**: 604 (1991). 9

Halperin E.C., Bentel G., and Heinz E.R. *Radiation therapy treatment planning in supratentorial glioblastoma multiforme: an analysis based in postmortem. Topographic anatomy with CT correlations*. Int. J. Radiat. Oncol. Biol. Phys. **17**: 1347 (1989). 84, 85

Hartmann G.H., Schlegel W., Sturm V., Kober B., Pastyr O., and Lorenz W.J.. *Cerebral radiation surgery using moving field irradiation at a linear accelerator facility*. Int. J. Radiat. Oncol. Bio. Phys. **11**: 1185-1192 (1985). 5, 7

Jones D., Christopherson D.A., Washington J.T., Hafermann M.D., Rieke J.W.,Travaglini J.J., and Vermuelen S.S. *A frameless method for stereotactic radiotherapy*. Brit. J. Radiol. **66**: 1142-1150 (1993). 9

Karzmark C.J. and Morton R.J. *A primer on theory and operation of linear accelerators in radiation therapy*. U. S. Department of Health and Human Services, Food and Drug Administration, Bureau of Radiological Health, Rockville, Maryland, (1981). 19

Kessler M.L. and Carson P.L. *Test object design and performance simulation for 3D imaging systems: spiral rod image distortion phantom*, Annual meeting of the Radiological Society of North America (1992). (abstract). 8

Khan F.M. *The Physics of Radiation Therapy*. 2nd edition, Williams and Wilkins, (1994). 18, 30

Kjellberg R.N., Shintani A., and Frantz A.G. *Proton beams in acromegaly.* N. Eng. J. Med. **278**: 689-695 (1968). 2

Kooy H.M., van Herk M., Barnes P.D., Alexander E. 3rd., Dunbar S.F., Tarbell N.J., Mulkern R.V., Holupka E.J., and Loeffler J.S. *Image fusion for stereotactic radiotherapy and radiosurgery treatment planning.* Int. J. Radiat. Oncol. Biol. Phys. **28**: 1229-1234 (1994). 8

Larsson B., Leksell L., and Rexed B. *The high energy proton beam as a neurosurgical tool.* Nature **182**: 1222-1223 (1958). 2

Larsson B., Liden K., and Sorby B. *Irradiation of small structures through intact skull.* Acta Radiol. TPB **13**: 513-534 (1974). 5

Lawrence J.H., Tobias C.A., Born J.L., Wang C.C., and Linfoot J.H. *Heavy particle irradiation in neoplastic and neurologic disease.* J. Neurosurg. **19**: 717-722 (1962). 2

Leavitt D.D., Gibbs F..A., Heilbrun M..P., Moeller J.H., and Tabach G.A. *Dynamic field shaping to optimize stereotactic radiosurgery.* Int. J. Radiat. Oncol. Biol. Phys. **21**: 1247-1255 (1991). 9

Leksell L. *The stereotaxis method and radiosurgery of the brain.* Acta Chir. Scand. **102**: 316-319 (1951). 2

Leksell L. *Cerebral radiosurgery I. Gamma thalamotomy in two cases of intractable pain.* Acta Chir. Scand. **134**: 585-595 (1968). 4

Leung P.M.K., Sontag M.R., Harrideo M., Chenery S. *Dose measurements in the build-up region for cobalt-60 therapy units.* Med. Phys. **3**: 169-172 (1976). 38, 42

Lunsford L.D. *Current worldwide role of gamma knife stereotactic radiosurgery.* Stereotactic radiosurgery update proceedings of the international stereotactic radiosurgery symposium, Pittsburgh, Pennsylvania, June 1991, Elsevier (1992). 4

Lutz W., Winston K.R., Maleki N. *A system for stereotactic radiosurgery with a linear accelerator.* Int. J. Radiat. Oncol. Bio. Phys. **14**: 373-381 (1988). 5, 7

Luxton G. and Jozsef G. *Dosimetric considerations in linac radiosurgery treatment planning of off-center and elongated targets* (abstract).. Int. J. Radiat. Oncol. Biol. Phys. (Suppl. 1). **19**: 262 (1990). 9

Lyman J.T., Phillips M.H., Frankel K.A, and Fabrikant J.I. *Stereotactic frame for neuroradiology and charged particle Bragg peak radiosurgery of intracranial disorders.* Int. J. Radiat. Oncol. Biol. Phys. **16**: 1615 (1989). 3

McGinley P.H., Butker E.K., Crocker I.R., and Landry J.C. *A patient rotator for stereotactic radiosurgery.* Phys. Med. Biol. **35**: 649-657 (1990). 7

McLaughlin W.L. and Chalkey L., *Low atomic numbered dye systems for ionizing radiation measurements*, Photo. Sci. Eng. **9**: 159-165 (1965). 27

McLaughlin W.L., Soares C.G., Sayeg J.A., McCullough E.C., Kline R.W., Wu A., and Maitz A.H. *The use of a radiochromic detector for the determination of stereotactic radiosurgery dose characteristics.* Med. Phys. **21**: 379-388 (1994). 28

Muench P.J., Meigooni A.S., Nath R., and McLaughlin W.L. *Photon energy dependence of the sensitivity of radiochromic film and comparison with silver halide film and LiF TLDs used for brachytherapy dosimetry.* Med. Phys. **18**: 769-775 (1991). 27

Padikal T.N. and Deye J.A. *Electron contamination of a high energy x-ray beam.* Phys. Med. Biol. **23**: 1086-1091 (1978). 38

Phillips M.H., Frankel K.A., Lyman J.T., Fabrikant J.I., and Levy R.P. *Comparison of different radiation types and irradiation geometries in stereotactic radiosurgery.* Int. J. Radiat. Oncol. Biol. Phys. **18**: 211-220 (1989). 62

Pike B., Podgorsak E.B., Peters T.M., and Pla C. *Dose distributions in dynamic stereotactic radiosurgery.* Med. Phys. **14**: 780-791 (1987). 34, 35

Pla. C. *A Macintosh based treatment planning system for brachytherapy and stereotactic radiosurgery.* In: Hounsell A.R., Wilkinson J.M., and Williams P.C., eds. Proc. 11th Int. Conf. on the use of computers in radiation therapy. Manchester, United Kingdom: 138-139 (1994). 34, 35, 64

Podgorsak E.B., Olivier A., Pla M., Hazel J., and deLotbiniere A. *Physical aspects of the dynamic stereotactic radiosurgery.* Appl. Neurophisiol. **50**: 263-268 (1987). 5, 7

Podgorsak E.B., Olivier A., Pla M., Lefebvre P.Y., and Hazel J. *Dynamic stereotactic radiosurgery.* Int. J. Radiat. Oncol. Biol. Phys. **14**: 115-126 (1988). 5

Podgorsak E.B., Pike G.B., Olivier A., and Souhami L. *Radiosurgery with high energy photon beams: a comparison among techniques.* Int. J. Radiat. Oncol. Biol. Phys. **16**: 857-865 (1989). 7

Ramani R., Lightstone A.W., Mason D.L.D., and O'Brien P.F., *The use of radiochromic film in treatment verification of dynamic stereotactic radiosurgery.* Med. Phys. **21**: 389-392 (1994). 28

Rice R.K., Hansen J.L., and Svensson G.K. *Measurements of dose distributions in small beams of 6 MV x-rays*, Phys. Med. Biol. **32**: 1087 (1987). 47, 56

Richardson, C. *Effect of chamber voltage on electron build-up measurements.* Radiology **62**: 584 (1954). 23

RTOG Protocol #93-05 *Radiosurgery Quality Assurance Guidelines*, Radiation Therapy and Oncology Group, Dosimetry Department, Philadelphia, Pennsylvania (1994). 61, 62, 63, 64, 66, 70, 72, 74, 94, 96

Sayeg J.A., Coffey C.W., and McLaughlin W.L. *The energy response of GafChromic radiation detectors*, Med. Phys. **17**: 521 (1990). (Proc. of 1990 AAPM Meeting). 27

Schad L.R., Lott S., Schmitt F., Sturm V., and Lorenz W.J. *Correction of spatial distortion in MR imaging: a prerequisite for accurate stereotaxy.* Journal of Computer Assisted Tomography **11**: 499-505 (1987). 8

Schell M.C., Smith V., Larson D.A., Wu A., and Flickinger J.C. *Evaluation of radiosurgery techniques with cumulative dose volume histograms in linac-based stereotactic external beam irradiation.* Int. J. Radiat. Oncol. Biol. Phys. **20**: 1325-1331 (1991). 62, 65

Serago C.F., Lewin A.A., Houdek P.V., Gonzalez-Arias S., Abitbol A.A., Marcial-Vega V.A., Pisciotti V., and Schwade J.G. *Improved LINAC dose distributions for radiosurgery with elliptically shaped fields.* Int. J. Radiat. Oncol. Biol. Phys. **21**: 1321-1325 (1991). 9

Serago C.F., Houdek P.V., Hartmann G.H., Saini D.S., Serago M.E., and Kaydee A. *Tissue maximum ratios (and other parameters) of small circular 4, 6, 10, 15, and 24 MV x-ray beams for radiosurgery.* Phys. Med. Biol. **37**: 1943-1956 (1992). 53

Serago C.F., Houdek P.V., Bauer-Kirpes B., Lewin A., Abitbol A., Gonzalez-Arias S., Marcial-Vega V., and Schwade J. *Stereotactic radiosurgery: Dose-volume analysis of linear accelerator techniques.* Med. Phys. **19**: 181-185 (1992). 62, 65

Sixel K.E. *Physical parameters of narrow photon beams in radiosurgery.* M.Sc. Thesis, McGill University, Montreal (1990). 42, 56

Sixel K.E. and Podgorsak E.B. *Build-up region and depth of dose maximum of megavoltage x-ray beams.* Med. Phys. **21**: 411-416 (1994). 38, 42

Walton L., Bomford C.K., and Ramsden D. *The Sheffield stereotactic radiosurgery unit: physical characteristics and principles of operation.* Br. J. Radiol. **60**: 897-906 (1987). 7

Zankowski C. *Monte Carlo analysis of the 10 MV x-ray beam from a CLINAC-18 linear accelerator.* M.Sc. Thesis, McGill University, Montreal (1996). 20, 38, 42